Improving the electronic communication between a porphyrin core and peripheral substituents: towards enhanced solar energy conversion.

Caitlin Kay Fulton

Master of Science by Research

University of York

Chemistry

December 2022

Abstract

The conversion of solar energy into a usable form *via* photocatalysis and photovoltaics is a continually growing area of research due to the ever-growing need to shift away from fossil fuel-derived energy. Porphyrins have become a focal point for the design of new dyes and photocatalysts due to their optical properties, high stability, scope of functionalisation and cheapness. This work synthesised a series of *meso*-substituted porphyrins with furan and thiophene based groups in an attempt to extend the conjugation of the porphyrin system. The synthesis of trans-5,15-di(methyl furan-2-carboxylate)10,20-diphenylporphyrin (26a) and trans-5,15-di(methylthiophene-2-carboxylate)10,20-diphenylporphyrin (27a) followed a Suzuki-Miyaura cross-coupling methodology. To get to this point, a modified Lindsey 2+2 condensation reaction, followed by di-bromination of a *trans*-5,15-diphenyl porphyrin was completed. The modified condensation reaction was the foundation of the synthetic pathway and resulted in exceptional yields of >40 %. Initially a palladium catalysed Miyaura-borylation of the furan and thiophene rings were undertaken but following complications in purification, an alternative C-H activated borylation reaction was undertaken using an [Ir(COD)(OMe)]$_2$ catalyst. This resulted in the successful synthesis of methyl 5-(4,4,5,5-tetramethyl-1,3,2-dioxaborolan-2-yl)-2-furancarboxylate (35) and methyl 5-(4,4,5,5-tetramethyl-1,3,2-dioxaborolan-2-yl)-2-thiophene-carboxylate (36), with yields of 51 % and 56 % respectively. Finally, the furan and thiophene-substituted porphyrins were synthesised in reasonable yields. These porphyrins were characterised and studied by UV-Vis spectroscopy and emission studdies. Both techniques gave evidence of increased extended conjugation in the free-base porphyrins compared to porphyrins with phenyl substituents. Supporting density functional theory (DFT) calculations confirmed that the red shift in the spectral data of the porphyrins containing the different 5-membered rings were due to a decrease in the dihedral angles along the porphyrin plane. Future work aims to tether the porphyrins to a dimolybdenum paddlewheel complex, so that the extent of the conjugation can be fully studied.

Contents

List of Tables

List of Figures

List of Abbreviations

DSSC – dye sensitised solar cell

bpy – 2,2-bipyridine

PCE – power conversion efficiency

OLED – organic light-emitting diode

MLCT – metal-to-ligand charge transfer

dcbH$_2$ – 2,2′-bipyridyl-4,4′-dicarboxylate

DMP – 2,9-dimethyl-1,10-phenanthroline

NHC – N-heterocyclic carbenes

NAD(H) – Nicotinamide adenine dinucleotide (+ hydrogen)

TON – turnover number

CNC – 2,6-*bis*(alkylimidazol-2-ylidene)pyridine

ISC – intersystem crossing

Mo$_2$-PWPC – dimolybdenum paddlewheel porphyrin conjugate

Mo$_2$-PW – dimolybdenum paddlewheel

HOMO – highest occupied molecular orbital

LUMO – lowest occupied molecular orbital

TLC – thin layer chromatography

DCM – dichloromethane

NMR (spectroscopy) – Nuclear magnetic resonance (spectroscopy)

NIS – N-iodosuccinimide

NBS – N-bromosuccinimide

APCI-MS – atmospheric pressure chemical ionization mass spectrometry

DMF – dimethylformamide

DMSO – dimethyl sulfoxide

THF – tetrahydrofuran

MTBE – methyl tert-butyl ether

COD – cyclooctadiene

dtbpy – 4,4'-di-tert-butyl-2,2'-bipyridine

B_2pin_2 – *bis*(pinacolato)diboron

COSY (NMR spectroscopy) – Correlated spectroscopy (NMR spectroscopy)

UV-Vis (spectroscopy) – Ultraviolet visible (spectroscopy)

DFT – density functional theory

Acknowledgements

There are quite a lot of people that I would like to acknowledge and thank as I have received a large amount of support, assistance, and love from such a large group of people. Firstly, Luke Wilkinson, who as my supervisor has given me so much of his time, support and patience. Without it, I would have struggled more though this masters than I already have. Without his advice (and pestering) I would have used used too many times in this thesis. Secondly, Jason Lynam. While I did not see him as much as Luke, his door was always open, and his pop culture references always brought some interesting topics into our regular meetings. Thirdly I want to thank Chris Goult, his support in the lab and in the office has meant that a good and successful day happened more than a bad unsuccessful one.

I of course want to thank Lucy, Elias, Imo, Dan and Oscar, the powerhouses of the Wilkinson group. Without them, I don't think being in the lab would have been as much fun. Thank you to the E214 lab! Alice, Fraser, Nick, Will, Ruhee, Grant have always given me help and advice.

I also want to thank all the staff in the chemistry department that have helped me this year - Heather Fish for NMR training and advice on running samples, Karl Heaton for his patience when running my many mass spectrometry samples, Iman Khazal for all her help in the E214 and all the advice on how to clean all the suborn porphyrin tar from my glassware.

I also want to acknowledge the support I received away from the lab. My weekly DnD quests with the Order of the Octopus and time with these friends meant so much to me and I will cherish the time I have had with them. I want to thank my family for always trying to be interested in what I am doing, even when they cannot understand what I am saying. I also want to thank Marcus, my boyfriend, for standing by me while I did this masters. His encouragement, love and pestering to go to sleep are what lead me to actually finishing this masters.

Lastly I want to acknowledge a younger me for deciding to do chemistry and for sticking though with it, even when there were many people who did not believe we could do it. We have proven that we can and that we can do it well!

Declaration

I declare that this thesis is a presentation of original work and I am the sole author. This work has not previously been presented for an award at this, or any other, University. All sources are acknowledged as References.

1. Introduction

Without major action to reduce the rise in global greenhouse gas emissions, the global average temperature will continue to increase by 2.5 °C , causing devastating and irreversible effects on the environment.[1] However, significant action has been taken by companies and governments to mitigate this rise. For example in 2015, as part of the "Paris agreement", 175 parties signed a legally binding treaty to reduce greenhouse gas emissions to limit global warming to far below 2 °C, and in 2021, the UK government developed the "Net Zero Strategy" aiming to be the first country to achieve "net zero" carbon emissions by 2050.[2, 3] Other individual companies, such as NASA, are working towards their own sustainability policies.[1] The Paris agreement provides a framework for financial, technical, and capacity building support, which has sparked new low-carbon solutions, new markets and development/growth into existing markets. These new and existing markets shift energy usage and production away from non-renewable sources (such as coal, gas, and oil) towards more sustainable and lower emission sources such as solar energy. Producing electricity from solar energy can offset the reliance on coal for electrical generation because the sun produces 173 000 TW of energy a year, which means it is the largest producer of 'clean' energy, delivering more energy to the surface of the earth in one hour than the world consumes in one year. Despite this, solar energy still contributes to only 1.4 % to the total global energy production.[4, 5] Continual development in solar conversion capabilities is the step forward to progress towards the goals of the Paris agreement. Despite low contribution to total global energy productions the markets for photosensitizers have shown steady growth in recent years.[6] While photovoltaic materials are used in the harvesting and storing of solar energy in accessible ways, photocatalysts are used in the photoreduction of water and CO_2 into usable fuels.

1.1.   A Brief Window into Photovoltaics – Dye Sensitized Cells.

Photovoltaic materials exhibit the photovoltaic effect, where a generation of current and voltage occurs when the material is exposed to light. This phenomenon is related to the photoelectric effect but the main difference between the two is that with the photovoltaic effect, the excited electron stays within the material rather than being ejected. Dye sensitized solar cells (DSSC) use photovoltaic materials (which are used as the dyes in the system); these can include: metal complexes,[7] organic structures,[8] or organometallic systems.[9] A typical DSSC consists of semiconductor electrode, redox electrolyte, dye, and counter electrode, which are structured as a sandwich cell, which is shown in Figure 1.
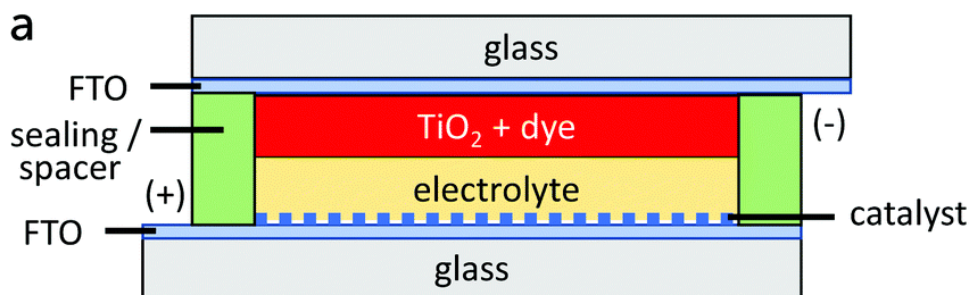
Figure 1: device structure of a sandwich cell for DSSC. FTO = fluorine-doped tin oxide. Image taken with permission from reference 7.[10]

Conventionally DSSC's use n-type, wide band-gap semiconductors to transport negative charges, and most examples mentioned in this discussion are related to this type but there are also p-type DSSC where the semiconductor is used to carry positive charges.[11] The mechanism of an n-type DSSC starts when the dye absorbs photons from light, to excite its electrons to a higher energy state. These high-energy electrons are ejected into the semiconductor, oxidizing the dye and initiating the current. The oxidized dye accepts an electron from the redox electrolyte/mediator, thereby regenerating the dye back to its ground state. In order to balance the charge and complete the circuit, the redox electrolyte/mediator is reduced by the counter electrode.[11]

A typical semiconductor electrode is a mesoporous TiO_2 surface. While SnO_2 and ZnO have also been used and studied, TiO_2 remains the most common electrode used in DSSC.[11, 12] A mesoporous surface is used because of its high surface area and increased external quantum efficiency, *i.e.* the ratio of charge carriers in the cell to the number of photons incident on the cell has increased. An increased surface area results in a greater proportion of dye being adsorbed to the surface, which would lead to an improvement of light harvesting capabilities. The electrolyte can also strongly influence the performance and stability of the cell. The I^-/I_3^- electrolyte has become an established and well used electrolyte, largely because it has good stability and an appropriate redox potential to regenerate the photo-oxidised state of many common dyes.[13, 14]

Despite the vital contributions from the aforementioned components, the dye itself is the major player of the DSSC and its ability to perform its core function affects the efficiency of the cell more than anything else. When designing a dye, certain points should be considered including (i) the photochemical stability, (*i.e.,* the likelihood the oxidised dye will undergo undesirable reactivity leading to bleaching); (ii) the panchromaticity, *i.e.,* the dye's ability to absorb solar energy across the electromagnetic spectrum; and (iii) factors that can promote a long-lived charge-separated state such as donor-acceptor structure. [10, 11, 15]

11

1.1.1. Transition Metal Complexes and Dyes

Transition metal complexes are popular choices for dyes, and this stems from the facile redox-chemistry of transition metals, and the advantageous energetic alignment between the metal d-orbitals and the π* orbitals of accompanying ligands. In particular, ruthenium(II) complexes with pyridyl-based ligands set the benchmark for competing dyes.[16] A typical $[Ru(bpy)_3]^{+2}$ based complex, as drawn in Figure 2, regularly reports power conversion efficiency's (PCE, *i.e.* the maximum power output of the device in relation to the power input and wavelengths used) > 11 % which was exceptional during the early development of DSSCs.[10]

(1)
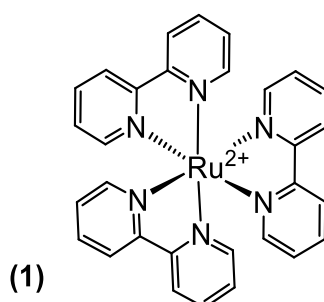
Figure 2: molecular structure of a $[Ru(bpy)_3]^{+2}$ (1)

Ruthenium(II) based dyes have been successful because they exhibit strong, broad absorption profiles that cover most of the visible region of the electromagnetic spectrum and possess long-lived photoexcited states.[17, 18] Figure 3, shows the structure and absorption spectra of a commercially available Ru-based dye, with absorbance ranging from 275-700 nm.[19]
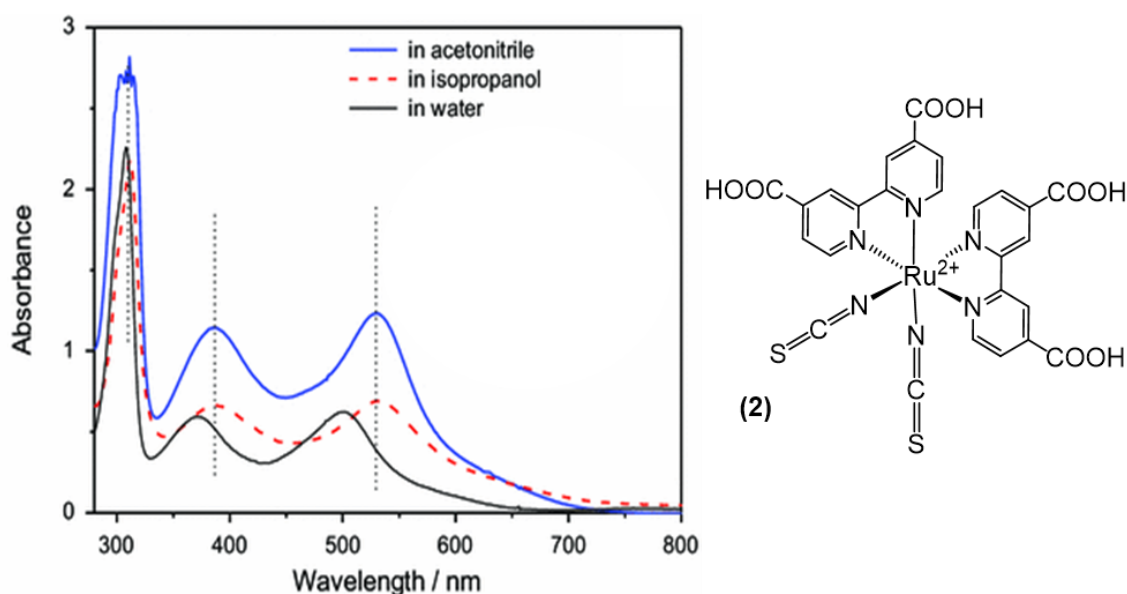
Figure 3: UV–Vis absorption spectra of (2) in water, acetonitrile, and isopropanol. Image taken with permission.[19]

Iridium(III) complexes are also familiar dyes for DSSC's. They are commonly used as emitters for OLED devices because they possess strong luminescence with long-lived photo excited states, are tuneable through modular synthesis, and exhibit high thermal and chemical stability.[20-22] Most of these properties match the criteria that are considered when designing an appropriate dye. However, despite these positives, they do not always perform as efficient dyes when compared to the performances seen in ruthenium(II) dyes, as they can possess lower molar extinction coefficients in regard to the MLCT bands. One approach to improving efficiencies of dyes is to improve the molar extinction coefficients of the metal-ligand charge transfer bands; the introduction of n-hexylthiophene based units to the 4 position of a modified terpyridine derivative ligand of a ruthenium(II) dye (3), produced novel sensitizers with strong absorptions at 350 nm, however the molar extinction coefficients were not always improved.[23] It was observed that changing the n-hexyl chains to a 2,6-diisopropylphenyl unit ((4), Figure 4) did slightly improve the molar coefficient values.[24] Coumarins and bodipy organic dyes are used in conjunction with metal complexes to improve efficiency and expand the wavelength range at which complexes absorb at.[25] For example, a coumarin ligand was shown to increase the molar coefficient of the MLCT in an iridium cyclometalated complex. For comparison, a ruthenium(II) dye - $[Bu_4N]_2[Ru(dcbH_2)(NCS)_2]$– exhibits a molar coefficient of 20000 $M^{-1}cm^{-1}$, whereas the iridium(III) coumarin comparison, $[Ir(C6)_2(dcbH_2)][PF_6]$ (dcbH$_2$ =2,2′-bipyridyl-4,4′-dicarboxylate) was double that.[25] The structure of which is shown in Figure 4, (5).
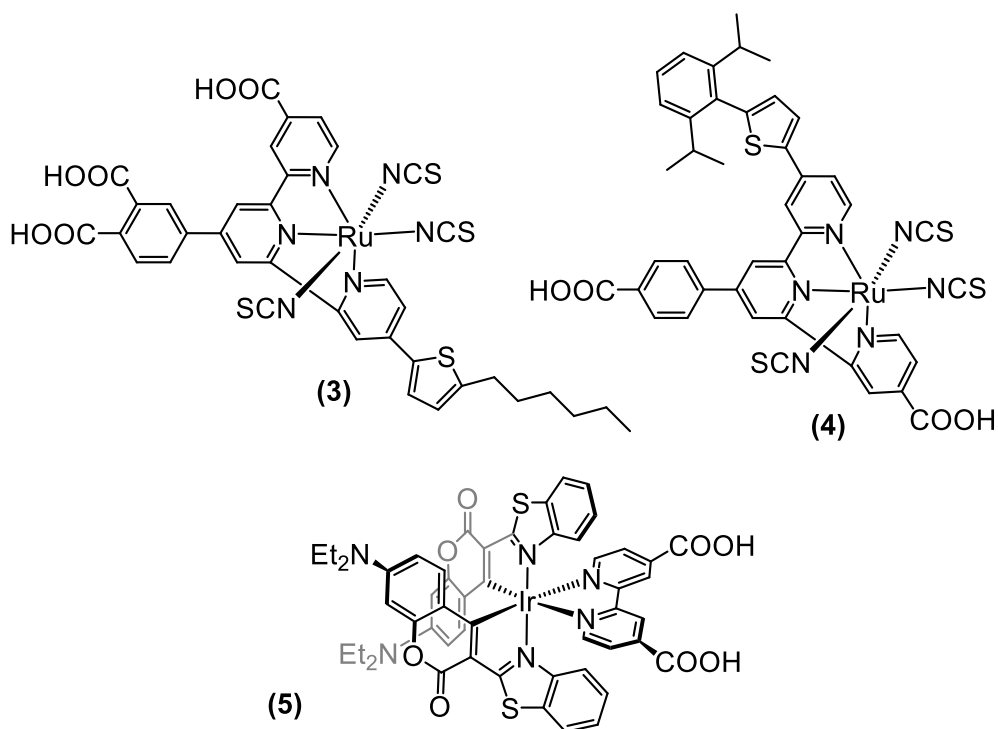
Figure 4: molecular structure of two ruthenium(II) complexes (3), (4) and [Ir(C6)$_2$(dcbH$_2$)]$^+$ (5); complex that use organic ligands specifically to improve the absorption of the complex.

1.1.2. Moving Away from Precious-metal Dyes

Despite their popularity and high PCE values, the metal complexes described in section 1.1.1 are not suitable for large industrial manufacture due to their cost and the scarcity of these metals. Hence why other approaches are taken, from using cheaper more abundant metals to having purely organic dyes.

Copper and iron are cheap and abundant metals that have been coined as possible alternatives to ruthenium and iridium. However, their PCE values significantly lag behind their competitors, while also hosting another range of problems to overcome. Copper complexes are unstable and incompatible with most mediator systems used in DSSC but a series of $[Cu(DMP)_2]^+$-based dyes (where DMP is 2,9-dimethyl-1,10-phenanthroline) (Figure 5, compound (6)) were shown to be stable under operating cell conditions.[26] Zhang *et al.* theoretically introduced N,N-diethyl-4-vinylaniline ancillary ligands to copper (I) complexes and their calculations and modelling showed that it would generate the highest light-harvesting efficiency while also producing efficient charge separated states. Despite attempts at improving the efficiencies of copper-based dyes the PCE is normally >5 %.[13, 27]

In the design of new dyes, Iron is attractive because it is exceptionally cheap and earth abundant. Fe(II) has a d^6 configuration similar to Ru(II), but this does not mean it has the same photophysical behaviours. $[Ru(bpy)_3]^{+2}$ complexes have long-lived photoexcited states (which can range from 100-1000 ns)[28] which result from a metal-to-ligand charge-transfer generating a metastable ^{3}MLCT state. However, the analogous ^{3}MLCT excited states of the Fe(II) counterparts are deactivated, possess energetically lower lying metal-centred excited states and have lifetimes which are drastically lower.[28] A potentially superior alternative to $Fe(bpy)_3^{2+}$-type complexes are those bearing N-Heterocyclic carbenes (NHCs) as ligands because these have shown to exhibit long-lived excited states which could potentially be harnessed.[13] ^{3}MLCT lifetimes of 9 ps could be reached for an iron(II) NHC complex (7).[29] However, upon replacing the NHC ligands with benzimidazolylidene-based ligands (compound (8) as shown in Figure 5) the lifetime was further increased to 16.4 ps.[30] The authors concluded that strong σ-donating ligands coordinating to Fe, combined with an increased delocalization of the electron in the ^{3}MLCT state leads to an increase in stability and therefore lifetime. Nonetheless, the PCE of these structures have only reached 1 % and more work is needed to establish these complexes as efficient and effective dyes for DSSC's.[13]
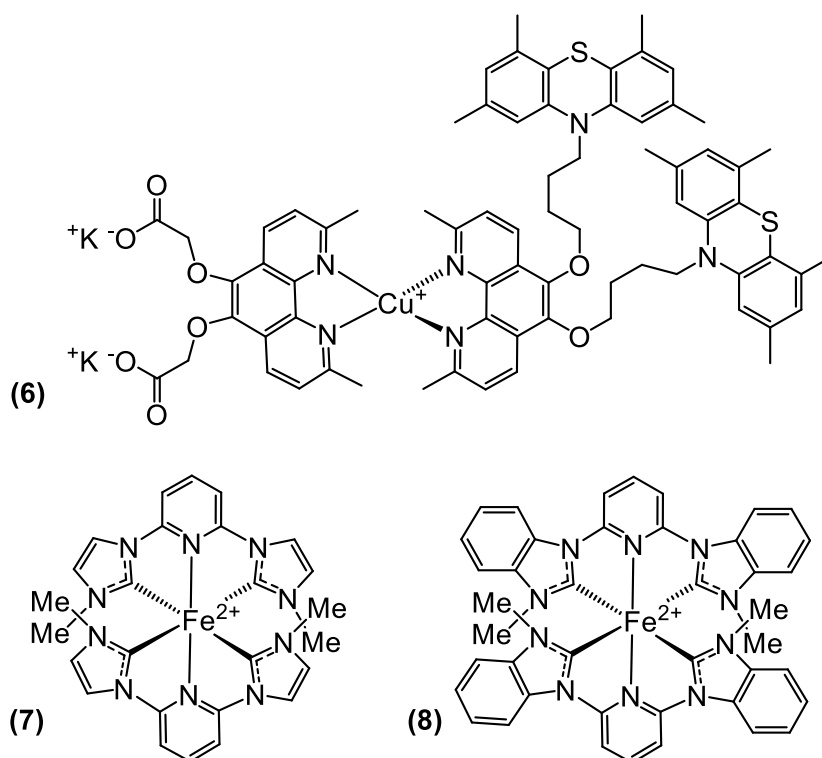
Figure 5: molecular structure of [Cu(DMP)₂]⁺ (6) and two iron(II) NHC complexes (7 and 8).

1.1.3. Purely Organic Dyes for DSSCs

Organic dyes with extended π-conjugated systems have also shown enormous potential as alternatives for DSSCs, as they have demonstrated greater PCE's than those observed with transition-metal complex dyes.[10] A few organic dyes have managed to exceed that of ruthenium(II)-based dyes, for example, a series of novel 4-hexyl-4H-thieno[3,2-b]indole based organic chromophores reached PCE values of up to 13.9 %.[31] Figure 6, compound (9) shows the most effective dye from this study. High performing organic-based dyes are based on amine donors because they have tuneable donation strength, have the potential for reversible oxidations and have multiple sites for functionlisation.[10, 15] Indoline-based donors are popular materials which have shown great success as dyes (Figure 6, compound (10)) with PCE values of above 9 %.[32] By increasing the bulk of the indoline donor with quinoxaline acceptors, dyes such as (Figure 6) have slightly improved PCE values up to 10.7 %.[33] Strong absorption into the near infrared-region is a property many organic dyes lack. Squaraine (*e.g.* compound (12), Figure 6) dyes are popularized as they can strongly absorb around 600-900 nm, while also possessing molar extinction coefficients up to and above 100,000 M^{-1} cm^{-1}.[10] Despite this favourable photophysical property, the PCE of squaraine dyes are found to be significantly lower compared to organic dyes discussed previously, but by extending the alkyl groups on the indoline groups to longer chains, as in compound (12), the PCE increased from 3.4 % to

7.7 %.[10] However, the long, complicated synthetic procedures of organic dyes pose a problem for industrial scale up.
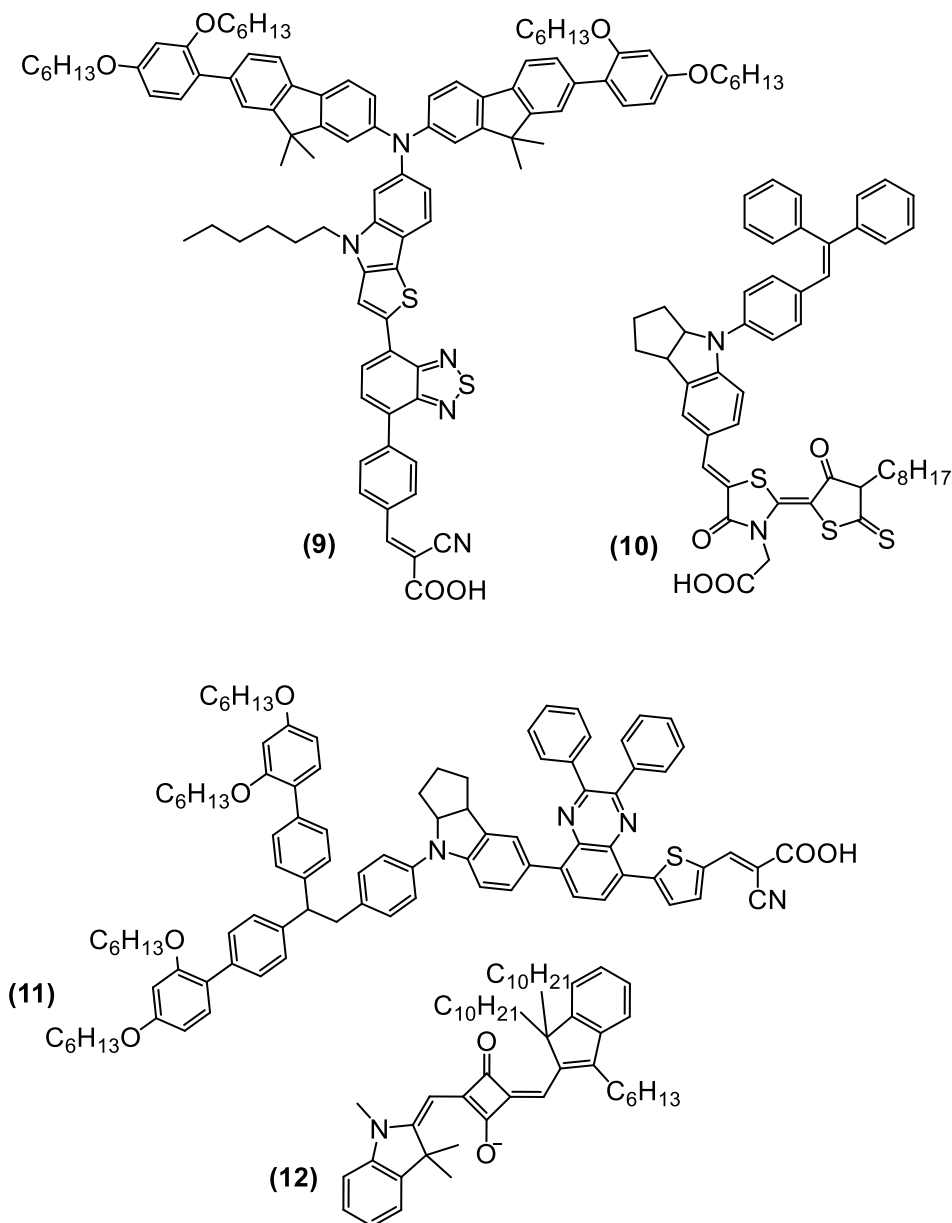
Figure 6: molecular structure of 4-hexyl-4H-thieno[3,2-b]indole based organic chromophore (9) and other organic structures used as dyes.

1.2.   A Window into Photocatalysts

A photocatalyst is another material that absorbs light to bring the material to a higher energy state but in contrast to a photovoltaic material, no current or voltage is generated, rather, the energy gained is transferred into a chemical reaction.[34] Perhaps the most famous

photocatalysts are those involved in photosynthesis, photosystem I and II. While Photosystem I uses light to catalyse the reduction of NADP (Nicotinamide adenine dinucleotide phosphate) to NADPH, Photosystem II catalyses the oxidation of water to oxygen. Water splitting, photoreduction of CO_2 and decomposition of small molecules are common processes that can be achieved by using a photocatalyst. Metal complexes,[18, 35, 36] organic dyes,[37] and metal-organic materials,[38-40] encompass many of the different types of materials that have been employed as photocatalysts. This review focusses exclusively on homogeneous catalysts.[41]

The majority of photocatalysts consist of a two-component system: a photosensitizer and catalytic centre. The photosensitizer absorbs photons from an incident light source to reach an excited state. An electron donor quenches the excited state of the photosensitizer, and during a reductive quenching process, the photosensitizer transfers the excited electron to the catalyst. The catalyst, which now contains the excited electron, has become a powerful reducing agent that is able to promote CO_2 reduction or H_2 prouduction.[41, 42] The electron transfer to the catalyst can happen intermolecularly, between a photosensitizer and catalyst that are two separate components, as shown in Figure 7 (A), but this transfer can also happen intramolecularly when the photosensitizer and catalyst are bridged, as shown in Figure 7 (B).[18, 41]
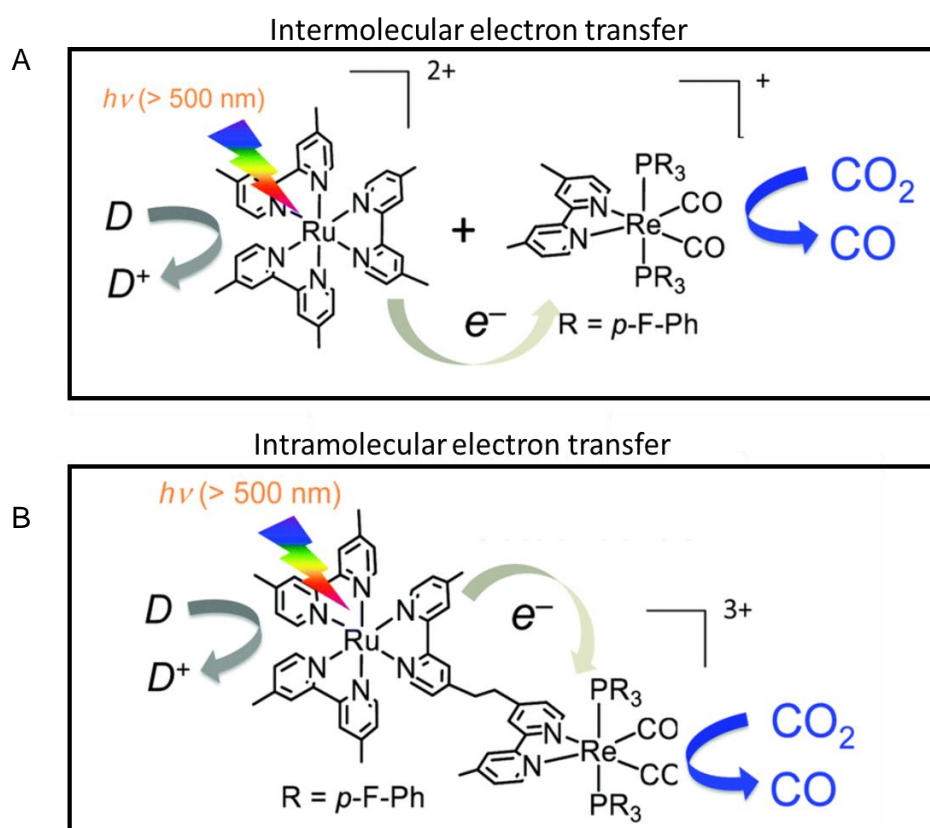
Figure 7: metal-complex-based homogeneous photocatalysts for CO2 reduction. A) Mixed system and B) supramolecular system.) Adapted with permission.[43]

Complementary to the design factors of DSSCs, the catalysts should be designed such that photoinduced electron transfer is favourable and that the charge-separated state has sufficient lifetime to perform chemistry. Ideally the catalytic system should also be photochemically stable, soluble in common organic solvents and water, and exhibit a sufficient excited-state lifetime for charge transfer.[34]

Also similar to DSSC's, ruthenium and iridium are popular and common metal complexes for solar catalysts due to their aforementioned ideal photophysical properties. An important metric in the way that catalysts are compared is by the use of turnover numbers (TON). TON is a measure of the number of catalytic cycles that can be performed before the catalyst starts to deteriorate.[40] The first reported case of a ruthenium(II) complex for the photocatalytic conversion of CO_2 to formate was by Lehn *et al.* The group used a $Ru(bpy)_3Cl_2$ (similar structure to compound (1) in Figure 2) photocatalyst which resulted in a TON of 4.[44] Since this first development great strides have been taken in improving the turnover number of ruthenium(II) catalysts. In recent years, pincer ligands, 2,6-*bis*(alkylimidazol-2-ylidene)pyridine (CNC) coordinated to Ru(II) (compound (13), Figure 8) have been used for photocatalytic reduction of CO_2. For example, the use of the CNC pincer ligands greatly improves the TON, to *ca.* 5600 in the formation of formate by photocatalytic CO_2 reduction.[45] In general the authors concluded that increasing the conjugation in ligand π-system would shift light absorption to lower energies, and increasing steric bulk on the ligands would limit catalyst-catalyst interactions. These design principles were adopted to produce compound (14) (Figure 8) which demonstrated an even greater TON of 33000.[46]
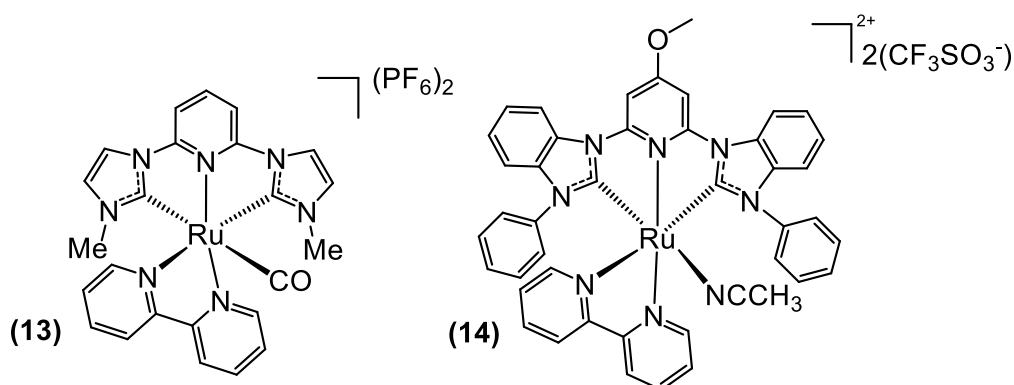
Figure 8: structures of [Ru(bpy)(CNC)]$^{2+}$ (13) and [(CNC)Ru(bpy)(CH$_3$CN)]$^{2+}$ (14), both incorporating CNC pincer-based ligands to improve the photocatalytic activity of the photocatalyst system.

Since its discovery, $[Ru(bpy)_3]^{2+}$ has become one of the most studied metal complexes for applications as a photocatalyst /chromophore. However, iridium(III) complexes are potentially superior to $[Ru(bpy)_3]^{2+}$ as sensitisers because they can possess larger molar extinction coefficients with ligand tuning, meaning that they can effectively absorb more light.

Additionally, some cyclometalated Ir(II) complex chromophores show improved luminescence properties, such as: long excited-state lifetimes in the µs time range, and tuneable emission wavelengths, compared to [Ru(bpy)$_3$]$^{2+}$.[18] The most efficient complex discussed in this is a cationic Ir(III) complex, as show in Figure 9, with ancillary 4,4'-*bis*(4-(triphenylsilyl)phenyl)-2,2'-bipyridine ligands which gave a TON of 17,000 in the photoreduction of water.[47]

(15)
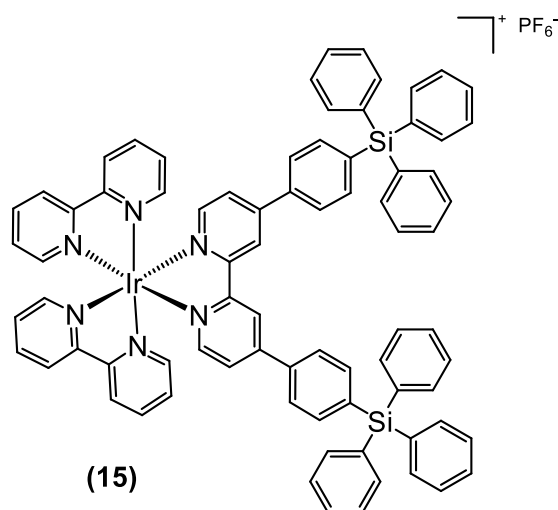
Figure 9: structure of a cationic Ir(III) chromophore with bulky triphenylsilyl groups (15).

Ru(II) and Ir(III) are frequently used as the photosensitizer/chromophore for photocatalytic processes (as stated above) because their ^{3}MLCT states are sufficiently long-lived for further chemistry to occur before relaxation down to the ground state. However, they are still expensive and scare materials. For these reasons, organic dyes such as boron dipyrromethene dyes (bodipy)[48] and coumarins can be used as chromophores for photocatalytic hydrogen evolution. A promising example of this approach, is compound (16) (Figure 10), which employed bodipys attached to [Ir(ppy)$_2$(bpy)]$^+$ complexes, the maximum TON output is improved to an impressive 115,000.[35] This was attributed to the efficient conversion of excited energy from the coumarin to the bodipy localized triple state.

(16)
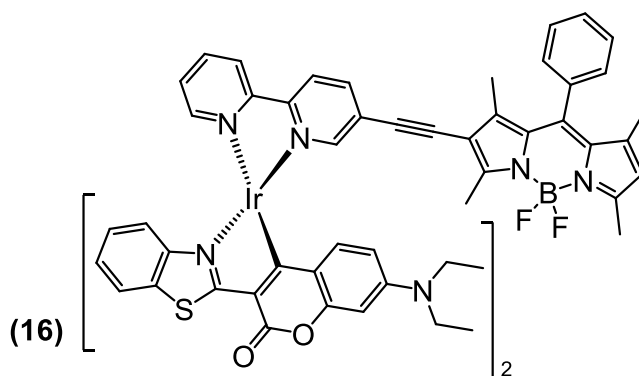
Figure 10: structure of a [Ir(ppy)$_2$(bpy)]$^+$ with a bodipy chromophore (16).

1.3.   Porphyrins – The Way Forward

The cost and scarcity of Ru(II) and Ir(III) make it difficult to scale to industrial manufacture for both dyes and photocatalysts, and while there has been research into cheaper alternatives, the alternatives lack in many ways, for example, copper-based dyes for DSSCs are still only able to access efficiencies of up to 5 %.

For these reasons, the design and development of new molecules used in solar energy conversion often take inspiration from nature and natural processes which are earth abundant. Plants are well known to use porphyrin-based pigments for natural photosynthesis and light harvesting processes.[49] Listed are some of the key factors that make porphyrins a sought after alternative; they have intense absorptions and molar extinction coefficients over a broad area of the visible spectrum,[15] they can be easily modified and functionalized to tune the properties of the porphyrin,[50-57] they are thermally stable compounds which are tolerant to atmospheric conditions, and they have been shown to exhibit relatively efficient photo- and thermally-induced electron transfer over large distances (40 Å).[39, 58]

1.3.1. What are Porphyrins?

Porphyrins are conjugated tetrapyrrole macrocycles that form a planar aromatic system with 22 π electrons.[59] The rigid planar molecule, (Figure 11) has twelve reaction sites (four *meso* and eight β positions) on the 'outer' part of the molecule and four sites in the porphyrin core that are accessible for C-X, C-C or N-M functionalization to tune the photo-electro properties of the porphyrins.[54, 60, 61] For example, it was shown that halogenation could be undertaken at different sites of an octaalklporpyrin, as drawn in Figure 11, resulting in a change in the fluoresce quantum yield and lifetime. The site of halogenation and the type of halogen had a great effect on the magnitude of the change and in this case, the change in fluorescence properties is a consequence of fluorescence quenching due to the heavy atom (i.e. Br, I) effect.[62] The effect that ferrocene substituents and different metal cores have on the redox properties of tetra substituted porphyrins have also been investigated.[63] Porphyrins tend to have one oxidation process while it was shown that the 5,10,15,20-tetraferrocenylporphyrins each have four oxidation processes (due to the four ferrocene substituents). The second, third and fourth oxidation processes are closely spaced to one another, and that the degree of separation varies on the type of metal centre present in the porphyrin core.
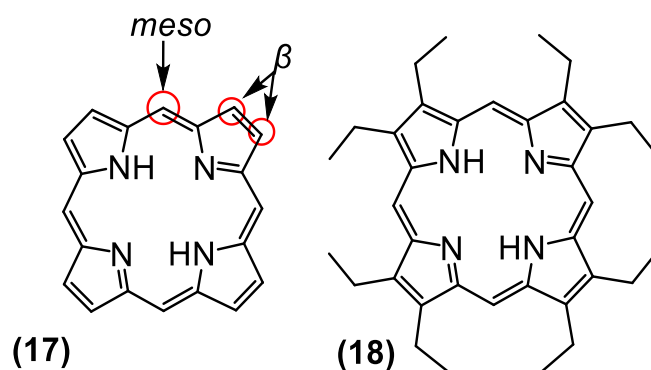
Figure 11: (17) structure of Porphine, with display of where the meso and β positions are located. (18) diagram of a free-base octaalkylporpyrin.

Porphyrins are brightly coloured and exhibit a well-recognized absorption spectra, a common example of a spectrum for a tetraphenylporphyrin is shown in Figure 12. A free-base porphyrin (a porphyrin without a metal ion in the centre) possesses D_{2h} symmetry, which results in five absorption bands present in the spectra: a single Soret band and four Q-bands; inserting a metal into the porphyrin core results in the symmetry increasing to D_{4h}. The Soret band is unchanged but the Q-bands have reduced from 4, to 2 bands.[53]

The Gouterman four orbital model (as shown in Figure 13a.) is commonly used to rationalise the absorption spectra of porphyrins. The absorption bands arise from electron transitions between two HOMO's (nearly degenerate a_{1u} and a_{2u} orbitals) and two LUMO's (degenerate e_g orbitals), as shown in Figure 13b. Orbital mixing due to configurational interactions splits the excited state into two ^1E_u states (Figure 13c), one at a higher energy with greater oscillator strength (the S_2 state), and a second at a lower energy with a lower oscillator strength (S_1). The former gives rise to the Soret band, whereas the latter is observed as the Q-bands.
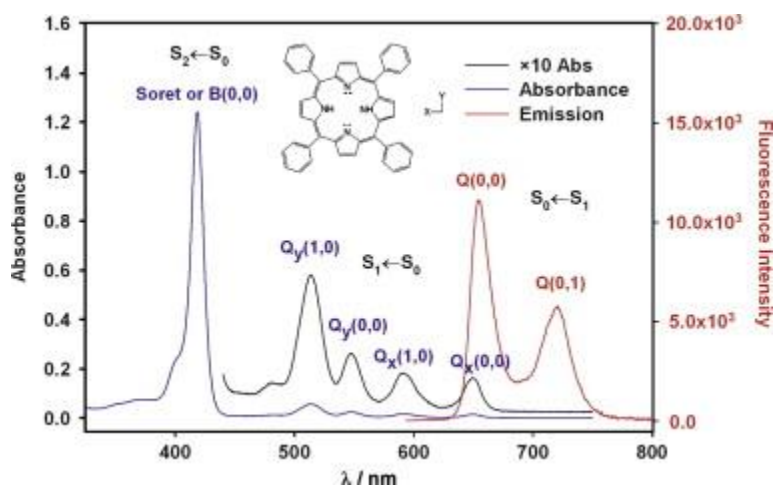
Figure 12: absorbance and fluorescence (λex = 418 nm) spectra of tetraphenylporphyrin in toluene. The tetraphenylporphyrin concentrations were 5 µM and 0.5 µM for absorbance and fluorescence, respectively. Image taken with permission from reference.[64]

21
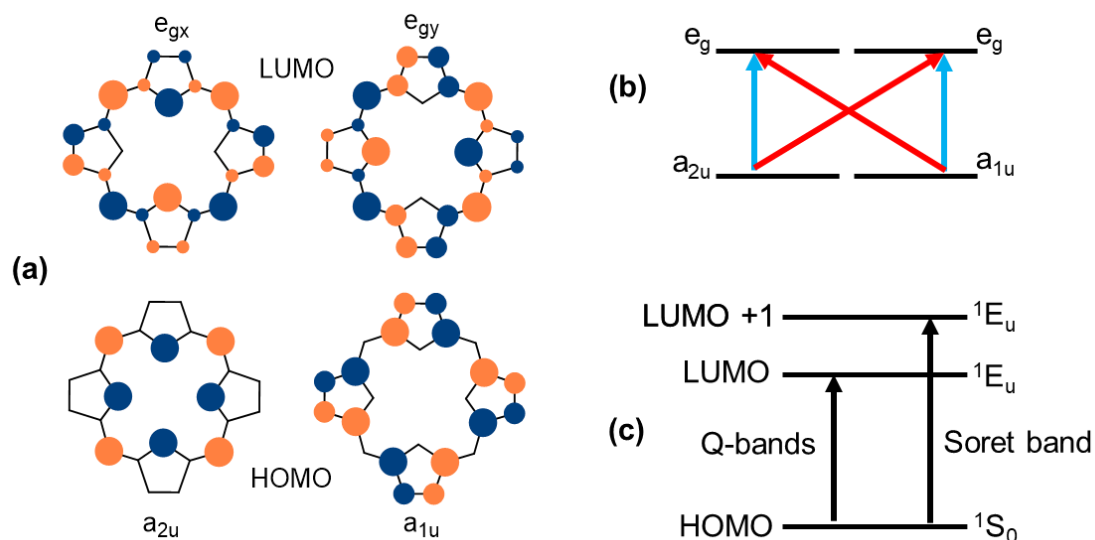
Figure 13: (a) porphyrin HOMO and LUMO based on the Gouterman 4-orbital model. (b) orbital diagram showing possible transitions of a free-base porphyrin system. (c) orbital diagram showing orbital splitting of excited state into two ^1E_u states.

Porphyrins are known to fluoresce and emit at 600-700 nm when excited around the Soret band (~400 nm).[53, 65] Referring to Figure 12, the emission spectra of tetraphenylporphyrin is overlayed with the relevant absorption spectrum. Fluorescence arises when an electron relaxes back down to the ground state after excitation from the ground state S_0 to any higher singlet excited state S_x. In some cases, intersystem crossing (ISC) occurs to form an excited triplet state (T_1) of similar energy to an S_x. The electron flips its spin during ISC going from S_x → T_1. Relaxation of the populated triplet (T_1) state down to the ground state (S_0) can occur alongside emission of a photon in a process called phosphorescence. However, in order to relax to the singlet ground state, the spin of the electron must flip back.[65, 66] Spin-flipping is a formally forbidden process, so phosphorescence generally takes much longer than fluorescence. Phosphorescence tends to only occur in porphyrins that bear heavy metal atoms because the greater spin-orbit coupling facilitates the intersystem crossing.[67] This phenomenon is illustrated in Figure 14.
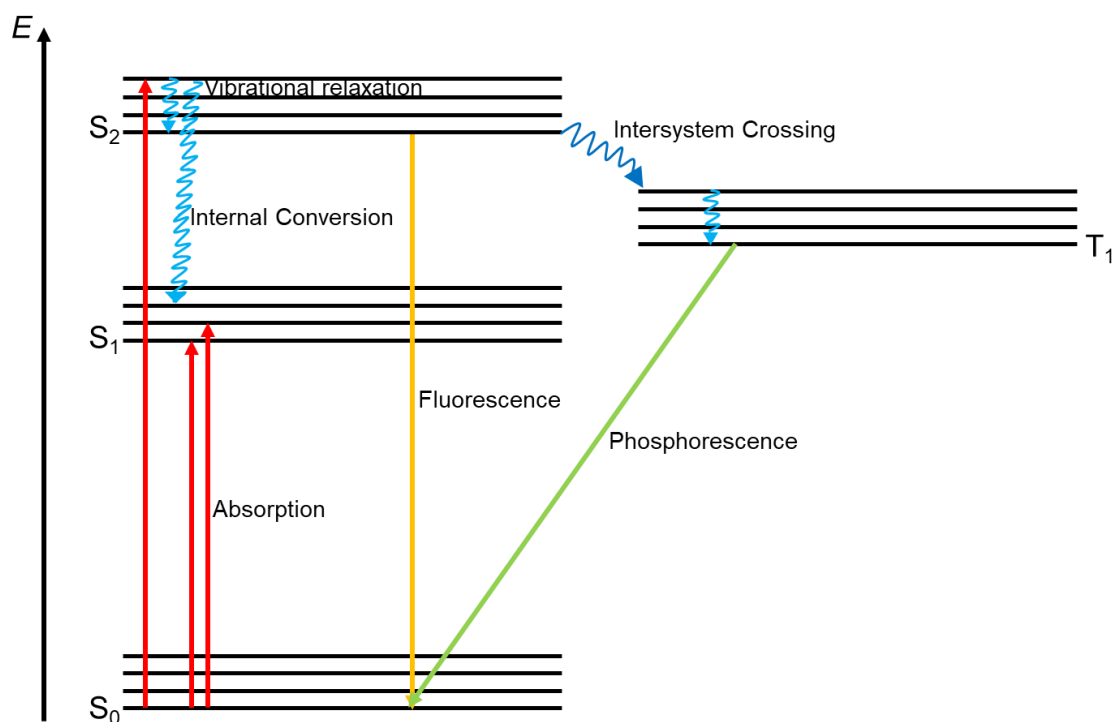
Figure 14: generic Jablonski diagram illustrating absorption and emission transitions.

1.3.2. Synthesis and functionalization of porphyrins

Many *meso*-substituted porphyrins are typically synthesized by a one-pot, mixed condensation reaction.[68] Adler and Longo developed a mixed condensation reaction in 1967, where different aldehydes and pyrroles were refluxed together in propionic acid at high temperatures,[69] Figure 15. Despite the fact that this is an effective and simple reaction, it is plagued by low yields (> 10 %) and difficulties in purification, due to formation of a statistical mixture of porphyrins caused by a lack of control over the reaction and formations of polypyrrole tar. However, it is still useful in synthesising a large range of functionalised porphyrins.[70]
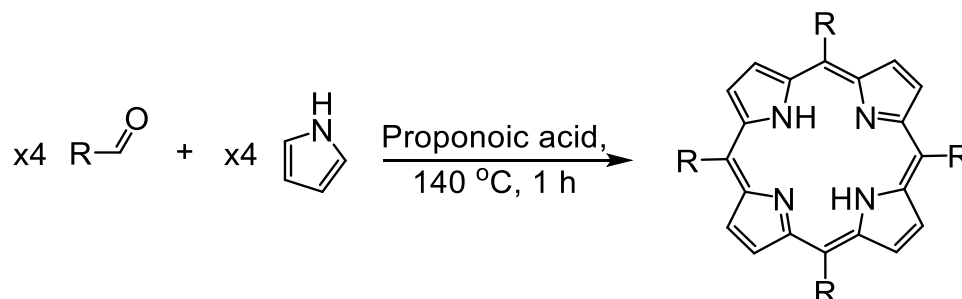
Figure 15: general reaction scheme of the Adler-Longo mixed condensation reaction for the synthesis of a porphyrin.

Building from this, in 1994, Lindsey's group developed a gentler 2-step, one-pot mixed condensation reaction: while it requires dilute conditions, an acid catalyst and oxidant (Figure 16), the overall procedure allows for a greater scope of functionalized porphyrin synthesis. This method enables aldehydes that are pre-functionalised with 'sensitive' groups to be directly converted to a porphyrin; it also allowed for greater yields of total product up to 40 %.[71, 72] However, this procedure still leads to a statistical mixture of porphyrins and polypyrrole tar that requires extensive purification and separation.
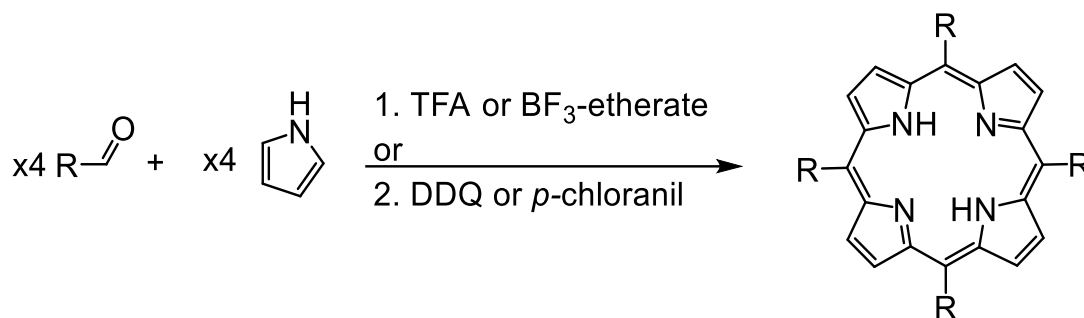
Figure 16: general reaction scheme for the Lindsey modified mixed condensation reaction.

Taking it even further, Lindsey's group then developed an alternate route which is well suited to directly access 5,15-disubsituted porphyrins (or *trans*-porphyrins).[59] As shown in Figure 17, it involves a 2+2 condensation between a dipyrromethane and aldehyde, it also requires high dilutions, an acid catalyst and oxidant.[73] High dilutions reduce oligomerisations but make it problematic to prepare in bulk due to the large amounts of solvents used. This procedure allows for the specific design of *trans*-porphyrins in higher quantities without all the purification difficulties that are seen in the previously mentioned statistical mixtures.[74]
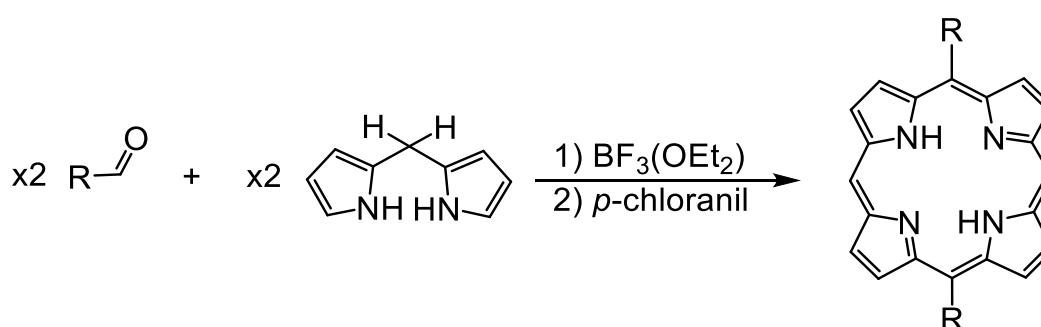
Figure 17: general reaction scheme of the Lindsey [2+2] mixed condensation reaction.

Targeted porphyrins can be synthesized via these methods with the relevant functional groups as reagents, however in a majority of current synthetic procedures for porphyrins, the relevant functional groups are attached in a later reactions.[50, 51, 59, 75] Organolithiation and cross-coupling reactions are popular methods to do this and are used to attach a range of functional groups – from alkenes and alkynes to imines and azo-based groups – this approach is more

commonly taken as it allows for more control and functionalisation towards complex target molecules. Transition metal catalysed reactions are one of the most widely investigated and used methods for functionalisation of porphyrins, especially palladium catalysed reactions. The common two cross-coupling reaction approaches for porphyrin functionalisation are Sonogashira and the Suzuki-Miyaura cross-coupling reactions.[51, 76] The Sonogashira reaction is a cross-coupling reaction between an aryl halide and terminal alkyne using a palladium catalyst and copper co-catalyst, (Figure 18a). It is a very important method for the formation of new $C(sp^2)$-$C(sp)$ bonds;[77-79] while the Suzuki-Miyaura reaction is a cross-coupling reaction between an organoboronic acid/ester and aryl halide using a palladium catalyst and base (Figure 18b). In porphyrin synthesis, both approaches form new C-C bonds from the conversion of a halogenoporphyrins.
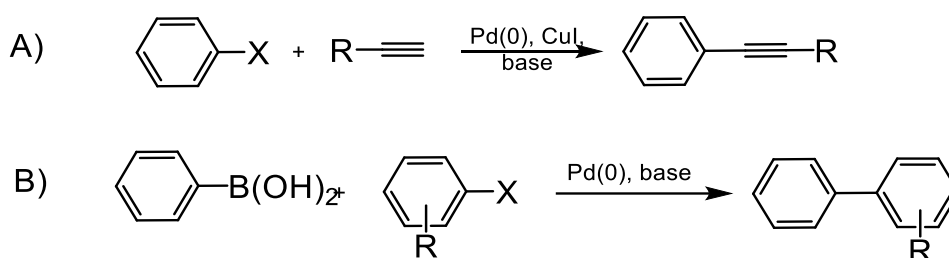
Figure 18: A) general reaction scheme for a Sonogashira cross-coupling between an aryl halide and terminal alkyne. B) general reaction scheme for a Suzuki-Miyaura cross-coupling reaction between a aryl halide and boronic acid. X = Br, I. R = PhOOCH3, H, Ph etc.

1.3.3. The Application of Porphyrins as Dyes

Porphyrins are readily used as dyes in DSSC due to their photophysical properties, they have also been stated to be one of the first class of dye to produce DSSC systems that have comparable PCE values to that of ruthenium(II) complexes.[10, 11] "Push-pull" porphyrin-based devices contain a donor-porphyrin-acceptor construction and are some of the most successful and commonly used design strategies for developing porphyrin based dyes; a basic example, compound (19) employs a diarylamine donor and benzoic acid acceptor and demonstrates an impressive 11 % PCE. An increase to 12.8 % results by addition of a 2,1,3-benzothiadiazole electron acceptor between the benzoic acid and the porphyrin (20).[10, 80] A problem that commonly befalls porphyrin dyes is the behaviour of dye aggregation which can reduced the electron injection efficiency of the DSSC, which further links into a reduction of the cell's overall efficiency. Suppression of this feat can easily be achieved by introducing either long alkoxy chains or bulky groups to the porphyrin.[10, 15]
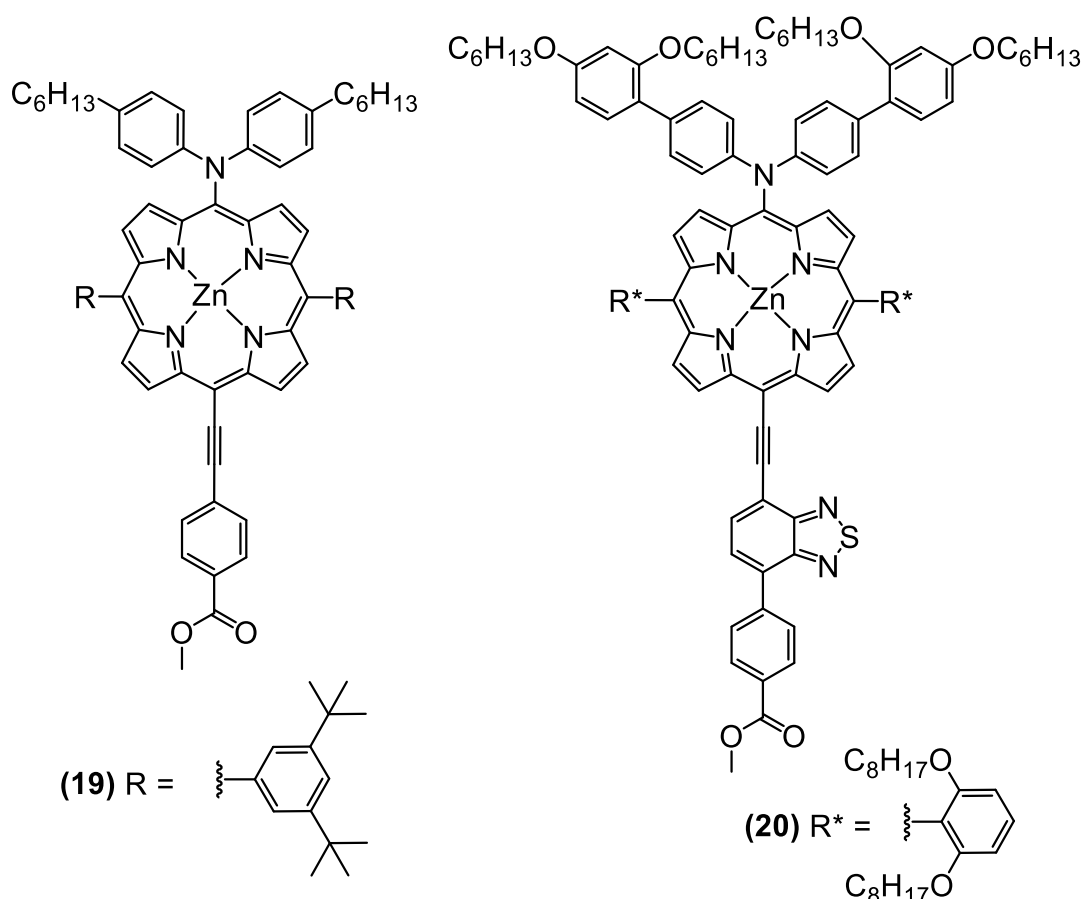
Figure 19: select structures of porphyrin dyes.

Suppressing dye aggregation is one of the many factors that is taken into consideration when designing push-pull porphyrin dyes; the type of anchoring group used to bind the porphyrin to the TiO_2 surface is another. Normally a carboxylic acid is used as the anchoring group but there are examples that have shown that by using a salicylic acid to form a tridentate anchoring group can improve the efficiency of electron ejection into the semiconductor surface.[81] Following this, the connection between the anchoring group and porphyrin also plays a significant role. According to one group, significantly increasing the distance between the anchoring group and porphyrin can negatively affect the efficiency of the cell, despite 'full' conjugation through the system, a chain containing four phenylethylene saw a decrease in efficiency by 10 % compared to a single phenylethylene group.[82] 5-membered heterocyclic spacers have also been used tailor the electronic coupling to the TiO_2 surface.[70]

1.3.4. Application of Porphyrins as chromophores for photocatalysis

While porphyrins have been established as effective dyes and therefore can be used to eliminate the need for expensive and scare materials currently used in DSSC, this is not the case for photocatalysts. In contrast to organic chromophores, porphyrins are more simplistic

to synthesise and have a broader range of tuneability. Instead of fully replacing metal complexes as fully fledged photocatalysts, porphyrins tend to be used in combination with metal complexes as a bioinspired approach to mimic natural processes like photosynthesis by using light absorption and charge-transfer processes to catalytically oxidise/reduce H_2O and CO_2.[42] As discussed, ruthenium(II) complexes are well used photocatalysts with impressive catalytic activities with ligand tuning. but weak absorption limits its capabilities.[16, 83] An approach by one group showed that coupling a ruthenium(II) complex to a asymmetric zinc porphyrin formed a system with decent improvement of absorption coefficients to that of just the metal complex – a increase by a factor of 100 (compound (21), Figure 20).[84]

Rhenium-porphyrin dyads have shown that a saturated bridge between the rhenium complex and porphyrin can greatly increase the TON in photocatalytic reduction of CO_2, when compared to a similar version that contains a methoxybenzamide spacer, the authors attributed it to flexibility of the Re(bpy) unit adopting the best orientation at the closest approach to the porphyrin. But the turnover number of (22) is stagnant at 330 despite increased stability.[38] The close proximity of a [Re(phen)(CO)$_3$Br] complex to a porphyrin unit (23) was shown to assist in suppressing electron accumulation on the porphyrin (as the complex act as an electron reservoir); coupled to the fact that the energy harvested was stored as a long-lived triplet state on the porphyrin, produced a suitable large TON of 1300.

(21)

(22)

(23)
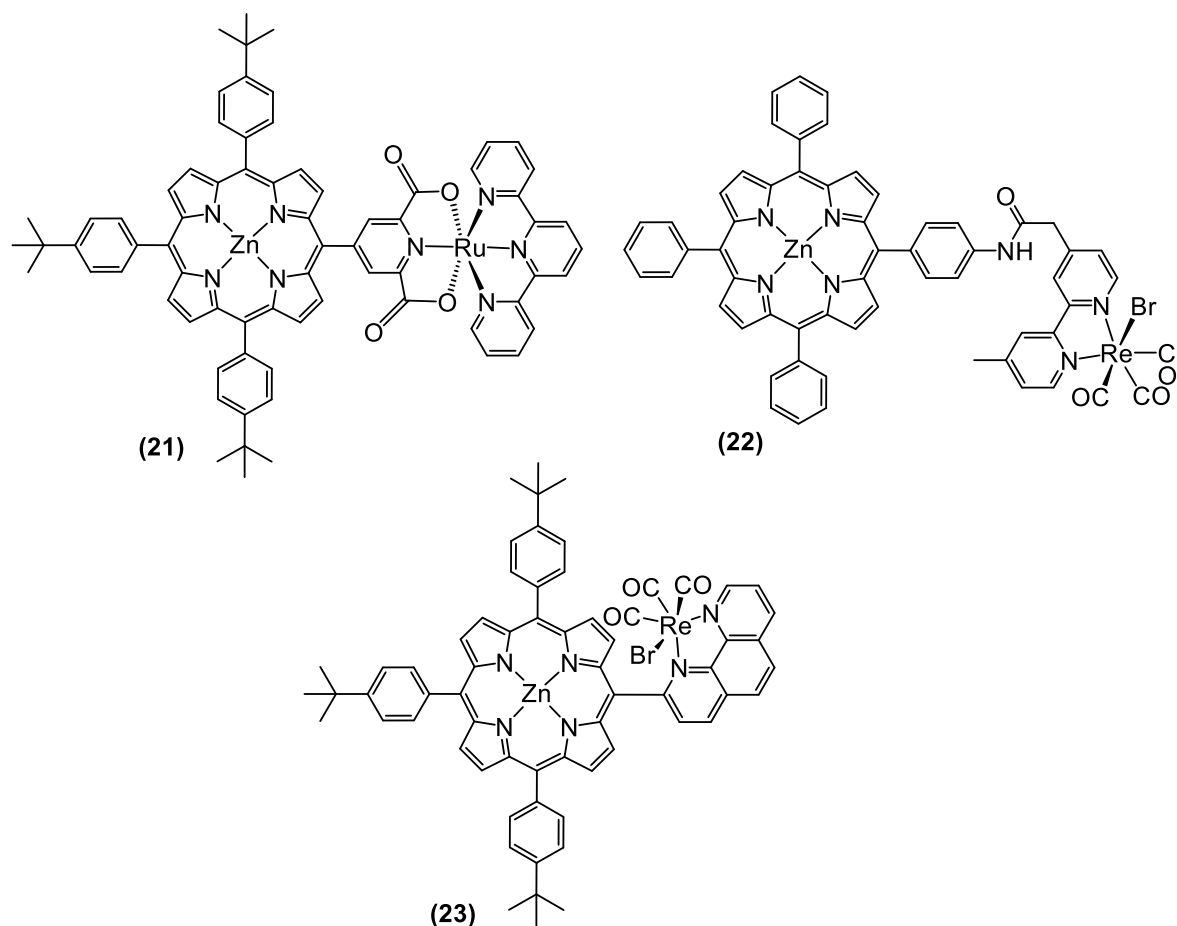
Figure 20: structure a ruthenium-porphyrin dyad (21), rhenium-porphyrin dyad with a methoxybenzamide bridge (22) and [Re(phen)(CO)₃Br] complex connected to a porphyrin (23).

In an attempt to move away from expensive metals like Ru(II) and Re(II), a dimolybdenum paddlewheel porphyrin conjugate (Mo$_2$-PWPC) was synthesised, the structure of which is shown in Figure 21. Use of this catalyst for water splitting has shown promising results with a TON of 640, but more remarkably it mimics photosystem I in terms of solar-energy conversion and was shown to successfully reduce NAD+ to NADH. But the TON of this reaction was drastically lower (TON of 40). The success of mimicking photosystem I was possible due to the possibility of multiple pathways for electron transfer from the Mo$_2$PW donor to the porphyrin acceptor from a broad energy threshold that covered the entire visible-light spectrum.
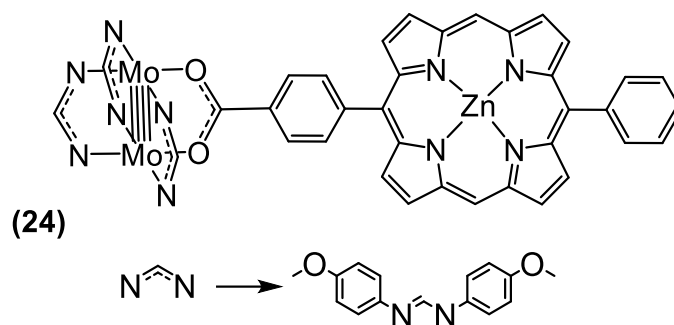
Figure 21: structure of a dimolybdenum paddlewheel porphyrin conjugate (Mo₂-PWPC) (24)

These are a select few examples that have been highlighted, a very recent review has also highlighted a broader range of homogenous and heterogenous catalysts that use porphyrins. However they summarised that while there has been advances in this area of photocatalysis, all examples mentioned in the review (and those mentioned in this discussion) suffer with poor activity/low efficiencies.[42]

1.3.5. The Problem.

The examples that have been discussed (section 1.3.4) all suffer from poor efficiencies (when compared to more successful metal complex catalysts)[47] which could be attributed to a lack of electronic communication between the porphyrin and metal complex. A common structural component that the porphyrin-metal complex conjugates possess is that the porphyrins are anchored to the complex *via* a phenyl bridge. The lack of electronic communication is considered to stem from poor π-orbital overlap between the phenyl bridge and porphyrin because of rotation along the C-C bond, caused by steric hindrance from the hydrogen atoms on the phenyl ring and the β position on the porphyrin. This rotation from the steric clash therefore causes the π-orbital overlap between these two groups to be out of phase to one another, which is shown in Figure 22, and limits the extended conjugation within the system.
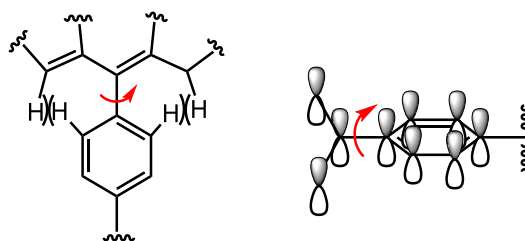
Figure 22: illustration of the steric clash and the resulting effect that the rotation has on π-orbital overlap.

The energy barrier of rotation is the energy that must be overcome for one full rotation around a bond, it is the difference in energy between the most stable and least stable conformations.

Steric hindrance within molecules (such as the hindrance between a porphyrin and phenyl bridge) can affect the barrier for rotation. At thermal equilibrium, the conformers can be relatively interchangeable, however at any given time it is more favourable for the molecule to be at a dihedral angle where there is the lowest energy conformation. Because of this, little electronic communication between the porphyrin and metal surface/complex is observed, rather than no electronic communication, as there are dihedral angles that are energetically accessible to allow for some π-orbital overlap. Looking at the HOMO energies of a Mo_2-PWPC (compound (24), Figure 27) it can be seen that there is significant electron density on each unit, but little electron density on the bridge. It gives clear indication that there is limited electron delocalisation between the two system.
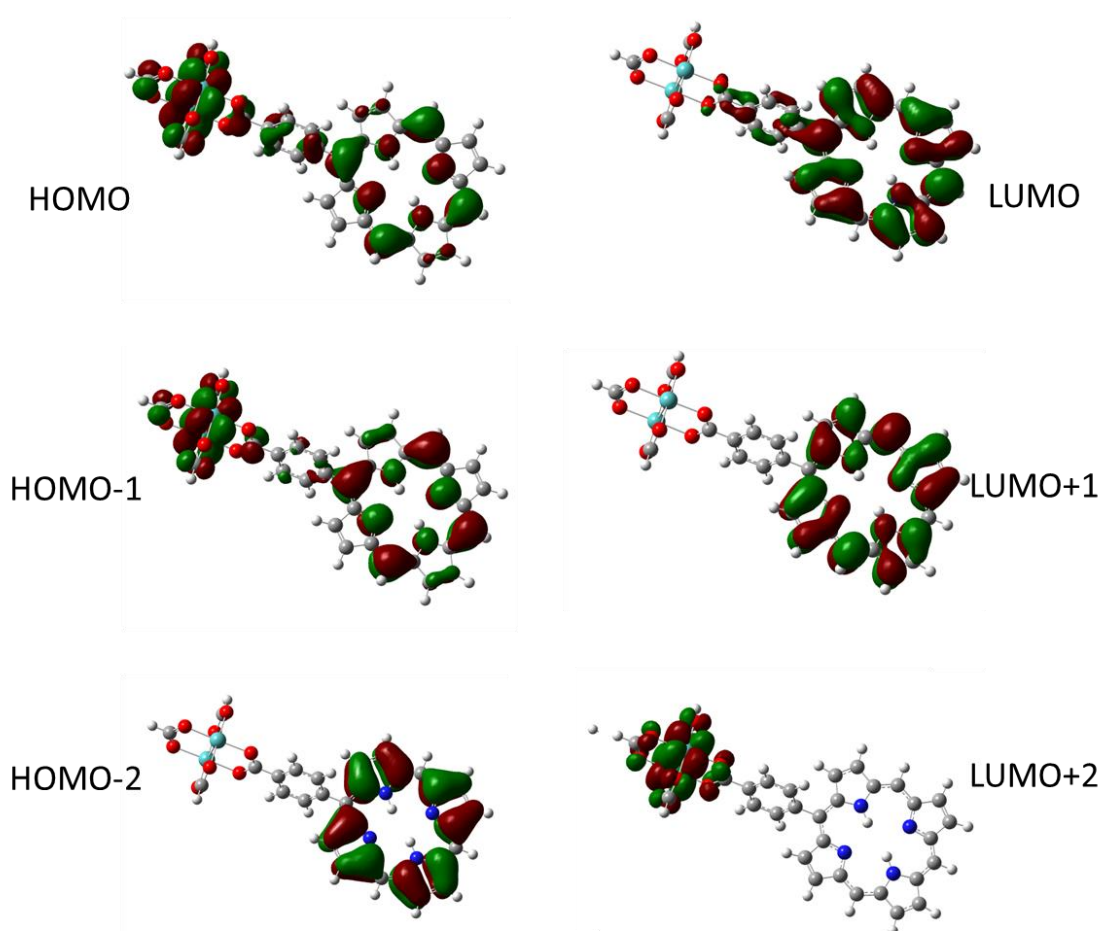
Figure 23: molecular orbital diagrams of compound (24) showing the electron density at the HOMO and LUMO energies.

Research into porphyrins as dyes in DSSC frequently vary the bridging group between the porphyrin and semiconductor surface. It is not uncommon to see the most effective dyes producing PCE values of 10-12 % containing an alkyne bridge.[11] Dye design and

investigations also incorporate other groups, such as: alkene spacers and azo groups ,[85] 5-membered heterocycles,[70, 71] or a combination.[82]

However, to the author's knowledge, there are no known examples of photocatalysts that contain different 'bridges' between a porphyrin and a metal complex that is not a phenyl ring. Therefore, it is of great interest to delve into varying the bridge between a porphyrin and metal complex to determine if different bridging groups can tune and improve the catalytic performance of these systems.

2. Aims of Project

The direction of this project is to delve into variation of the bridging unit between a porphyrin and metal complex. The main aim is to synthesise and characterise a series of porphyrins that each contain different *meso*-substituents that will act as the bridging unit when eventually coupled to a metal complex (in this case a dimolybdenum paddlewheel unit). The different *meso*-substituents will range between an alkyne extension between the porphyrin and phenyl ring ((25), Figure 24), to replacement of the phenyl group with different 5-membered heterocyclic rings (compounds (26 and 27), Figure 24).
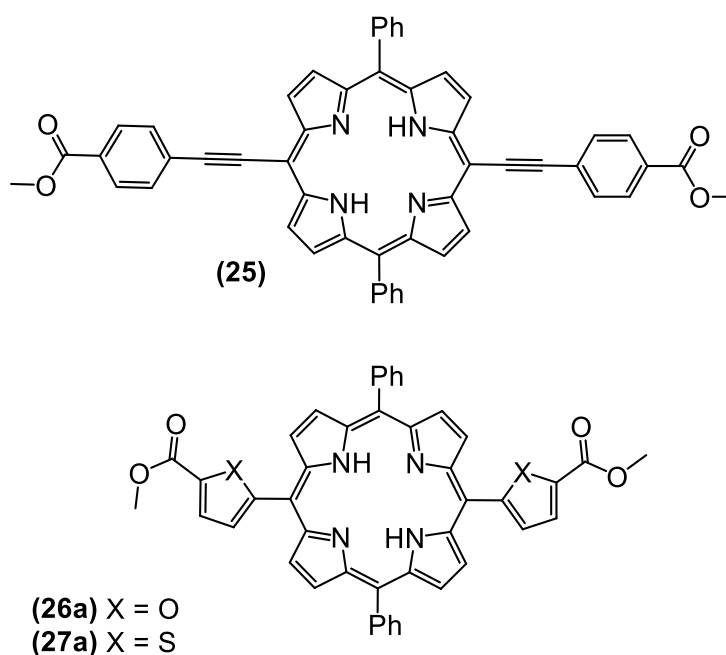
Figure 24: structures of the target compounds for this project.

The effect these substituents may have on the structure is as follows; the alkyne functional group will act as a spacer unit between the porphyrin and phenyl ring, which by extension will eliminate rotation along the C-C bond. However, if rotation still occurs the alkyne unit may exhibit continual π-orbital overlap as the alkyne is cylindrically symmetrical and would continue to stay in-phase despite rotation. The rotational barrier would be at a lower energy as full 'free' rotation can occur. The 5-membered heterocyclic rings are a smaller size to that of the phenyl ring and may possess smaller dihedral angles and therefore smaller energy barriers to overcome, compared to that of the phenyl ring. Addition of these groups will possibly tune and change the photophysical properties of the porphyrin as they are expected to extend the conjugation of the porphyrin macrocycle.
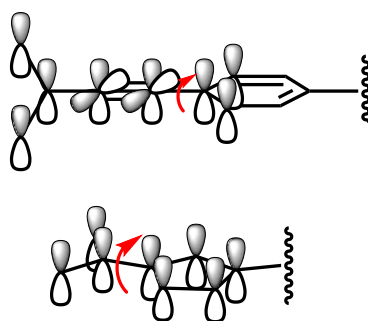
Figure 25: π-orbitals of an alkyne bridge (top) and 5-membered heterocyclic ring (bottom).

UV-Visible spectroscopy and emission studies will be used to probe the photophysical properties of the synthesised compounds. A change in peak position will indicate whether there has been successful extension of the conjugation of the porphyrins. The scale of the change would indicate the extent that different sized groups and dihedral angles have on the electronic resonance of the compounds.

While this approach can be applied to other porphyrin-metal dyads, this project is aimed to be directed towards the overall improvement of Mo_2-PWPC because it is a focal interest in the overall scheme of the research group that this project is based in. It also fits into the idea of using cheaper alternatives to ruthenium(II) as photocatalysts. Computational chemistry calculations used to support and build on the work are therefore based on Mo_2-PWPC structures.

3. Results and Discussion

3.1. Porphyrin Synthesis

3.1.1. Towards halogenated porphyrins

The first stages of the project predominately focused on synthesising a suitable supply of halogenated porphyrins: the steps towards this target are highlighted in Figure 26. This is because aryl halides are important synthetic precursors as they provide access to a broad range of chemical activity. In particular, cross-coupling reactions such as Sonogashira or the Suzuki-Miyaura reactions.[77-79, 86, 87] The brominated porphyrins will be vital in giving access towards both Sonogashira and the Suzuki-Miyaura cross-coupling reactions, for the synthesis of the target compounds (25, 26 and 27).
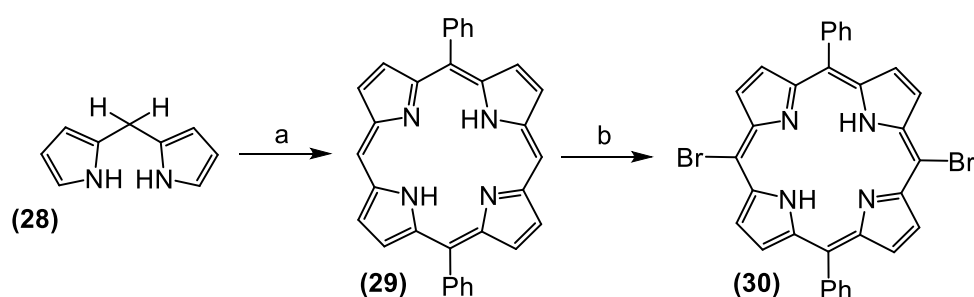
Figure 26: reaction scheme for the synthesis of (30). a) BF$_3$(OEt$_2$), benzaldehyde, p-chloranil. b) NBS, pyridine.

Dipyrromethane (28) was formed by reaction of 100 equivalents of pyrrole to one equivalent of *para*-formaldehyde with an InCl$_3$ catalyst at 55 °C for 2 hours, Figure 27. Due to light sensitivity and degradation of (28) over time, the reaction was kept in the dark and work-up procedures were performed in low light environments. The reaction was straightforward and required minimal purification – an orange oil was triturated against petroleum ether to produce a light brown solid in near quantitative yields. It is noted that *para*-formaldehyde is insoluble in pyrrole, which is why the reaction is heated to 55 °C. It is also heated to induce thermal 'cracking' of *para*-formaldehyde into formaldehyde, which is soluble. Other aldehydes/ketones (such as benzaldehyde) are more soluble and do not require such significant heating.[88]
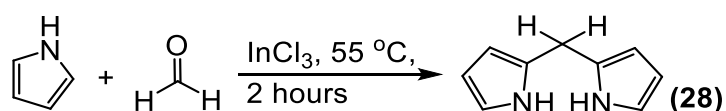
Figure 27: reaction scheme for the acid catalysed condensation reaction between formaldehyde and pyrrole for the synthesis of dipyrromethane (28).

The synthesis of *trans*-5,15-diphenylporphyrin (29) was achieved using the Lindsey 2+2 condensation method – which in this case is a reaction between dipyrromethane (28) and

equal equivalents of benzaldehyde as shown in the general scheme in Figure 17.[59, 72, 73] The reaction was performed with a Lewis acid catalyst, boron trifluoride etherate ($BF_3(OEt_2)$) - at room temperature for 3 hours before oxidation with *p*-chloranil. *P*-chloranil is considered a mild oxidant and therefore requires heating at reflux for full oxidation of the porphyrinogens into porphyrins to occur. The crude TLC, (Figure 28) of the product demonstrated that this material was a combination of (29), polypyrrole tar and in some cases *cis*-5,10-diphenylporphyrin. Despite the selection of this method for its regioselective synthesis of the *trans*-isomer, scrambling results in the presence of the *cis*-isomer. Removal of the majority of the polypyrrole tar *via* a silica gel plug, before column chromatography, resulted in cleaner separation of the two porphyrin isomers. Nonetheless, due to the similar R_f values, column chromatography needed to be performed many times to achieve full separation. The best results were achieved when wide and long columns were used in conjunction with a mixed solvent mobile phase of dichloromethane (DCM) and petroleum ether (approximately in a 7:3 ratio), this was demonstrated by greater separation seen on TLC, shown in Figure 28. Following this method, compound (29) was isolated as a dark purple solid in yields of around 20 %.
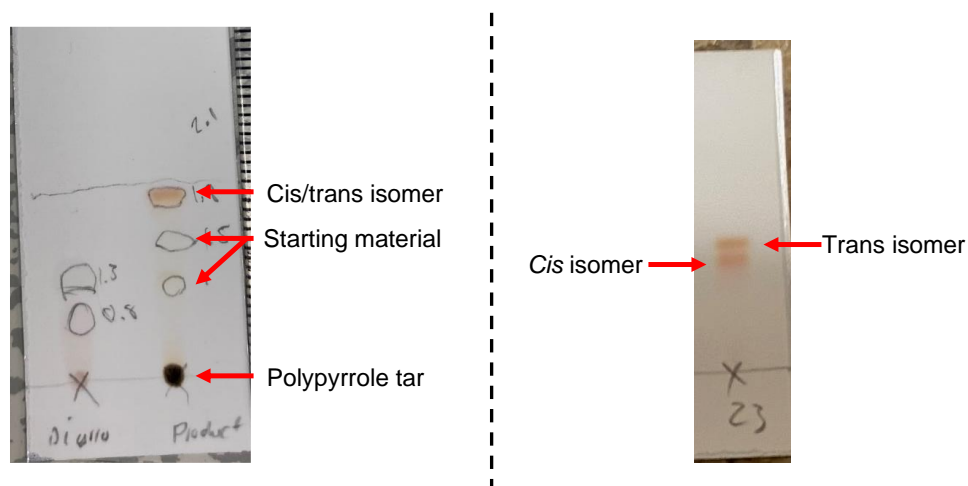
Figure 28: (left) image of a TLC plate (DCM eluent) showing the cis/trans isomer, starting materials and polypyrrole tar of the crude products of (29). (right) Image of the cis and trans isomeric separation of (29) using 7:3 DCM:petroleum ether eluent.

^{1}H NMR spectroscopy of compound (29), Figure 29, shows that in the aromatic region there are β-pyrrole hydrogen nuclei appearing as two, 2H doublets at 9.38 and 9.09 ppm, and the phenyl resonances from the *meso*-substituents present as two multiplets at 8.26 and 7.80 ppm. A singlet resonance at 10.32 ppm was assigned to the hydrogen nuclei at the *meso*-positions that are not occupied by phenyl rings. Out of the aromatic region, a singlet resonance at -3.12 ppm was assigned to the N*H* groups. The anisotropic effect is the cause of the high upfield shift of the N*H* inner core protons. Aromatic compounds exhibit anisotropy; π-electrons in an aromatic ring are delocalised, and when an external magnetic field is applied, the

electrons move around the ring. The movement of electrons in the interior part of the ring opposes the external magnetic field, which results in significant shielding of the inner protons.
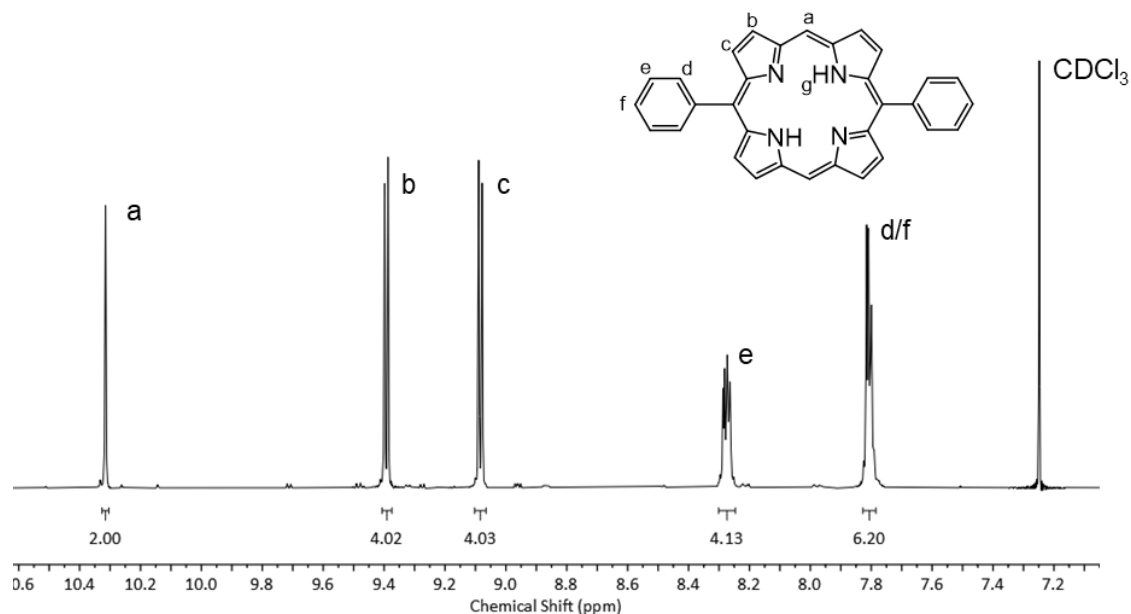
Figure 29: ^{1}H NMR spectrum (CDCl$_3$, 298 K, 400 MHz) of the aromatic region of compound (29).

Iodination's are sterically demanding and according to Dolphin *et al.*,[89] failure of these reactions for octaethyl- and tetraphenylporphyrin were because of steric hindrance by the alkyl/phenyl substituents, which prevents the iodine ion from efficient electrophilic attack on the porphyrin ring but 5,15-diphenylporphyrins that lack β-pyrrolic substituents are not hindered enough. The phenyl group is said to not be sterically bulky enough to encourage *meso-meso* diiodination, but rather mono-substitution at one *meso*-position and a second substitution at a β position on the porphyrin.[56, 89]

Coupling the possibility of iodination at a β-position and the time it takes to iodinate with *N*-iodosuccinimide (several days with significant excess of reagent),[90] the decision was taken to brominate compound (29), as it is more routinely used.[52, 82, 85, 91] Compound (29) was brominated at both available *meso*-positions with excess amounts of *N*-bromosuccinimide (NBS) and an acid scavenger (pyridine) at 0 °C. The excess of NBS meant that there was conversion to the di-bromated porphyrin (30), while equal equivalents of (29) and NBS resulted in the mono-brominated porphyrin, as shown in Figure 30. For (30), loss of the 2H resonance at 10.32 ppm, indicated that both *meso*-positions were occupied by nuclei other than protons, while for the mono-brominated version the integration of this resonance decreased to 1H, as shown in Figure 31.
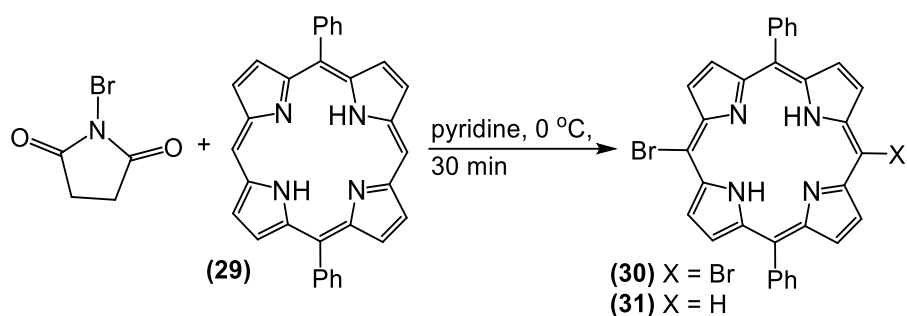
Figure 30: general reaction scheme for the halogenation of compound (29) to compounds (30) and (31)
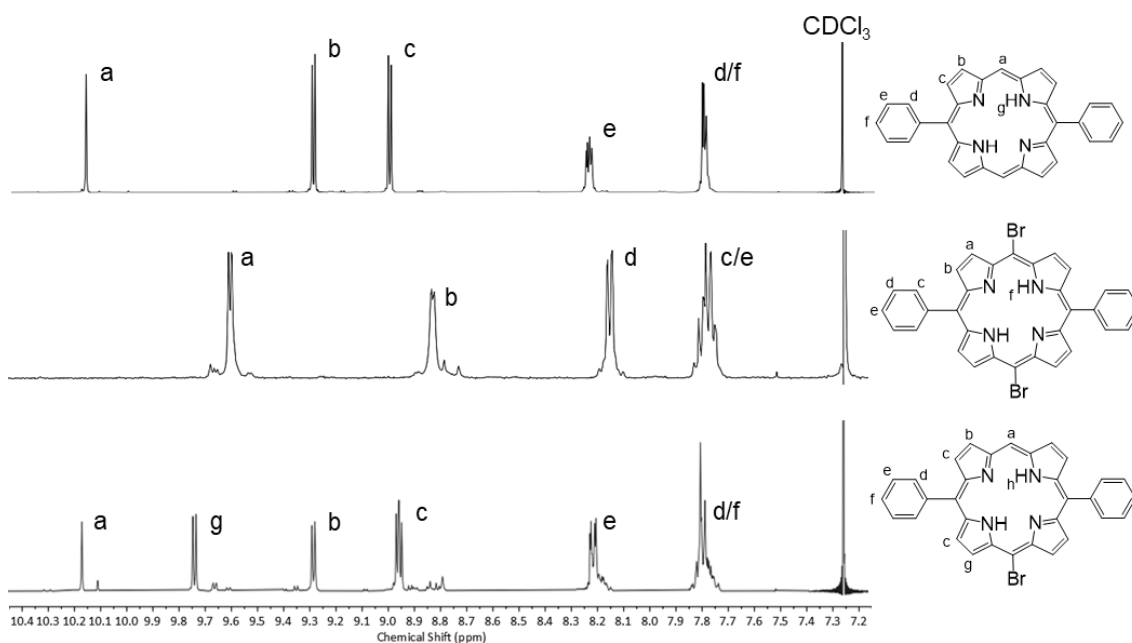
Figure 31: ^{1}H NMR spectrum (CDCl$_3$, 298 K, 400 MHz) overlay of the aromatic region of compounds (29) (top), (30) (middle) and (31) (bottom).

3.1.2. Metallation of the porphyrin core

The next stage of the project focused on the synthesis of metallated porphyrins (in this case zinc metallation) and was a necessary step because of the presence of the copper co-catalyst that is used in Sonogashira cross-coupling reactions. The co-catalyst easily binds to the four nitrogen atoms in the porphyrin core, which results in negative consequences on the reaction. Mainly, without the co-catalyst, the reaction may not proceed. Even though a Suzuki-Miyaura cross-coupling reaction does not contain or require a copper co-catalyst (and therefore does not need a metallated porphyrin), having access to it would also allow comparison with the free-base porphyrin and would highlight further ways of tuning the photophysical properties of the porphyrin. Additionally, the zinc core could be removed post reaction. Compound (32) was synthesized by two approaches – as demonstrated in Figure 32.

37
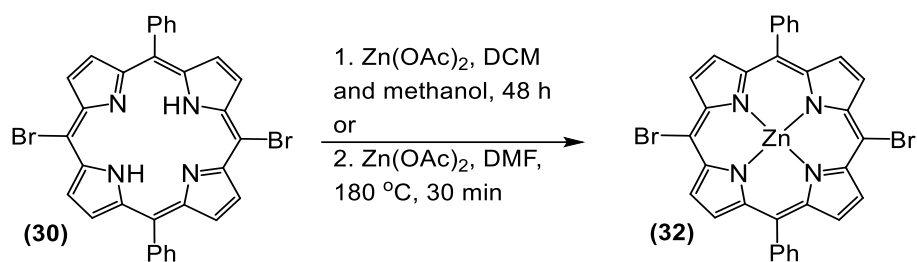
Figure 32: synthetic procedure for the synthesis of (32) via two methods.

The first approach involved using 2 equivalents of zinc acetate and compound (30) in 3:1 DCM:methanol at room temperature until full conversion. But even after 48 hours, full conversion was not seen (shown by the presence of starting material in APCI-MS, Figure 33).

Meas. m/z	#	Ion Formula	m/z	err [ppm]	err [mDa]	mSigma	Mean err [ppm]
680.927460	1	C32H19Br2N4Zn	680.926239	1.8	1.2	70.6	4.7
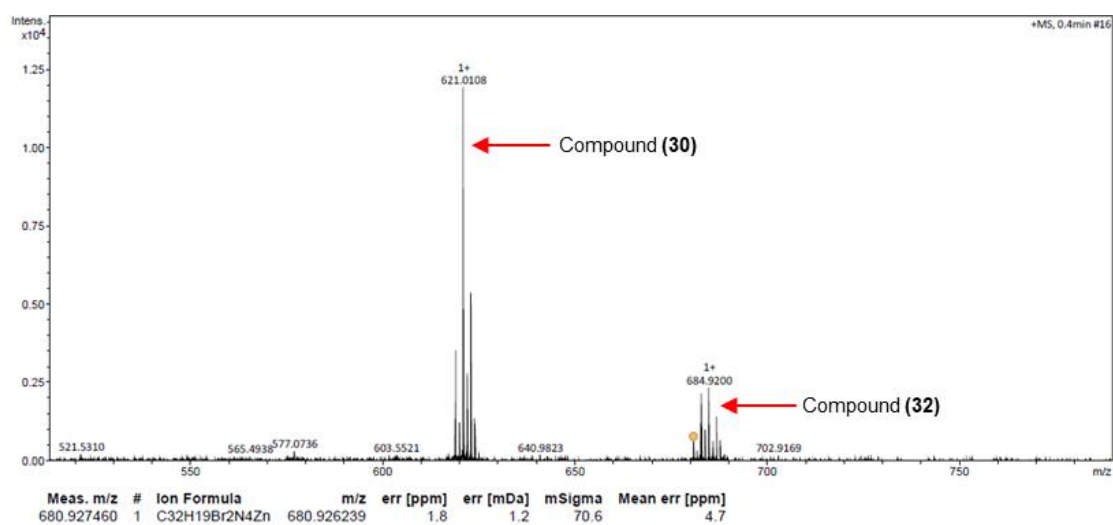
Figure 33: APCI-MS spectrum of the crude product taken after 48 h, showing some formation of (32).

Thus, a second approach was taken in an attempt to obtain purer material; microwave assisted synthesis.[92] It was hoped that using this method, would reduce the reaction time, promote full conversion to (32) and to increase the collected yield of product. Six equivalents of zinc acetate and compound (30) in DMF were added to a thick-walled glass tube, with the microwave set at 300 W, the reaction mixture was heated to 180 $^{\circ}$C for 30 minutes. Gratifyingly, a purple solid was collected in 63 % yield. The poor solubility of (32) made it difficult to collect clear NMR spectral data and several deuterated solvents were used in order to try collect better resolved spectra. In the end, DMSO-d_6 gave the best solubility and allowed for clear identification, assignment, and integration of signals. Coordination of zinc results in the loss of the two hydrogens that were attached to the nitrogen atoms in the centre of the porphyrin and so from this, the successful synthesis of compound (32) was confirmed by the loss of the N*H* singlet resonance at -2.25 ppm, as shown in Figure 34.

38
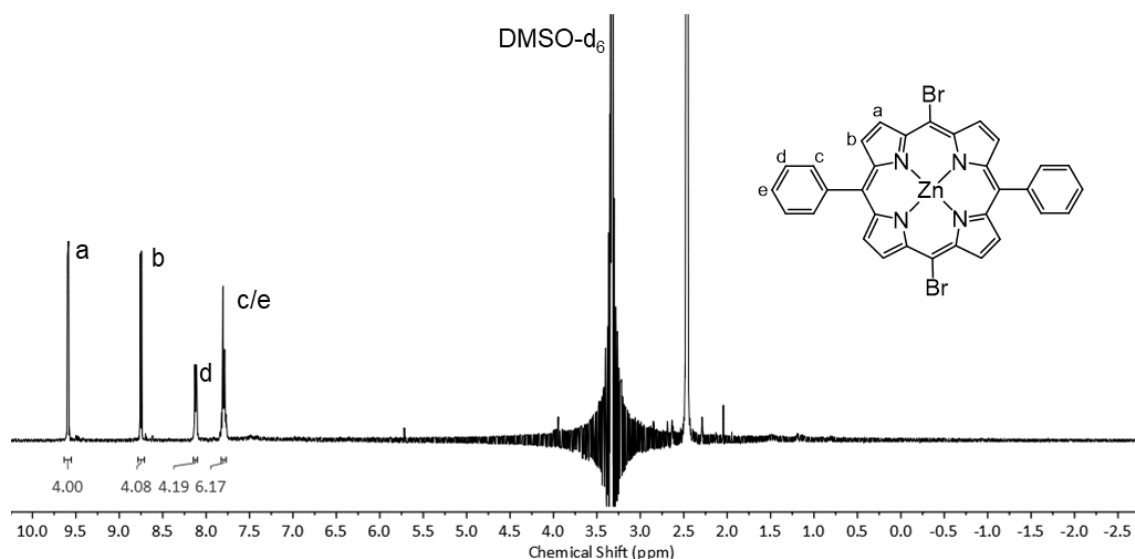
Figure 34: ^{1}H NMR spectrum (DMSO-d_6, 298 K, 400 MHz) of compound (32), showing no resonance at -2.25 ppm.

Both compound (30) and (32) were collected as purple solids in high yields, however due to the low yields of (29), the supply of (30) and (32) were limited. Hence increasing the yields of (29), was needed to efficiently progress forward to the next stages of synthesis. Due to the high volumes of solvent used in the synthesis of compound (29) (ca. 1 L of DCM per reaction), it was difficult to significantly scale the reaction up to produce more of compound (29). However, one method that has been used to improve the yields of a tetra-phenylporphyrins, involved the addition of zinc acetate to a standard Adler-Longo procedure.[93, 94]

According to Calvin *et al.* the yield of the resulting zinc(II) tetra-phenylporphyrin was double that of the non-zincated version (i.e. 5 % *vs.* 10 %).[17] Appling this to the current conditions used in the synthesis of compound (29), a new synthetic scheme can be followed (Figure 35), where compound (33) was synthesized from a reaction between equal equivalents of dipyrromethane (28) and benzaldehyde to 2.5 equivalents of zinc acetate resulting in the isolation of a maroon solid at >40 % yield. While also increasing the yield of product, there was no formation of the *cis*-isomer which made purification of the compound much simpler, and a silica gel plug was only required to remove some polypyrrole tar present. Compound (33) can then be brominated in a similar fashion to (29).
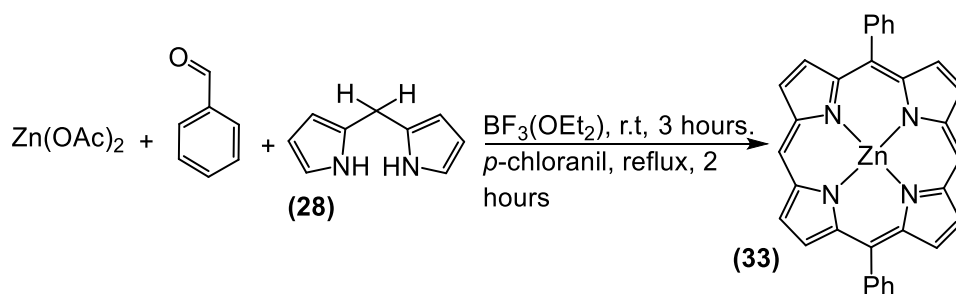
Figure 35: reaction scheme towards the synthesis of (33) by zinc templatation.

In the case of compound (33), similar resonances are observed in the aromatic region to that of compound (29), with the biggest difference between the spectra seen in the loss of the N-*H* resonance at -3.12 ppm.

3.2. Cross-Coupling reactions

3.2.1. Sonogashira cross-coupling

The first focus in the next stages of synthesis was directed towards the synthesis of compound (34), where there was mixed success despite prevalent and successful literature in synthesizing this type of porphyrin.[81, 95] Addition of an alkyne to the porphyrin has been demonstrated before by following a Sonogashira cross-coupling reaction; which is a reaction between a arylhalide and terminal alkyne in the presence of a palladium catalyst, copper iodide co-catalyst and base, as shown in Figure 18 from section 1.3.2. Synthesis of compound (34) was a targeted molecule of the project because the compound was expected to produce the best opportunity for electronic communication when tethered to a Mo_2-PW complex. Initial synthesis involved reacting one equivalent of compound (32) with 6 equivalents of methyl 4-ethynylbenzoate and 5 mol% of $PdCl_2(PPh_3)_2$ and CuI in a 1:1 THF:NEt$_3$ solvent mixture for about 18 hours at room temperature, as shown in the reactions scheme in Figure 36.
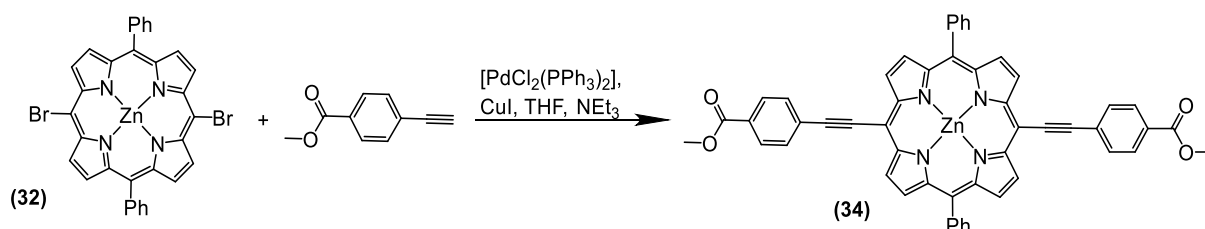
Figure 36: reaction scheme for the synthesis of compound (34), via a Sonogashira cross-coupling reaction.

After the first attempt using these conditions, some formation of (34) was seen in the crude APCI-MS, however there was still starting material also present, as shown in Figure 37. The poor solubility of compound (32) was considered a factor towards the poor conversion into the

targeted product. However, it was later realized that the sample of (32) used for this specific reaction was not pure and contained compound (30). This can be seen in Figure 37. The consequence of the presence of the free-base porphyrin in this reaction may also result in the copper (from the CuI co-catalyst) binding itself to the porphyrin core, and therefore reducing the amount of co-catalyst, severely limiting the reaction progress. However, there was no indication of the copper binding to compound (32), and the limiting factor of this reaction was attributed to the poor solubility of the porphyrin in solution.
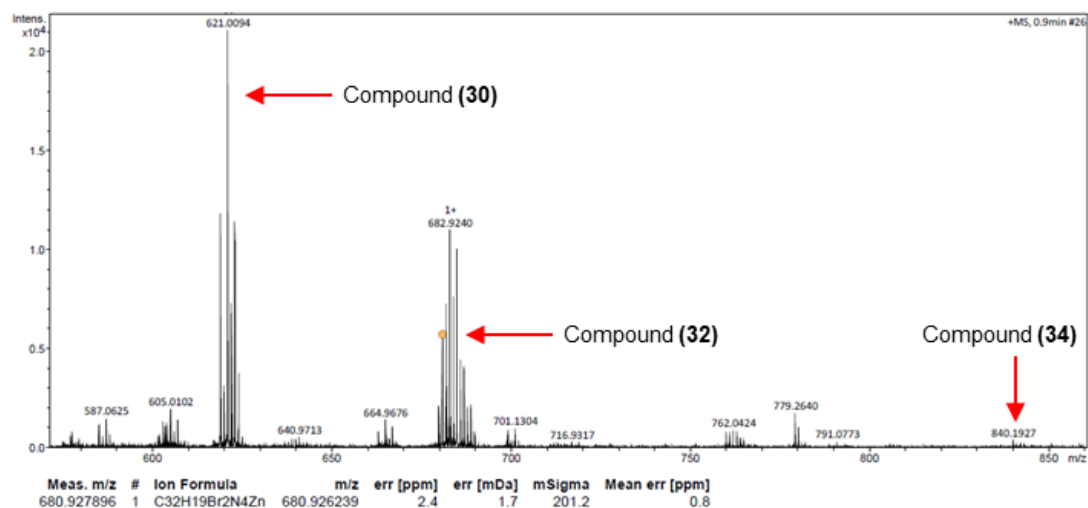
Figure 37: APCI-MS spectrum of the crude product from the synthesis towards (34).

In an attempt to improve the yield of compound (34), a literature search into the conditions used by different groups that performed Sonogashira reactions on halogenated porphyrins was completed and is summarised in Table 1. By looking at the conditions others have used, it was expected to see if there were common factors towards successful Sonogashira cross-couplings on porphyrins.

Table 1: reaction conditions used in Sonogashira cross-coupling reactions upon porphyrins. a. entry is superscripted with the relevant reference to literature b. equivalents of alkyne per one equivalent of porphyrin c. NEt$_3$ is used universally as the base in conjunction to the solvent.

Entry[a]	Equivalents of terminal alkyne[b]	Reaction Time	Temperature (°C)	Solvent[c]	"Pd" Catalyst	Catalyst mol%	CuI mol%	Yield (%)
1[81]	2	6 h	Reflux	THF	PdCl$_2$(PPh$_3$)$_2$	16	24	82
2[96]	6.7	14 h	55	THF	Pd(PPh$_3$)$_4$	6	6	98
3[97]	3	4 h	80	Toluene	Pd$_2$(dba)$_3$ and PPh$_3$	6	25	66
4[98]	10	>18 h	Reflux	THF	Pd(PPh$_3$)$_4$	10	10	78
5[99]	5	12 h	r.t	THF	PdCl$_2$(PPh$_3$)$_2$	25	25	84
6[100]	3	12 h	50	THF	Pd(PPh$_3$)$_4$	10	10	71
7[101]	3	48 h	40	THF	Pd(PPh$_3$)$_4$	15	15	82
8[102]	10	1.5 h	80	Toluene	Pd$_2$(dba)$_3$ and PPh$_3$	7	25	78

From some common factors seen in Table 1, a few changes were made to the conditions used; the first major change was increasing the mol% of catalyst and co-catalyst from 5 mol% each to 12 mol% each, and the second major change was heating the reaction to 80 °C. The total volume of solvent was also increased (which was expected to assist with the solubility of the porphyrin) and the ratio between THF and NEt$_3$ was changed. So from this, to synthesise compound (34), six equivalents of methyl 4-ethynylbenzoate were combined with (32), using 12 mol% of PdCl$_2$(PPh$_3$)$_2$,12 mol% of CuI and a 7:3 THF:NEt$_3$ solvent mixture at 80 °C. In this case, according to APCI-MS (Figure 38), compound (34) was isolated after several separation attempts but identification by ^{1}H NMR spectroscopy proved difficult. Similar to (32), several deuterated NMR solvents were used but the solid continued to be poorly soluble in the solvents and the spectra stayed poorly resolved, which meant compound (34) could not be identified with certainty.

Meas. m/z	#	Ion Formula	m/z	err [ppm]	err [mDa]	mSigma	Mean err [ppm]
841.176291	1	C52H33N4O4Zn	841.178774	3.0	2.5	54.3	5.6
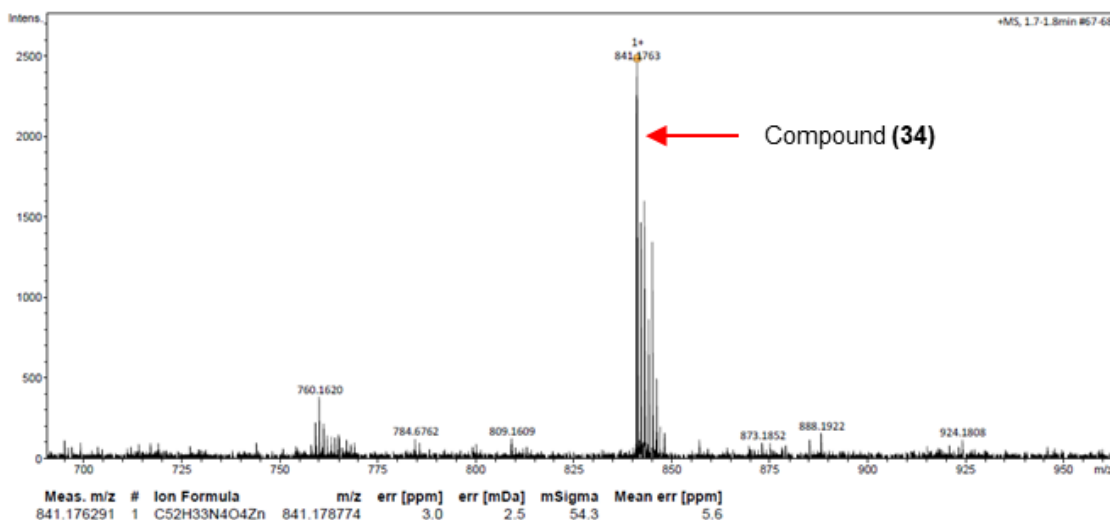
Figure 38: APCI-MS spectrum of a column fraction isolating compound (34)

3.2.2. Suzuki-Miyaura Cross-coupling

Due to the difficulty in isolating compound (34) and subsequent characterisation by NMR spectroscopy, it was decided to start synthetic attempts towards compounds (26) and (27). It was stated previously that a Suzuki-Miyaura cross-coupling is a reaction between an aryl halide and boronic acid/ester with a palladium catalyst and base, as drawn in Figure 18.[52, 103] While the halide reactant has already been synthesised (compounds (30) and (32)), the boronic acid/ester was still required, which in this case would be on the 5-membered heterocyclic rings. Therefore, before Suzuki-Miyaura reactions could take place, the different 5-membered heterocyclic rings needed to be borylated. Borylation of these groups were chosen over borylation of the porphyrins because the current yields and supply of the halogenated/metallated porphyrins are limited, addition of an extra synthetic step would severely reduce the amount available. It was more efficient and time effective to borylate the furan and thiophene rings as the precursors are commercially available and do not require complicated and time-consuming synthesis to make.

3.2.2.1.   Borylation reactions

Initially a palladium catalysed Miyaura-borylation was undertaken; a [Pd(PPh$_3$)$_4$] catalyst, coupled with KOAc in toluene with an excess of B$_2$pin$_2$ was first used (Figure 39).

43
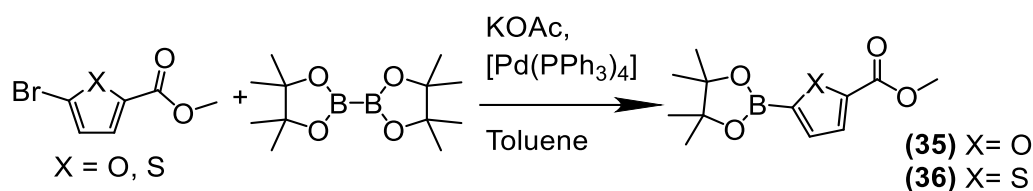
Figure 39: reaction scheme for the synthesis of (35) and (36) via [Pd(PPh₃)₄] catalysed Miyaura-borylation.

While the reaction seemed to have worked, as the product was detected by ESI-MS, the product could not be isolated to determine a yield. A different catalyst and solvent was then used, these were [Pd(dppf)Cl$_2$] and dry dioxane respectively, as according to literature, is more effective and commonly used.[104] Once again, the reaction formed the desired product but purification proved difficult again and the product could not be isolated. Borylated compounds are notoriously difficult to purify *via* column chromatography,[105] and are known to streak/stick along the silica, which was possibly why the product could not be isolated in both cases. However it has been demonstrated that aryl boronic 1,1,2,2-tetraethylethylene glycol esters [ArB(Epin)s] (Figure 40) are an effective way to overcome this problem.[105] While these [ArB(Epin)s] could be an effective way to increase yields and ease the purification methods, they are not commercially available and it was not feasible to prepare these in the timescale of this project.
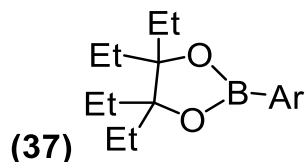
Figure 40: image of an aryl boronic acid 1,1,2,2-tetraethylethylene glycol ester or [ArB(Epin)s] (37)

A homo-coupled product – such as dimethyl 2,2'-bifuran-5,5'-dicarboxylate – was also formed in the reaction mixture. Homo-coupling (*i.e.* the coupling of two aryl bromides together) occurs in this reaction when the newly formed arylboronic ester reacts with the starting aryl halide, as the conditions of the Miyaura-Borylation reaction are similar to Suzuki-Miyaura conditions. However, the use of potassium acetate as a base should be ideal for these reactions as it does not easily facilitate Suzuki-Miyaura cross-coupling to the extent of a stronger base does, but homo-coupling can still occur.[104]

Due to the challenges associated with the Miyaura-Borylation of compounds (35) and (36), a different approach was undertaken; C-H activated borylations. C-H bond activation reactions have been employed regularly by others to overcome the difficulties seen in palladium catalysed Miyaura-borylation.[106, 107] While a number of metal complexes have been used, the

focus was directed to an [Ir(COD)(OMe)]₂ catalyst ((1,5-Cyclooctadiene)(methoxy)iridium(I) dimer) and 4,4'-di-tert-butyl-2,2'-bipyridine (dtbpy) co-catalyst. Compounds (35) and (36) were synthesised from the relevant furan/thiophene, 0.5 equivalents of B_2pin_2 and [Ir(COD)(OMe)]₂ (1.5 mol%) and dtbpy (3 mol%) in methyl tert-butyl ether (MTBE) to give an orange solid, (Figure 41). Purification was simple. Compound (35) required recrystallization from hot toluene and compound (36) precipitated out of a toluene solution when hexane was added.
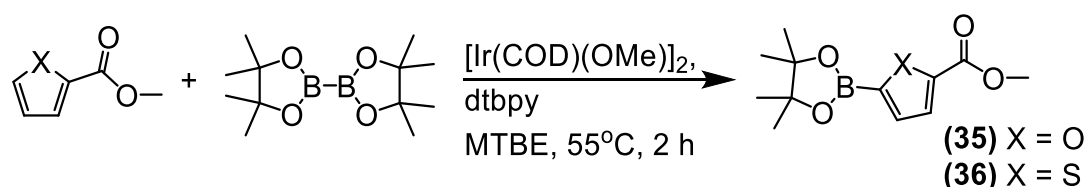
Figure 41: reaction scheme for the synthesis of compounds (35) and (36) via iridium catalysed C-H activated borylation.

In the ¹H NMR spectra of compounds (35) and (36), the CH protons of compound (36) (on the thiophene ring) are downfield shifted towards 7.79 ppm and 7.53 ppm compared to that of compound (35) (compared to the ¹H NMR spectra in Figure 42). Sulfur is less electronegative and less electron withdrawing than oxygen, so the protons on compound (36) experience less de-shielding. Both (35) and (36) show a characteristic singlet resonance at 3.87 ppm for a CH₃ group on the ring and another 12H singlet resonance at 1.32 ppm for the two CH₃ groups located on the boron-pinacol ester.
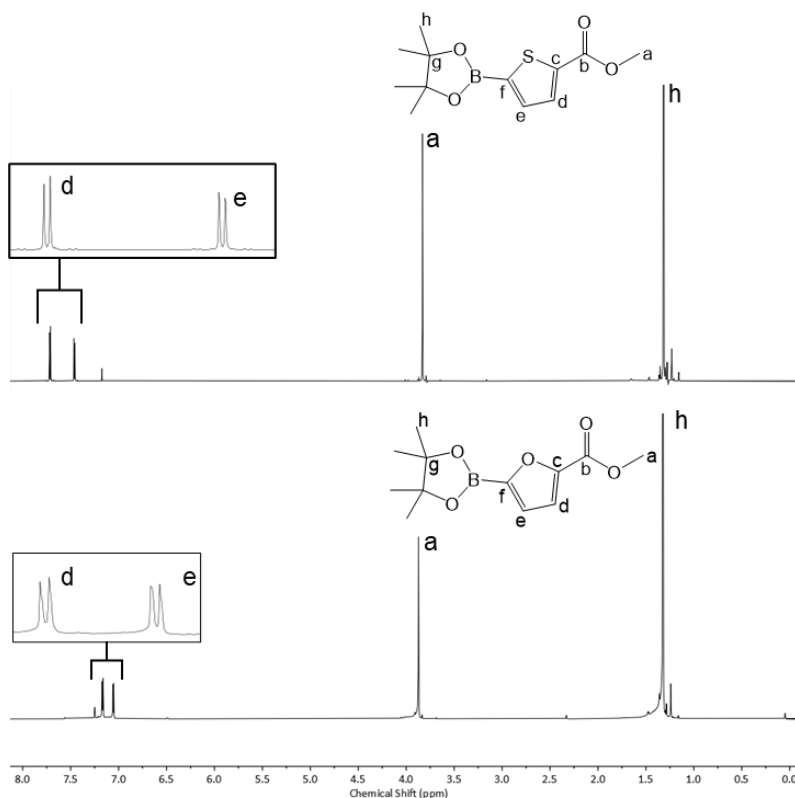
There were concerns for the stability of the compounds because while boronic pinacol-esters are more stable then boronic acids because the σ-donating ability of the carbons attached to the oxygens of the boronate esters; they are presumed to conjugate more effectively into the electron-deficient boron centre.[108] However, it has been highlighted that electron rich heterocyclic rings (such as furan and thiophene rings) can undergo protodeboronation when exposed to water or basic conditions,[104] so before progressing to the next synthetic step a systematic study into the air stability of both compounds was required. Small amounts of the compounds were placed in a vial and left under atmospheric conditions at room temperature. Then they were analysed by ^{1}H NMR spectroscopy to determine if the sample would degrade over time, significant reduction of the compound peaks and formation of new resonance peaks would indicate degradation of the product. Compound (36) was seen to be stable even after 4 days where, as shown in Figure 43, there were no peaks that corresponded to the degradation of the product.
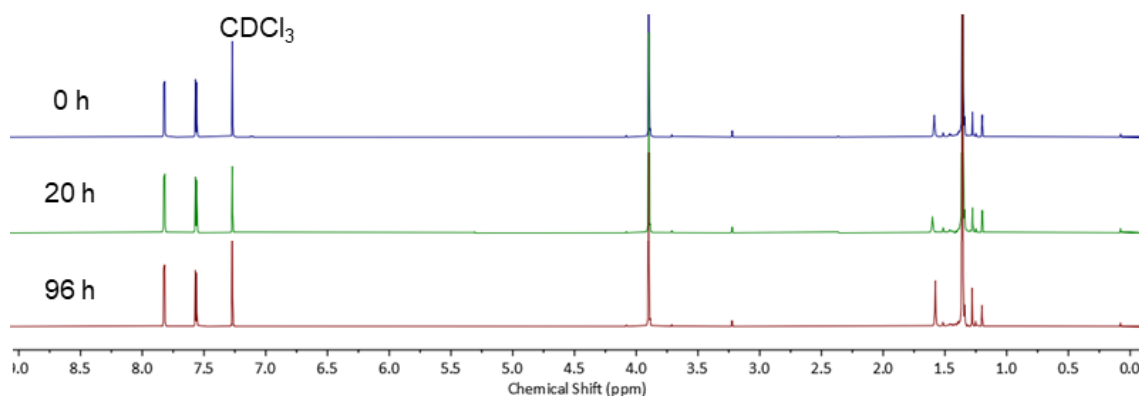
Figure 43: ^{1}H NMR stacked spectrum (CDCl$_3$, 298 K, 400 MHz) of compound (36) after 0h, 20 h and 96 h.

Analysis of the stability of compound (35) was completed in a shorter time frame but again it was shown that there were no peaks corresponding to the degradation products, as shown in Figure 44.

3.2.2.2. Suzuki-Miyaura reactions.

With access to the newly borylated heterocycles, it was possible to work towards coupling these to the porphyrins. The first conditions used for the Suzuki-Miyaura reactions, were chosen based on common conditions seen in a broad literature search, rather than following a singular literature procedure. The conditions for these reactions are summarized in Table 2. The literature search was based on general Suzuki-Miyaura reactions upon porphyrins and was not limited to the cross-coupling of 5-membered heterocyclic rings. Porphyrins containing thiophene based groups (such as (27a) and (27b)) are known, but the novelty arose in the synthesis of compounds (26a) and (26b).

Table 2: reaction conditions used for Suzuki-Miyaura cross-coupling reactions on porphyrins. a. entry superscript is in relation to the reference for literature used. b. in a mixed solvent system a ratio of 2:1 is typically used. c. an excess of equivalents of base is used in each example.

Entry[a]	Equivalents of boronic acid/ester	Reaction Time	Temperature (°C)	Solvent system[b]	Base[c]	Catalyst	Catalyst mol%	Yield (%)
1[87]	12	15 min	80	THF	K$_3$PO$_4$	Pd(PPh$_3$)$_4$	12	60-98
2[96]	3	21 h	100	Toluene / DMF	Cs$_2$CO$_3$	Pd(PPh$_3$)$_4$	46	/
3[98]	4	12 h	80	THF / water	Ba(OH)$_2$	Pd(PPh$_3$)$_4$	5	96
4[109]	/	12 h	Reflux	THF	K$_3$PO$_4$	Pd(PPh$_3$)$_4$	10	30-70
5[110]	12	48 h	90	Toluene / water	K$_3$PO$_4$	Pd(PPh$_3$)$_4$	25	40
6[110]	4	4 h	130	Toluene / DMF	Cs$_2$CO$_3$	Pd(PPh$_3$)$_4$	12.5	12

As with a Sonogashira reaction, a high catalyst loading was required. Excess boronic ester should give the opportunity for full substitution at both halogenated sites, and a strong base (such as K$_3$PO$_4$) was chosen to assist in the transmetallation step as the porphyrin is sterically demanding.[104] The synthesis of the free-base compounds (26a) and (27a) and the metallated

compounds (26b) and (27b) were achieved by reacting the required porphyrin with an excess of selected boronic ester, 14 equivalents of K_3PO_4 and [Pd(PPh$_3$)$_4$] (14.5 mol%) in dry THF for 24-48 h at 80 °C, Figure 45. The yields of all the compounds were varied, ranging from 10 % to 43 %.
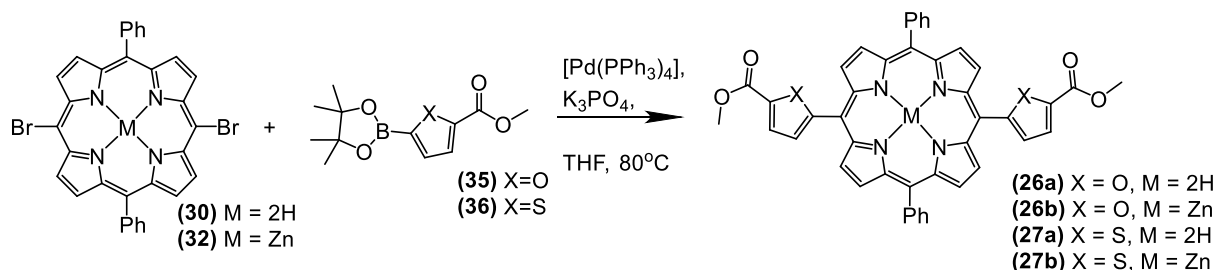
Figure 45: general reaction scheme towards the synthesis of the targeted compounds following a Suzuki-Miyaura cross-coupling reaction.

The reaction for the synthesis of compound (26a) did not reach full conversion, even after 24 h. The compound was isolated as a purple solid, in 10 % yield. The low yield was attributed to loss of material while performing multiple column separations and significant formation of several side-products as observed by APCI-MS; the monosubstituted species, 5-(methyl furan-2-carboxylate)15-bromo,*trans*-10,20-diphenyl porphyrin and the dehalogenated mono-substituted species 5-(methyl furan-2-carboxylate)*trans*-10,20-diphenyl porphyrin (Figure 46).
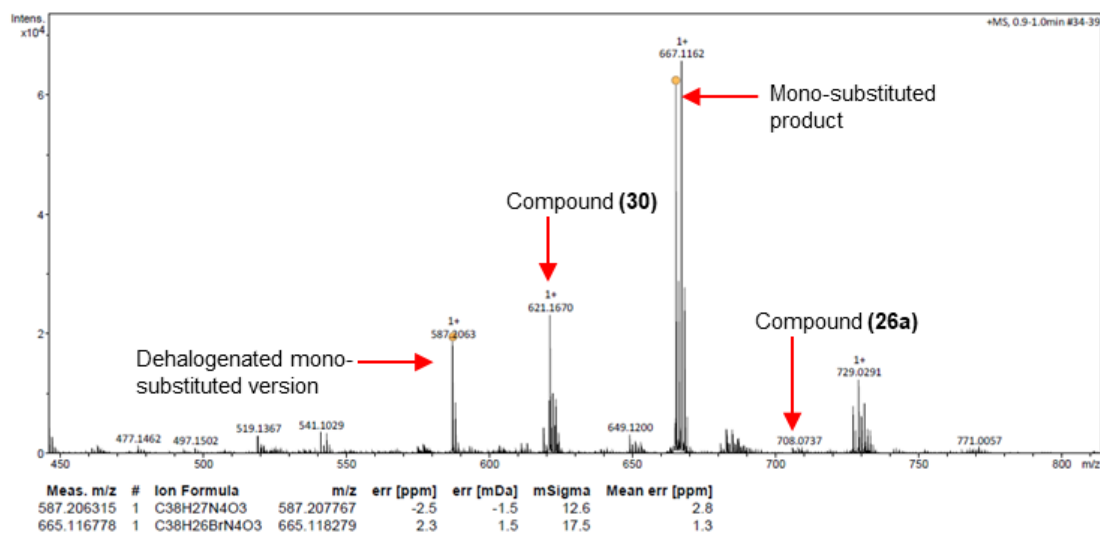
Figure 46: APCI-MS spectrum of the crude product from the synthesis of compound (27a) showing the formation of several side-products.

Homo-coupling and dehalogenation are unfortunate common issues that arise in Suzuki-Miyaura reactions. The homo-coupled product, while not shown in Figure 46, was thought to be formed through oxidative processes from the presence of O_2 in the reaction mixture, which would mean future reaction required more rigorous air exclusion techniques to eliminate and

reduce this side-reaction – this process is also seen in Sonogashira cross-coupling reactions. Consideration of smaller equivalents of boronic ester has shown reductions in the formation of the homo-coupled product as it forces the transmetallation step to be the rate determining step over oxidate addition.[104] Dehalogenation of the porphyrin substrates was thought to derive from displacement of the halide from the Ar-Pd-X species from solvent (e.g. methanol), with subsequent β-elimination to Ar-Pd-X, followed by reductive elimination to ArH (Ar in this case is the porphyrin macrocycle).[111]

However (27a) was isolated after column chromatography and characterised by APCI-MS and NMR spectroscopy. The ^{1}H NMR spectrum of (27a) was expected to show 6 proton environments in the aromatic region, however, the presence of only 5 proton environments was observed (Figure 47). As expected, the C-H protons of the pyrrole region appear as two 2H doublets at 9.13 ppm and 8.90 ppm, with the signals of the phenyl ring appearing at 8.20 ppm and 7.78 ppm, but a second doublet related to a CH on the furan ring was missing. Using COSY ^{1}H/^{1}H NMR experiments it was determined that there was a stacked overlap of two different resonances (Figure 48) and it was demonstrated that the CH resonance from the furan overlaps with the signal assigned to the 6H protons at the ortho and meta positions on the phenyl ring. It should be noted that a 6H singlet resonance at 4.04 ppm is characteristic of the CH$_3$ group seen on the two esters.
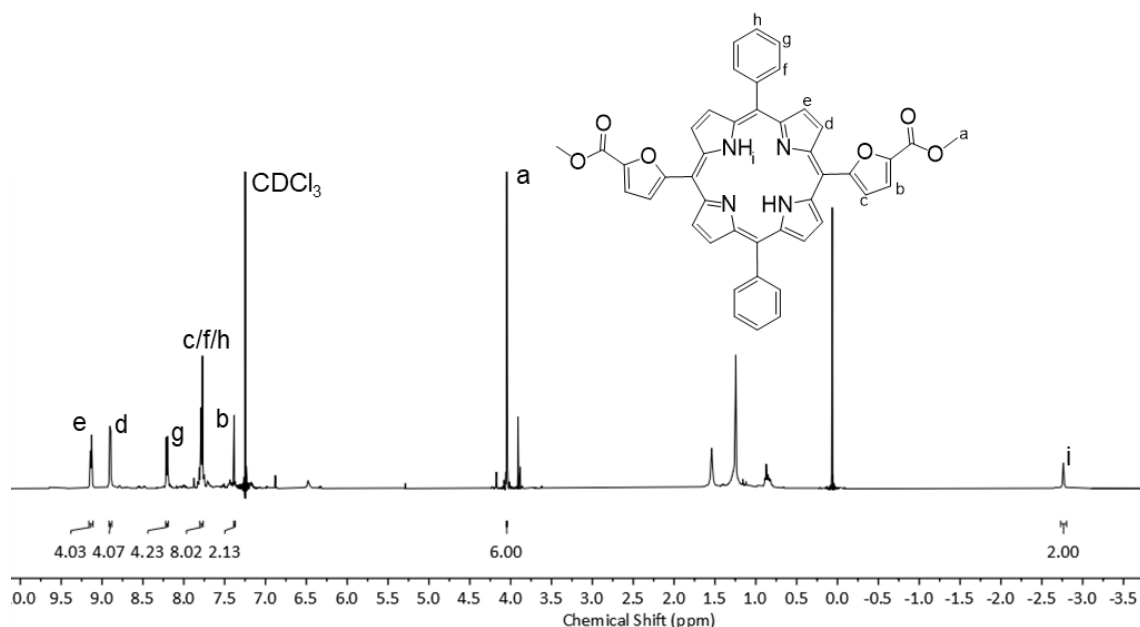
Figure 47: ^{1}H NMR spectrum (CDCl$_3$, 298 K, 400 MHz) of compound (26a).
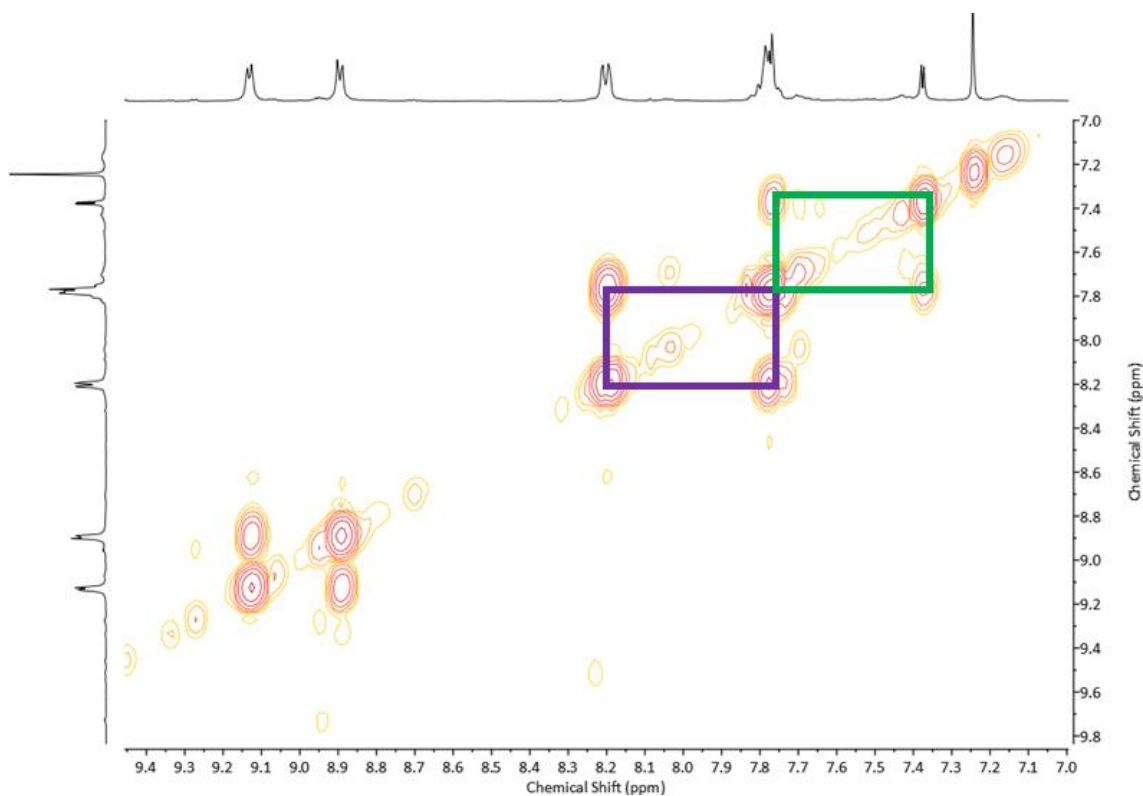
Figure 48: COSY NMR spectrum (CDCl₃, 298 K, 400 MHz) of (26a) of the aromatic region, showing that stacked signals at 7.78 ppm. (purple square = f/h-g coupling, green square = c-b coupling)

The metallated version, compound (26b) was synthesized in a similar way but had double the reaction time and no similar side products were observed in the crude material, as shown in APCI-MS (Figure 49).
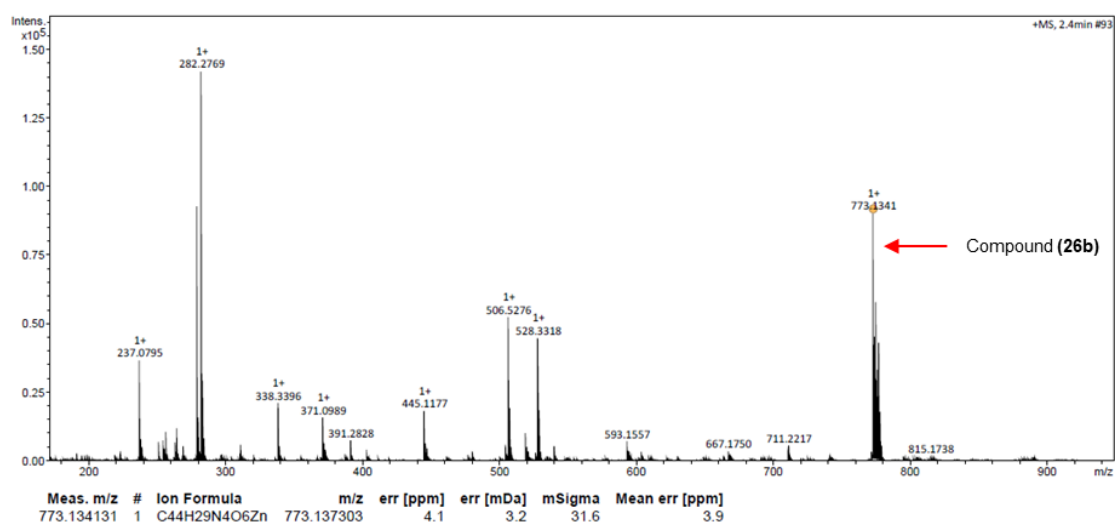
Figure 49: APCI-MS spectrum of the crude mixture of (26b), showing no formation of other identifiable side prodcuts.

A short column and a cold hexane wash was required to purify (26b), and a green-tinted purple solid was collected in 35 % yield. Increasing reaction times and having a metallated porphyrin seems to have an effect on the yield; similar patterns were expected for the thiophene based porphyrins – compounds (27a) and (27b). With the exception of no singlet resonance at -2.76, which would correspond to the two N*H* protons of the free-base porphyrin, analysis of (26b) by ^{1}H NMR spectroscopy showed similar resonances to that of its free-base counterpart, including the overlapping resonance signals at 7.78 ppm.

Compounds (27a) and (27b) were synthesized using the same conditions. Attachment of the thiophene based carboxylate was relatively more successful, in terms of yields and purification, than that of the furan. (27a) was isolated as a dark purple solid in 43 % yield, which, when in solution, is more red in colour; (27b) was isolated as a pink solid in 22 % yield. The ^{1}H NMR spectra (Figure 50) for (27a) show a similar signal pattern as (26a) but with a small up-field shift of the signals. There is still overlap of resonance signals, however the overlap is between the 2H C*H* proton on the thiophene rings and 4H C*H* signal at the *meta* positions of the phenyl rings. These were again clarified by COSY ^{1}H/^{1}H NMR, Figure 51. The same applies with the metallated counterpart.
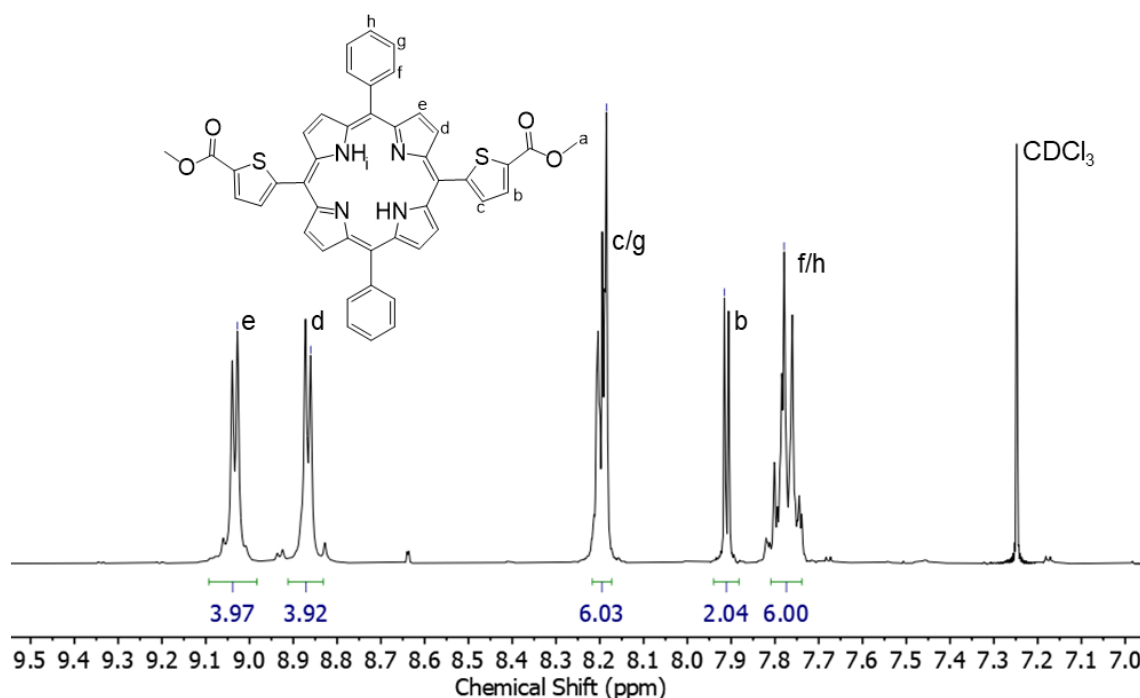
Figure 50: ^{1}H NMR spectrum (CDCl$_3$, 298 K, 400 MHz) of the aromatic region of compound (27a).

51
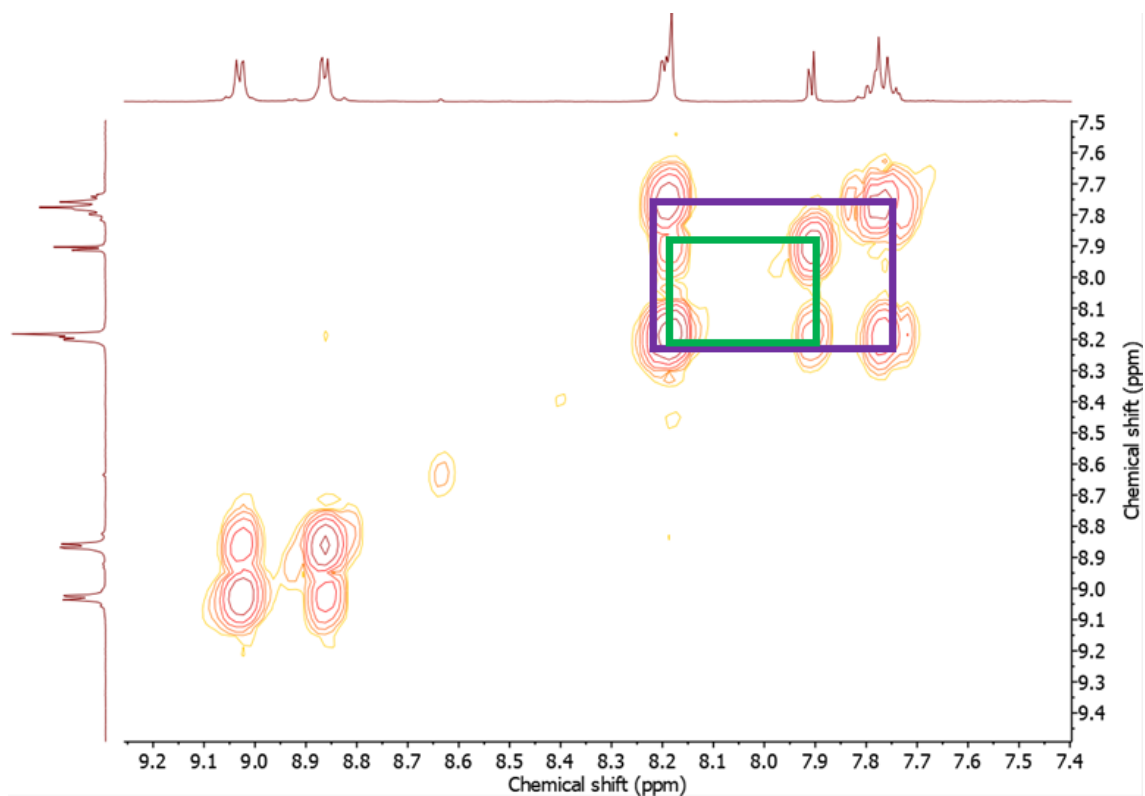
Figure 51: COSY NMR spectrum (CDCl$_3$, 298 K, 400 MHz) of (27a) of the aromatic region, showing stacked signals at 8.18 ppm. (purple square = f/h-g coupling, green square = c-b coupling)

3.3. Further characterisation

To determine the effect that the different linker groups have on the optical properties of the porphyrin, the compounds were studied by UV/Vis spectroscopy and Fluorescence spectroscopy. A comparison between the starting 'unsubstituted' porphyrin (29) and the targeted compounds would highlight the overall significant changes that the 5-membered heterocyclic rings have on the porphyrin system; while comparison with compound (38) would highlight the significance of any changes in the spectra in respect to the system we are trying to improve upon. Computational calculations, performed by Dr. Martin Bates, are used to further explain, and expand upon the findings.

(26a) X = O, M = 2H
(26b) X = O, M = Zn
(27a) X = S, M = 2H
(27b) X = S, M = Zn
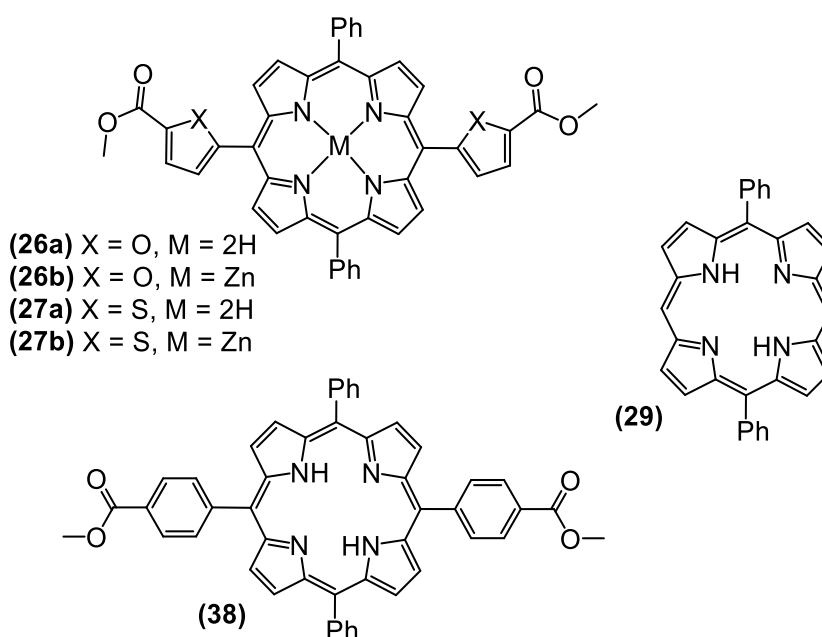
Figure 52: structures of porphyrins (26a), (26b), (27a), (27b), (29) and (38), which further characterisation were done upon.

3.3.1. UV-Visible Spectroscopy

Compounds (26a), (27a), (29) and (38) displayed the characteristic spectrum expected for free-base porphyrins; a Soret band and four Q-bands. While compounds (26b) and (27b) exhibited the characteristic spectrum expected for a metallated porphyrin; a single Soret band and two Q-bands. The spectra are shown in Figure 53, and the results summarised in Table 3. The Soret bands arises from the $a_{1u}(\pi) \rightarrow e_{gy}(\pi)$ transition and is arises when there is a transition to the second excited state from the ground state, while the less intense Q-bands arise from the $a_{2u}(\pi) \rightarrow e_{gx}(\pi)$ transition and arise from excitement to the first excited state. These transitions are shown in a modified Jablonski diagram in Figure 54, highlighting the absorption transitions.
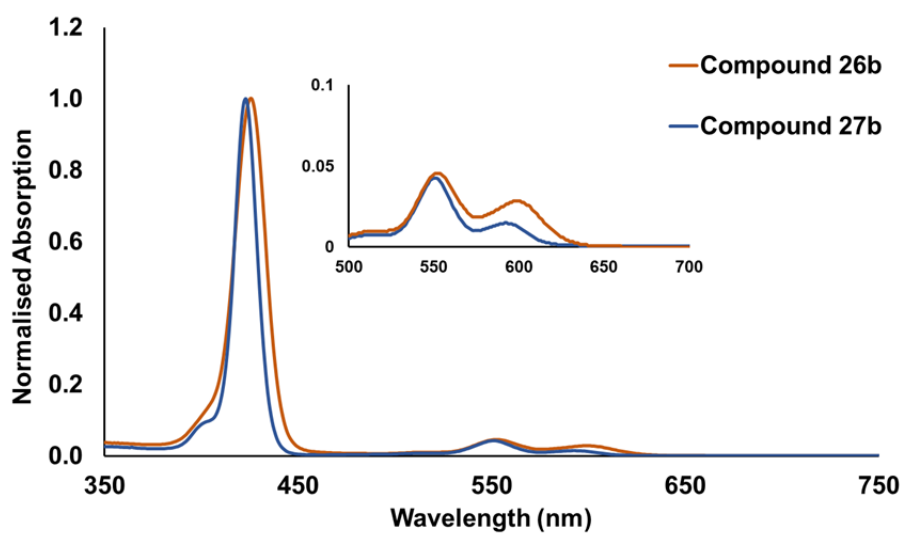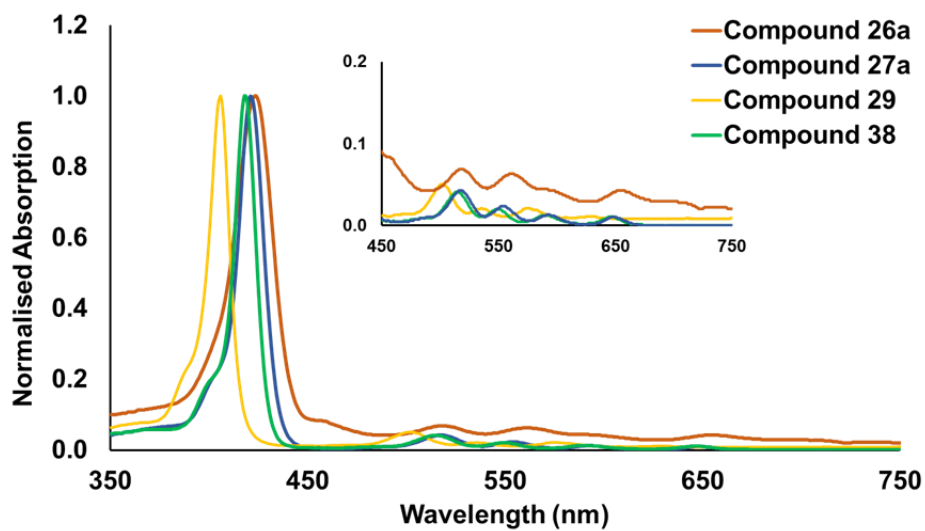
Figure 53: UV-Visible spectra of further characterised compounds in DCM. (top) is the spectrum for the free-base porphyrins. (bottom) the spectrum for the metallated porphyrins

Table 3: UV-Visible spectra data (λ$_{max}$ / nm, ε / M^{-1} cm^{-1}) of compounds (26a), (26b), (27a), (27b), (29) and (38) in DCM solution.

Porphyrin	λ$_{max}$ / nm (ε / M^{-1} cm^{-1})				
	Soret band	Q-band 1	Q-band 2	Q-band 3	Q-band 4
(26a)	425 (3.58 x 10^5)	520 (1.33 x 10^4)	562 (1.28 x 10^4)	598 (6.67 x 10^3)	656 (6.01 x 10^3)
(26b)	426 (3.49 x 10^5)	-	552 (1.57 x 10^4)	599 (9.93 x 10^3)	-
(27a)	421 (2.12 x 10^5)	517 (8.75 x 10^3)	554 (4.98 x 10^3)	592 (2.84 x 10^3)	648 (2.29 x 10^3)
(27b)	423 (6.42 x 10^5)	-	551 (1.99 x 10^4)	592 (6.64 x 10^3)	-
(29)	406 (5.11 x 10^5)	502 (2.10 x 10^4)	536 (6.57 x 10^3)	574 (6.12 x 10^3)	629 (1.85 x 10^3)
(38)	419 (4.28 x 10^5)	514 (1.47 x 10^4)	549 (7.05 x 10^3)	590 (4.46 x 10^3)	646 (3.71 x 10^3)

Figure 54: illustration showing the absorption transitions of the Soret and Q-bands.

Early studies into the effect that 5-membered heterocycles have on the optical properties of porphyrins were attributed to the induction effect of the *meso*-subsituents.[112] It was later deduced that a red shift and broadening of the absorption and fluoresce bands was due to an increase of π-delocalisation (through conjugation) because of stronger resonance interactions

between the porphyrin and 5-membered heterocyclic rings.[113, 114] A red shift in absorption and emission spectra is related to an increase in wavelength and decrease in photon energy, and when a compound is 'red shifted' less energy is required to excite the electrons to a higher state. In an aromatic system, such as a porphyrin, the degree of conjugation in the system greatly effects the shift of absorption peaks; the greater conjugation results in a smaller energy gap between the HOMO and LUMO orbitals. A smaller energy gap between the HOMO-LUMO orbitals results in less energy required to promote an electron to the higher energy state. Hence, if a compound is less conjugated – like compound (29) – then more energy is required to promote the $a_{1u}(\pi) \rightarrow e_{gy}(\pi)$ transitions and therefore the absorption peaks are at a lower wavelength.

Addition of different *meso*-substituents could expand the conjugation of the porphyrin macrocycle. The free-base porphyrins (26a) and (27a) exhibit a Soret band at 421 and 425 nm respectively and are shown to be significantly red shifted in comparison to compound (29) by 15 - 19 nm, which is highlighted in Figure 55, showing just the Soret band. A similar pattern in the shifts of the Q-bands is also seen. Compound (38) was also shown to significantly red shift compared to (29) by 13 nm. However, it was previously stated in section 1.3.5, that the conjugation of this bridging group is limited from rotation of the phenyl group out of the plane of the porphyrin ring, which leads to poor π orbital overlap. The absorption peaks for (26a) and (27a) are 6 nm and 4 nm red shifted respectively to (38) (Figure 55), indicating that there is some improved orbital overlap.
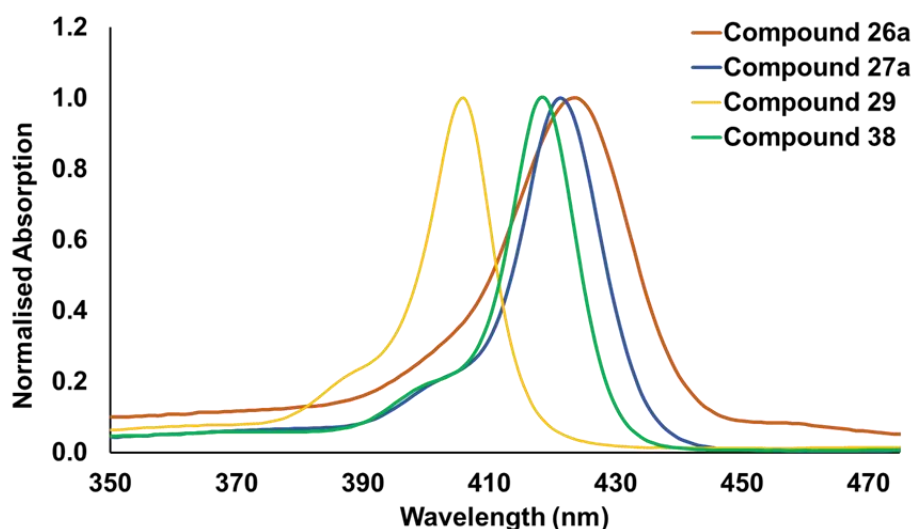
Figure 55: select region of the UV-Visible spectrum for compounds (26a), (27a), (29) and (38) showing the peak separation of the Soret band.

The metallated porphyrins (26b) and (27b) exhibit Soret bands at 423 and 426 nm respectively and are red shifted by 17-20 nm in comparison to the 'unsubstituted' precursor (29), as shown

in Figure 53. The minor changes in Soret band peak shifts, in comparison with their free-base counterparts, are attributed to addition of the metal ion to the porphyrin core. When a porphyrin core is occupied by a metal (in this case Zn(II)), the zinc ion accepts the lone pair electrons of the nitrogen atoms, while the electrons of the zinc ion are donated to the porphyrin molecule. This forms delocalised π bonds that allow for the easy flow of electrons into the π-system, while also increasing the electron density of the porphyrin, which thus reduces the energy for electron transitions to an excited state.[53] Another effect that the metal core has on the porphyrin is seen in the reduction in the number of Q-bands present in the spectra. Which is the result of the symmetry increase of the porphyrin to a D_{4h} symmetry.

3.3.2. Emission Studies

The fluorescence spectra of free-base porphyrins (26a), (27a), (29) and (38) and metallated porphyrins (26b) and (27b) are shown in Figure 56, with the data summarised with the quantum yields in Table 4.

Table 4: emission spectral data of (26a), (26b), (27a), (27b), (29) and (38) in DCM solution. Emission was seen after excitation into the relevant Soret Band.

Porphyrin	Emission (λ_{em}/nm)	Quantum Yield (Φ_f)
(26a)	674	0.067
(26b)	632	0.057
(27a)	660, 723	0.016
(27b)	610, 654	0.045
(29)	636, 698	0.036
(38)	602, 652	0.044
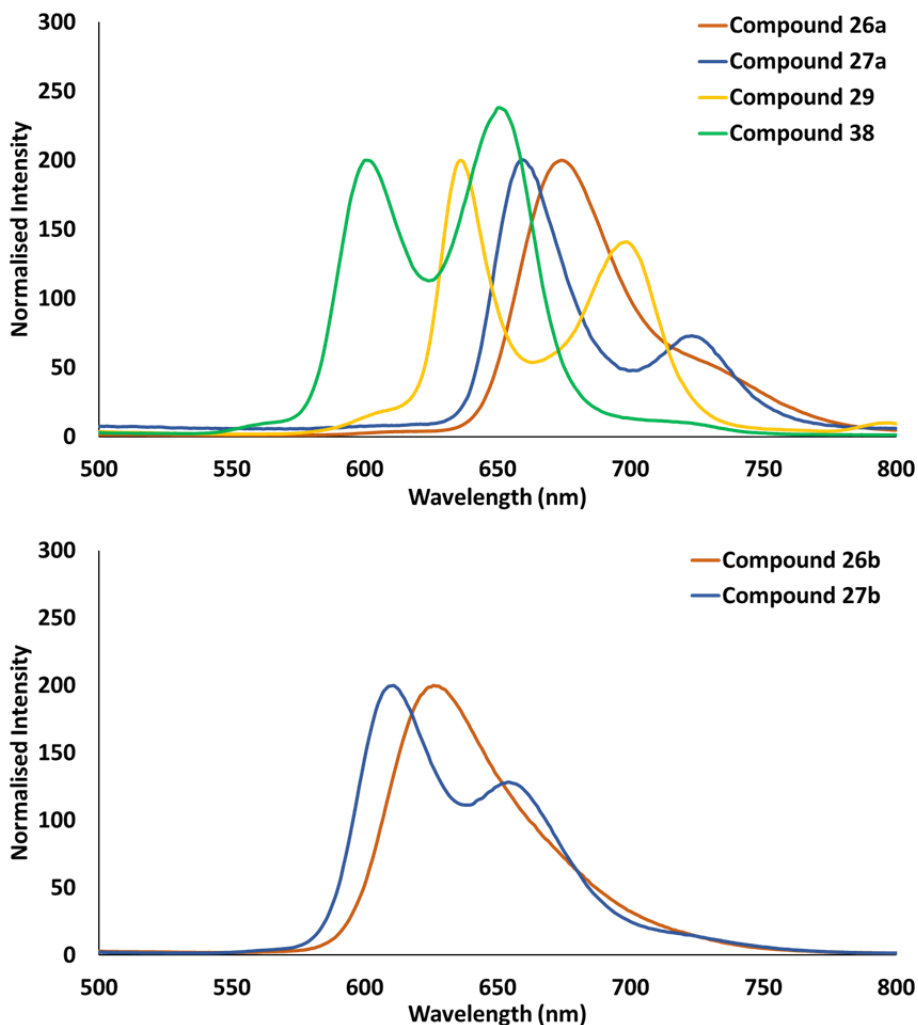
Figure 56: emission spectra of free-base porphyrins (top) and metalloporphyrin (bottom) in DCM solution. Spectra has been formatted to a normalised intensity.

Upon excitation of the Soret band, fast vibrational relaxation back down to the first excited state results in the emission spectra being derived from the Q-bands, according to Kasha's Rule.[115] With the exception of compounds (26a) and (26b), two peaks are seen in the spectra. Compounds (26a) and (27a) continue to show a red shift in peak position in comparison to (29) and (38), which correlates well with the UV-vis data. The emission of compounds (26a) and (27a) show a red shift peak positions by 58-72 nm respectively in comparison with (38), which supports the explanation that the 5-membered rings are increasing the conjugation of the porphyrin system.

The heavy atom effect not only greatly impacts the emission of metalloporphyrin (26b) and (27b) but also compound (27a). Zinc and sulfur atoms are classed as heavy atoms and when they are present in a molecule that fluoresces it can reduce the fluorescence and quantum yields seen in the compounds by enhancing non-radiative pathways. Overall, the quantum yields of these compounds are low, with compound (26a) having the highest value of 0.067.

The furan based porphyrins (26a) and (26b) are slightly higher in value to that of the thiophene based porphyrins (27a) and (27b), which agrees with the heavy atom effect mentioned previously. With exception of compound (27b), compound (29) possess the smallest quantum yield, this again correlates to the overall increase in conjugation of the different *meso*-substituents. Quantum yields are difficult to consistently compare to literature values, while the trends between the literature and these results follow a similar fashion,[53] the values themselves can be vastly different.

3.3.3. Computational Rationalisation

Computational calculations using DFT were employed to gain insight into the electronic communication between the synthesised porphyrins and Mo_2 paddlewheel complexes. The calculations show that in the optimum geometries of the Mo_2-porphyrin conjugates, the aromatic linker group (phenyl, furan, thiophene) are all coplanar with the Mo_2 bond and will allow maximum orbital overlap between the Mo_2-δ orbitals and the ligand π system. Crucially however, the dihedral angles between the linker and the porphyrin are not planar and so a disruption of the communication between the Mo_2-δ orbitals and porphyrin will be observed. The presence of the Mo_2 groups in the calculations is unlikely to provide any steric influence on the dihedral angle between the linker and the porphyrin so these calculations can therefore provide a reasonable explanation of the observed spectral data for the free porphyrins above. The steric requirements for the 5-membered heterocyclic rings are smaller compared to the 6-membered phenyl group. This means that there is greater opportunity for effective overlap of the π-orbitals in the system because of a reduced energy barrier between the porphyrin and bridging unit. According to the calculations, the dihedral angles between the porphyrin and the linker decrease in order of phenyl bridge (65°) > thiophene bridge (63°) > furan bridge (47°), and this correlates with the red shift pattern in the spectral data, illustrating that there is a greater scope of conjugation throughout the system. Theoretically an alkyne bridge will have a dihedral angle of 14°, which means that the spectral data would possibly show the greatest red shift in comparison of the other bridges. It also indicates a greater degree of 'free' rotation.

Molecular orbital diagrams may give insight into the level of delocalisation of a paddlewheel porphyrin conjugate, the extent of the electron density on the bridging unit correlates to the level of extended conjugation that the conjugates process. For the paddlewheel porphyrin conjugate with phenyl linker there is very little electron density on the bridging unit at HOMO-1 and HOMO, while comparison with the furan and thiophene based units shows an improvement, Figure 57. The apparent increase of electron density on the furan and thiophene bridging units indicate that these compounds have a greater extent of conjugation though the

Mo$_2$-PWPC. Which agrees to the idea that the smaller the dihedral angle increases conjugation.
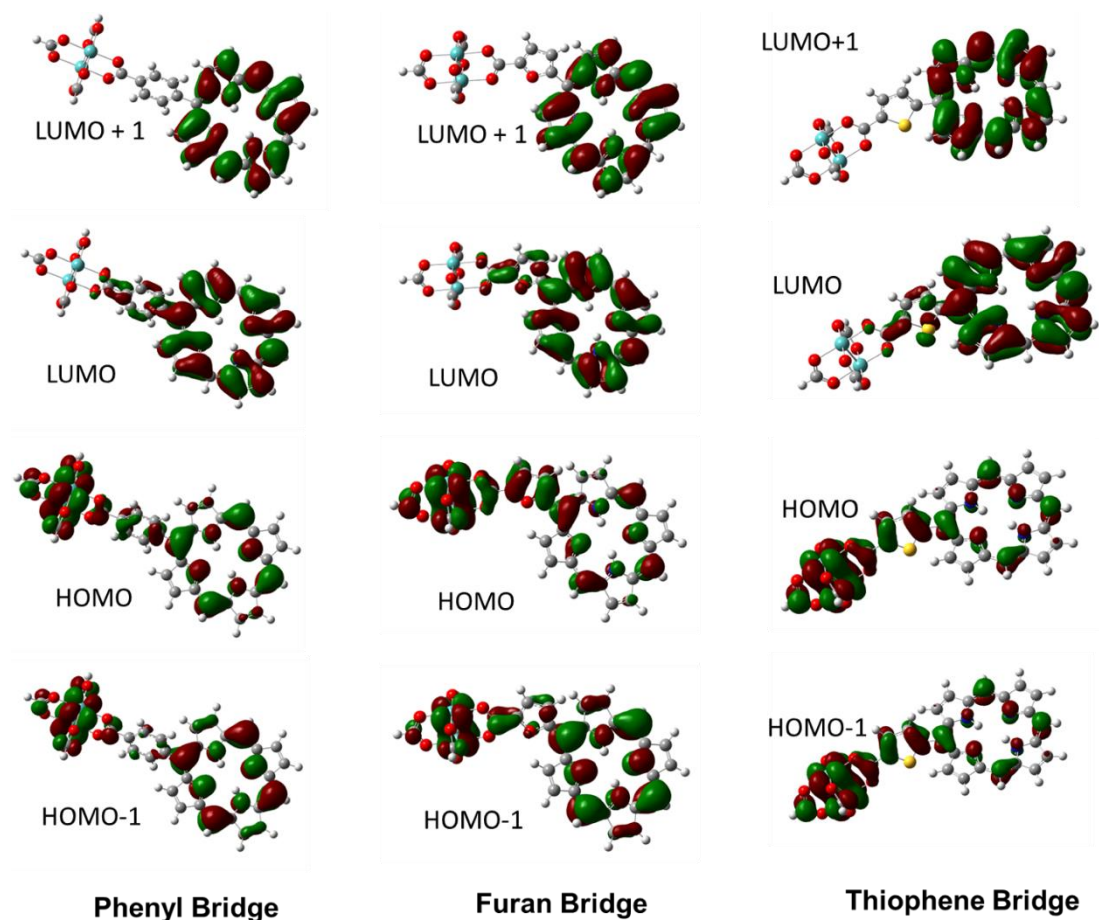
Figure 57: molecular orbitals of Mo2-PWPC with varying bridging units.

4. Conclusion and Future Work

Through this project, a new synthetic procedure was developed for the synthesis of compound (33). Assisting the Lindsey [2+2] condensation method with zinc templatation lead to great success at improving the yields in the initial synthesis of the porphyrin precursor, in comparison to the synthesis of (29), the yield was almost double. This early success led to significant ease in synthesising the halogenated porphyrins required for the different cross-coupling reactions. From that synthesis a series of porphyrins with varying *meso*-substituents produced four novel products, compounds (26a), (26b), (27a) and (27b) of varying yields. UV-vis spectroscopic data show that there is significant red shift between the Soret bands of the porphyrin containing phenyl *meso*-substituents (38) and the 5-membered rings (26) and (27). This led to the conclusion that there has been an extension to the conjugation of the porphyrin macrocycle. Despite assumptions that the thiophene group may produce more significant red

shifting of the Soret band, because inclusion of sulphur into the backbone of a conjugated linker tends to lower the LUMO energy by a small amount because the orbital overlap is better for S-Carbon than O-Carbon (sulfur is a bigger atom). This was not the case. In fact there was almost no difference between the furan and thiophene based *meso*-substituents of compounds (26a) and (27a). Emission studies matched the UV-vis spectroscopic data. Overall it was shown that the different *meso*-substituents decrease the dihedral angle between the porphyrin and bridging unit.

Future work would involve working towards clearer identification and synthesis of compound (34); it would be beneficial to determine if that specific structure, for which there is possibility of 'free-rotation' around the C-C bond, shows better extended conjugation to that of the porphyrins that have been made. As stated previously theoretically (based on DFT calculations) the alkyne bridging group has the smallest dihedral angle of 14°, and with this small angle it should possess the greatest extent of conjugation between the paddlewheel and porphyrin units. Optimization of the Suzuki-Miyaura reactions is also needed and further study into the lifetimes of the synthesised porphyrins will indicate whether the low fluorescence and quantum yields were due to other transitions (phosphorescence) taking place. Tethering a paddlewheel unit to the synthesized porphyrins and studying the photophysical and electrochemical properties of these conjugates is the obvious next step in quantifying the effect that the different bridging units have.

5. Experimental

5.1. Materials

Unless stated all reagents were obtained from commercial sources and used as received without further purification. 5,15-*bis*-(4-COOMephenyl)-10,20-diphenylporphyrin, compound (38), was synthesised by a previous BSc student, Imogen Walsh. Anhydrous tetrahydrofuran (THF) and dichloromethane (DCM) were obtained from Innovative Inc. PureSolv® solvent purification system. Pyrrole (Alfa Aesar) was dried over calcium hydride and freshly distilled before use. Methyl tert-butyl ether (MTBE) was stored under an inert atmosphere. All reactions involving inert atmospheric conditions were performed using standard Schlenk line techniques.

5.2. Instrumentation and Methods

^{1}H, ^{13}C and ^{11}B NMR spectra were recorded on JEOL ECX400 or JEOL ECS400 spectrometer, operating at 400 MHz, 101 MHz and 128 MHz respectively. All spectral data were acquired at 298 K and ^{1}H and ^{11}B NMR were recorded with proton decoupling. Chemical shifts are reported as parts per million (ppm) and coupling constants (J) are reported in hertz (Hz). The residual solvent peaks: δ_H 7.27 and δ_C 77.16 for CDCl$_3$, δ_H 2.50 for d_6-DMSO, were used as reference. The multiplicity abbreviations used: br broad, s singlet, d doublet, m multiplet. ^{13}C NMR peak assignments were only given where definitive assignment could be made with assistance from 2D NMR. Mass-spectra were obtained by the University of York Mass Spectrometry Service, using atmospheric pressure chemical ionisation (APCI) and electrospray ionisation (ESI) on a Bruker compact® time of flight mass spectrometer. Microwave assisted synthesis was conducted on a CEM Discover SP in thick walled vials. Infrared (IR) spectra were recorded on a PerkinElmer UATR 2 spectrometer as a thin layer dispersed from DCM solution; data points are reported in cm^{-1}. UV/Visible spectra were measured in DCM on a Shimadzu UV-1800 UV-Visible Spectrophotometer, using a 1 cm quartz cell. λ_{max} were reported in nm and molar extinction coefficients (ε) are reported in M^{-1} cm^{-1}. Emission spectra were measured on a Hitachi F-4500 fluorimeter, employing an Xe lamp, at room temperature. Fluorescence quantum yields (Φ_f) for the compounds (26a), (26b), (27a), (27b), (29) and (38) were calculated in aerated DCM solutions, using [Ru(bpy)$_3$][PF$_6$]$_2$ in aerated water as a standard (Φ_f = 0.04)[116], according to equation.[116]

$$\phi_a = (I_a/I_b)\,(A_b/A_a)\,(n_a/n_b)^2 \times \phi_b$$

Where 'a' refers to the sample and 'b' to the standard; I is the integrated intensity of the spectrum; A is the absorbance at λ_{ex}; Φ_f is the fluorescence quantum yield in the solvent of choice; n is the refractive index of the solvent.

5.3. Synthesis

5.3.1. Dipyrromethane (28)
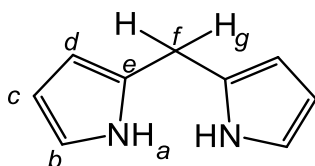
A suspension of formaldehyde (2.152 g, 71.66 mmol) in dry pyrrole (500 mL) was degassed under a flow of nitrogen and kept in the dark. Indium chloride (1.225 g, 5.538 mmol) was added, and the mixture was heated to 55 °C for 2.5 h. The reaction vessel was removed from the heat and quenched by addition of solid sodium hydroxide (8.591 g, 214.6 mmol) and stirred for an additional hour. The cooled solution was filtered, and the filtrate concentrated until an orange oil remained and the pyrrole recovered. The oil was extracted with 20 % ethyl acetate/hexanes (100 mL) and washed with water (75 mL). The solvent was removed under reduced pressure and the residue triturated with petroleum ether (40-60 °C) to afford an orange solid (7.245 g, 49.59 mmol, 69 % yield).

¹H NMR: (400 MHz, CDCl₃) δ$_H$: **a** 7.82 (s, 2H, 2 x NH), **b** 6.65 (m, 2H, 2 x CH), **c** 6.14 (m, $^3J_{H\text{-}H}$ = 2.9, 2H, CH), **d** 6.03 (m, 2H, 2 x CH), **g** 3.97 (s, 2H, CH_2).

¹³C NMR (101 MHz, CDCl₃) δ$_C$: **e** 129.4 (2 x CH), **b** 117.5 (2 x CH), **c** 108.4 (2 x CH), **d** 106.6 (2 x CH), **f** 26.4 (1 x CH₂).

ESI-MS: calc. for $C_9H_{11}N_2$ [M+H]⁺ m/z 147.0917, found m/z 147.0917 [M+H]⁺.

IR (FTIR): 3369, 1563, 1469, 1421, 1313, 1255, 1113, 1088, 1023, 984, 788, 708, 646, 539.

5.3.2. *Trans*-5,15-diphenylporpyrin (29)
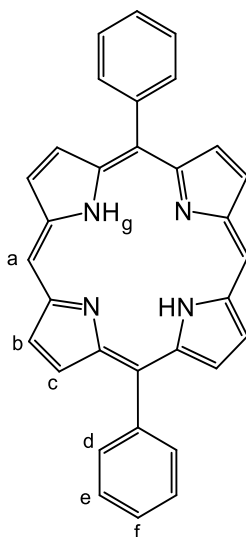
Dipyrromethane (0.288 g, 1.97 mmol) and BF$_3$(OEt$_2$) (0.07 mL, 0.6 mmol) were added to dry DCM, followed by dropwise addition (over 10 minutes) of benzaldehyde (0.22 mL, 2.1 mmol). The solution was stirred at room temperature for 3 h, before addition of *p*-chloranil (0.475 g, 1.97 mmol) and the resulting red solution was heated at reflux for 1 h. The solution was cooled and concentrated under reduced pressure. The crude product was passed through a silica plug (DCM) before purification by column chromatography (silica-gel, 6:4 DCM : petroleum ether (40-60 °C)). The sample was finally recrystallised (DCM/hexanes) to give a purple solid (0.089 g, 0.192 mmol, 19 % yield).

^{1}H NMR (400 MHz, CDCl$_3$) δ$_H$: **a** 10.32 (s, 2H, 2 x C*H*), **b** 9.38 (d, $^3J_{H-H}$ = 4.9, 4H, 4 x C*H*), **c** 9.09 (d, $^3J_{H-H}$ = 4.4, 4H, 4 x C*H*$_\beta$), **e** 8.26 (m, 4H, 4 x C*H*), **d/f** 7.80 (m, 6H, 6 x C*H*), **g** -3.12 (s, 2H, 2 x N*H*).

^{13}C NMR (101 MHz, CDCl$_3$) δ$_C$: 147.3, 145.3, 141.3, 135.0, 131.7, 131.2, 127.8, 127.1, 119.2, 105.4.

APCI-MS: calc. for C$_{32}$H$_{23}$N$_4$ [M+H]$^+$ m/z 463.1917, found m/z 463.1921 [M+H]$^+$.

UV/Vis (CHCl$_3$): λ$_{max}$ (ε) = 406 (5.11 x 10^8), 502 (2.10 x 10^7), 536 (6.57 x 10^6), 574 (6.12 x 10^6), 629 (1.85 x 10^6).

IR (FTIR): 2962, 2924, 1259, 1086, 1014, 956, 853, 725, 737, 699.

5.3.3. Zinc (II) *trans*-5,15-diphenyl porphyrin (33)
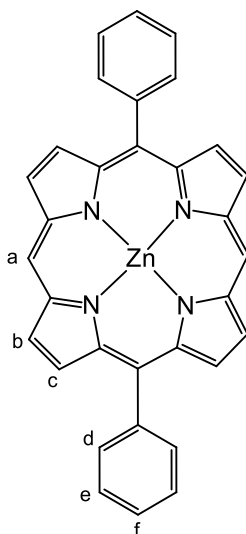
Dipyrromethane (0.972 g, 6.65 mmol) and benzaldehyde (0.80 mL, 5.2 mmol) were added to degassed DCM (800 mL) and stirred for a few minutes before addition of of $BF_3(OEt_2)$ (0.16 mL, 1.3 mmol) and $Zn(OAc)_2$ (2.747 g, 14.97 mmol). The solution was stirred at room temperature for 3 h in darkness, before addition of *p*-chloranil (1.826 g, 7.427 mmol) and the resulting red solution was heated at reflux for 1 h. The solution was cooled and concentrated under reduced pressure. The crude product was passed through a silica plug to remove the majority of the polypyrroles tar (DCM) before further purification by column chromatography (silica-gel, 6:4 DCM). If necessary, the sample was washed with hexane to remove grease and yield a red/maroon solid (0.911 g, 1.97 mmol, 66 % crude yield).

1H NMR (400 MHz, CDCl_3) δ_H: **a** 10.31 (s, 2H, 2 x C*H*), **b** 9.42 (d, $^3J_{H-H}$ = 4.5, 4H, 4 x C*H*), **c** 9.14 (d, $^3J_{H-H}$ = 4.4, 4H, 4 x C*H*), **e** 8.26 (m, 4H, 4 x C*H*), **d/f** 7.80 (m, 6H, 6 x C*H*).

APCI-MS: calc. for $C_{32}H_{21}N_4Zn$ [M+H]$^+$ m/z 525.1052, found m/z 525.1043 [M+H]$^+$.

IR (FTIR): 3394, 1408, 1306, 1199, 1064, 994, 882, 856, 734, 724, 701.

5.3.4. 5-bromo-*trans*-10,20-diphenylporpyrin (31)
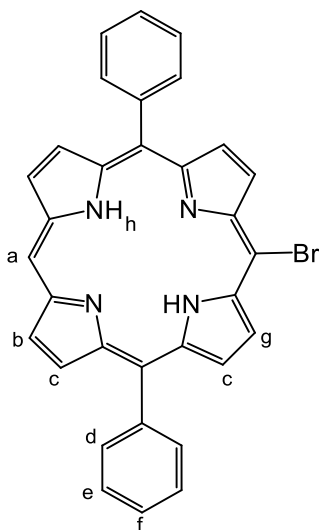
5,15-diphenylporphyrin (0.100 g, 0.216 mmol) was dissolved in chloroform (100 mL) and cooled to 0 °C. Pyridine (0.4 mL), followed by N-bromosuccinimide (0.039 g, 0.216 mmol) were added to the cooled flask. The reaction was followed by TLC (1:1 DCM /hexane) until completion. The reaction was quenched with acetone (8 mL) and the solvent removed under reduced pressure. The crude product was separated by flash column chromatography (silica-gel, 6:4 DCM : petroleum ether (40-60 °C)). If necessary, the product was purified by recrystallisation (DCM/ petroleum ether (40-60 °C)) to give a dark purple solid (0.062 g, 0.114 mmol, 52 % yield).

^{1}H NMR (400 MHz, CDCl$_3$) δ$_H$: **a** 10.16 (s, 1H, C*H*), **g** 9.74 (d, $^3J_{H-H}$ = 5.3, 2H, 2 x C*H*), **b** 9.28 (d, $^3J_{H-H}$ = 4.8, 2H, 2 x C*H*), **c** 8.89 (m, 4H, 4 x C*H*), **e** 8.20 (m, 4H, 4 x C*H*), **d/f** 7.79 (m, 6H, 6 x C*H*), **h** -3.11 (s, 2H, 2 x N*H*).

^{13}C NMR (101 MHz, CDCl$_3$) δ$_C$: 141.5, 138.5, 135.6, 134.8, 128.0, 127.0, 120.4, 105.7.

APCI-MS: calc. for C$_{32}$H$_{22}$^{79}BrN$_4$ [M+H]$^+$ m/z 541.1022, found m/z 541.1029 [M+H]$^+$.

UV/Vis (CHCl$_3$): λ$_{max}$ (ε) = 414 (4.07 x 10^8), 511 (1.79 x 10^7), 545 (5.93 x 10^6), 587 (5.14 x 10^6), 643 (2.60 x 10^6).

IR (FTIR): 2209, 2972, 963, 792, 723, 700.

5.3.5. *Trans*-5,15-dibromo 10,20-diphenyl porphyrin (30)
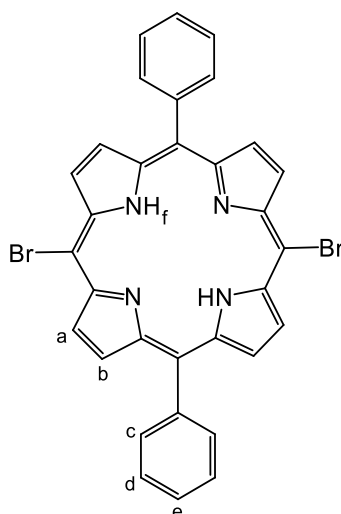
Trans-5,15-diphenylporphyrin (0.198 g, 0.427 mmol) was dissolved in chloroform (100 mL) and cooled to 0 °C. Pyridine (0.4 mL), followed by N-bromosuccinimide (0.159 g, 0.894 mmol) were added to the cooled flask. The reaction was followed by TLC (1:1 DCM /hexane) until completion. The reaction was quenched with acetone (8 mL) and the solvent removed under reduced pressure. The product was washed with methanol and purified by recrystallisation (DCM/ petroleum ether (40-60 °C)) to give a dark purple solid (0.210 g, 0.307 mmol, 69 % yield).

^{1}H NMR (400 MHz, CDCl$_3$) δ$_H$**: a** 9.60 (d, $^3J_{H\text{-}H}$ = 4.9, 4H, 4 x C*H*), **b** 8.82 (d, $^3J_{H\text{-}H}$ = 4.4, 4H, 4 x C*H*), **d** 8.14 (m, 4H, 4 x C*H*), **c/e** 7.78 (m, 6H, 6 x C*H*), **f** -2.25 (s, 2H, 2 x N*H*).

^{13}C NMR (101 MHz, CDCl$_3$) δ$_C$: 143.9, 134.5, 126.9, 125.1.

APCI-MS: calc. for C$_{32}$H$_{21}$^{79}Br$_2$N$_4$ [M+H]$^+$ m/z 619.0274, found m/z 619.0140 [M-H]$^+$.

UV/Vis (CHCl$_3$): λ$_{max}$ (ε) = 420 (3.05 x 10^8), 520 (1.28 x 10^7), 555 (9.17 x 10^6), 599 (4.58 x 10^6), 657 (4.05 x 10^6).

IR (FTIR): 1463, 1334, 996, 960, 793, 789, 736, 694.

5.3.6. Zinc (II) *trans*-5,15-dibromo 10,20-diphenyl porphyrin (33)
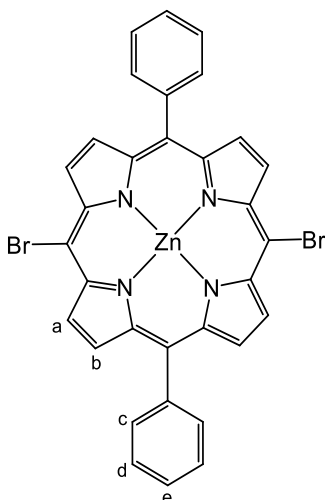
In a 10 mL thick-walled glass tube, *trans*-5,15-dibromo-10,20-diphenylporphyrin (0.100 g, 0.161 mmol) and zinc acetate (0.181 g, 0.986 mmol) was dissolved in DMF (6 mL). The vessel was sealed and placed in the microwave. The microwave was set to 300 W and the reaction vessel was heated to 180 °C and stirred for 30 min. The vessel was cooled and solvent was removed under reduced pressure. The solid was extracted in DCM (30 mL) and washed with aqueous $NaHCO_3$ (3 x 25 mL). The organic layer was dried with a brine wash and solvent removed under reduced pressure, leaving a green/purple solid (0.070 g, 0.102 mmol, 63 %).

^{1}H NMR (DMSO, 298 K, 400 MHz) δ_H: **a** 9.58 (d, $^3J_{H-H}$ = 5.2, 4H, 4 x C*H*), **b** 8.75 (d, $^3J_{H-H}$ = 6.9, 4H, 4 x C*H*), **d** 8.11 (m, 4H, 4 x C*H*), **c/e** (m, 6H, 6 x C*H*).

APCI-MS: calc. for $C_{32}H_{20}N_4{}^{79}Br_2Zn$ [M+H]$^+$ m/z 680.9262, found m/z 680.9278 [M+H]$^+$.

UV/Vis (CHCl$_3$): λ_{max} (ε) = 423 (2.15 x 10^8), 554 (7.01 x 10^6), 594 (2.36 x 10^6).

IR (FTIR): 1709, 1334, 996, 960, 793, 784, 736, 694.

5.3.7. General procedure A, for C-H activated borylation

[Ir(COD)(OMe)]$_2$ (1.5 mol%), 4,4'-di-tert-butyl-2,2'-bipyridine (dtbpy) (3.0 mol%) and *bis*(pinacolato)diboron (0.5 equiv) were added to a reaction vessel fitted with a condenser and placed under a nitrogen atmosphere. Dry MTBE (6 mL) was added, followed by the chosen furan/thiophene (1 equiv) and the mixture stirred at 55 °C for 1-3 h. The reaction vessel was cooled, and the solvent removed under reduced pressure followed by recrystallization.

5.3.7.1. Methyl 5-(4,4,5,5-tetramethyl-1,3,2-dioxaborolan-2-yl)-2-furancarboxylate (35)
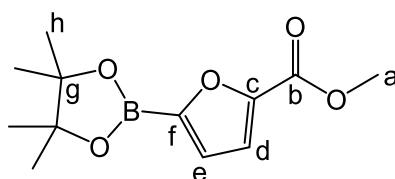
Compound (35) was synthesized according to general procedure A using [Ir(COD)(OMe)]$_2$ (0.040 g, 0.060 mmol), dtbpy (0.032 g, 0.12 mmol), *bis*(pinacolato)diboron (0.504 g, 1.99 mmol) and methyl 2-furate (0.42 mL, 4.0 mmol) and MTBE (12 mL), with a reaction time of 3 h. Recrystallization from hot toluene yielded an orange solid (0.514 g, 2.03 mmol, 51 % yield).

^{1}H NMR (400 MHz, CDCl$_3$) δ$_H$**: d** 7.17 (d, $^3J_{H-H}$ = 3.7, 1H, C*H*), **e** 7.05 (d, $^3J_{H-H}$ = 3.7, 1H, C*H*), **a** 3.87 (s, 3H, C*H$_3$*), **h** 1.32 (s, 12H, 4 x C*H$_3$*).

^{13}C NMR (101 MHz, CDCl$_3$) δ$_C$: **b** 159.2 (1 x C_q), **c/f** 148.5 (2 x C_q), **e** 124.1 (1 x C*H*), **d** 118.0 (1 x C*H*), **g** 84.3 (1 x C_q), **a** 52.1 (1 x C*H$_3$*), **h** 24.8 (4 x C*H$_3$*).

^{11}B NMR (128 MHz, CDCl$_3$) δ$_B$: 27.7 (brs, 1 x B).

ESI-MS: calc. for C$_{12}$H$_{18}$BO$_5$ [M+H]$^+$ m/z 253.1242, found m/z 253.1253 [M+H]$^+$.

IR (FTIR): 2979, 1726, 1575, 1536, 1435, 1381, 1358, 1328, 1286, 1208, 1139, 1111, 1018, 988, 965, 925, 851, 819, 765, 713, 699, 667, 602, 577.

5.3.7.2. Methyl 5-(4,4,5,5-tetramethyl-1,3,2-dioxaborolan-2-yl)-2-thiophene-carboxylate (36)
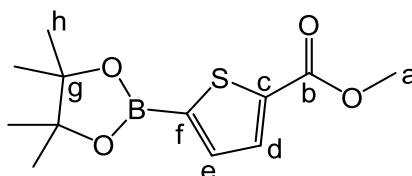
The compound was synthesized according to general procedure A using [Ir(COD)(OMe)]$_2$ (0.036 g, 0.050 mmol), dtbpy (0.028 g, 0.11 mmol), *bis*(pinacolato)diborane (0.451 g, 1.76 mmol) and methyl 2-thiophenecarboxylate (0.41 mL, 3.5 mmol) and MTBE (12 mL), with a reaction time of 2 h. Addition of hexane yielded an orange precipitate (0.531 g, 1.98 mmol, 56 % yield).

^{1}H NMR (400 MHz, CDCl$_3$) δ_H: **d** 7.79 (d, $^3J_{H\text{-}H}$ = 3.5, 1H, C*H*) **e** 7.56 (d, $^3J_{H\text{-}H}$ = 3.8, 1H, C*H*), **a** 3.87 (s, 3H, C*H$_3$*), **h** 1.33 (s, 12H, 4 x C*H$_3$*)

^{13}C NMR (101 MHz, CDCl$_3$) δ_C: **b** 162.7 (1 x C_q), **c/f** 140.1 (2 x C_q), **e** 136.9 (1 x C*H*), **d** 133.9 (1 x C*H*), **g** 84.6 (1 x C_q), **a** 51.5 (1 x C*H$_3$*), **h** 24.7 (4 x C*H$_3$*).

^{11}B NMR (128 MHz, CDCl$_3$) δ_B: 27.9 (brs, 1 x B).

APCI-MS: calc. for C$_{12}$H$_{18}$BO$_4$S [M+H]$^+$ m/z 269.1013, found m/z 269.1010 [M+H]$^+$.

IR (FTIR): 2972, 1714, 1526, 1460, 1442, 138, 1372, 1345, 1289, 1269, 1241, 1193, 1141, 1096, 1056, 1016, 960, 851, 823, 752, 664, 564, 522.

5.3.8. General Procedure B, for Suzuki-Miyaura cross-coupling

In a reaction vessel fitted with a condenser, porphyrin (1.0 equiv), boronic ester (5 equiv), K$_2$PO$_4$ (18 equiv) and [Pd(PPh$_3$)$_4$] (14.5 mol%) were added, placed under a nitrogen atmosphere and dissolved in dry THF (40 mL). The reaction was stirred at 80 °C to completion (at least 20 h) as determined by TLC (DCM). The solution was cooled to room temperature and the solvent removed under reduced pressure. The residue was extracted into CH$_2$Cl$_2$ and washed with saturated aqueous NaHCO$_3$ and H$_2$O; the organic layer was dried with brine and the solvent removed under reduced pressure. The crude product was purified by flash column chromatography (silica) and washed with cold hexane.

5.3.8.1. *Trans*-5,15-di(methyl furan-2-carboxylate)10,20-diphenyl porphyrin (26a)
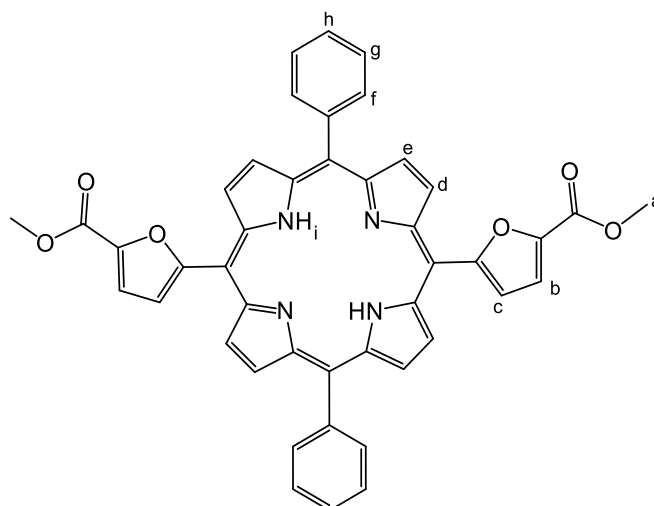
Compound (26a) was synthesised according to general procedure B, using 0.101 g of compound (35) (0.147 mmol), 0.124 g methyl 5-(4,4,5,5-tetramethyl-1,3,2-dioxaborolan-2-yl)furan-2-carboxylate (0.491 mmol), 0.475 g K_2PO_4 (2.24 mmol) and 0.030 g of [Pd(PPh$_3$)$_4$] (0.026 mmol) and 50 mL of THF, with a reaction time of 24 h. Column chromatography (silica gel: DCM) yielded a purple solid (0.012 g, 0.022 mmol, 10 % yield).

¹H NMR: (400 MHz, CDCl$_3$) δ_H: **e** 9.14 (d, $^3J_{H-H}$ = 5.5, 4H, 4 x C*H*), **d** 8.91 (d, $^3J_{H-H}$ = 4.1, 4H, 4 x C*H*), **f** 8.22 (d, $^3J_{H-H}$ = 8.3, 4H, 4 x C*H*), **c/f/h** 7.77 (overlayed m, 8H, 8 x C*H*), **b** 7.38 (d, $^3J_{H-H}$ = 4.1, 2H, 2 x C*H*), **a** 4.04 (s, 6H, 2 x C*H*$_3$), **i** -2.76 (s, 2H, 2 x N*H*).

¹³C NMR (101 MHz, CDCl$_3$) δ_C: 158.3, 145.5, 141.8, 134.7, 132.2, 130.1, 128.1, 127.0, 121.7, 119.6, 118.5, 51.98.

APCI-MS: calc. for $C_{44}H_{31}N_4O_6$ [M+H]$^+$ m/z 711.2238, found m/z 711.2210 [M+H]$^+$.

UV/Vis (CHCl$_3$): λ_{max} (ε) = 427 (3.58 x 10^8), 520 (1.33 x 10^7), 562 (1.28 x 10^7), 598 (6.67 x 10^6), 656 (6.01 x 10^6).

Fluorescence (CHCl$_3$): λ_{em} at excitation 419 nm: 674 nm.

Quantum Yield (CHCl$_3$): Φ_a = 0.067.

IR (FTIR): 2924, 1726, 1302, 1205, 1139, 971, 799, 729, 702.

5.3.8.2. Zinc (II) *trans*-5,15-di(methyl furan-2-carboxylate)10,20-diphenyl porphyrin (26b)
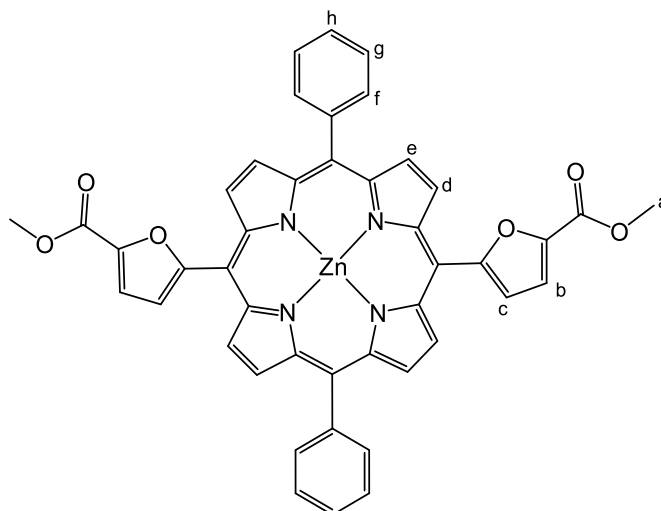
Compound (26b) was synthesised according to general procedure B, using 0.051 g of compound (35) (0.073 mmol), 0.075 g methyl 5-(4,4,5,5-tetramethyl-1,3,2-dioxaborolan-2-yl)furan-2-carboxylate (0.29 mmol), 0.236 g K_2PO_4 (1.09 mmol) and 0.010 g of [Pd(PPh$_3$)$_4$] (0.088 mmol) and 50 mL of THF, with a reaction time of 48 h. Column chromatography (silica gel: DCM) yielded a green/purple solid (0.016 g, 0.020 mmol, 35 % yield).

^{1}H NMR: (400 MHz, CDCl$_3$) δ_H: **e** 9.20 (d, $^3J_{H-H}$ = 4.6, 4H, 4 x C*H*), **d** 9.00 (d, $^3J_{H-H}$ = 4.8, 4H, 4 x C*H*), **f** 8.20 (d, $^3J_{H-H}$ = 5.9, 4H, 4 x C*H*), **c/f/h** 7.78 (overlayed m, 8H, 8 x C*H*), **b** 7.37 (d, $^3J_{H-H}$ = 3.44, 2H, 2 x C*H*), **a** 3.99 (s, 6H, 2 x C*H$_3$*).

^{13}C NMR (101 MHz, CDCl$_3$) δ_C: 159.1, 145.3, 142.4, 134.6, 133.2, 131.5, 127.9, 126.9, 119.6, 117.8, 52.2.

APCI-MS: calc. for C$_{44}$H$_{29}$N$_4$O$_6$Zn [M+H]$^+$ m/z 773.1373, found m/z 773.1349 [M-H]$^+$.

UV/Vis (CHCl$_3$): λ_{max} (ε) = 426 (3.49 x 10^8), 552 (1.57 x 10^7), 599 (9.93 x 10^6).

Fluorescence (CHCl$_3$): λ_{em} at excitation 422 nm: 632 nm.

Quantum Yield (CHCl$_3$): Φ_a = 0.082.

IR (FTIR): 2950, 1720,1485, 1303, 1139, 1002, 795, 718.

5.3.8.3. T*rans*-5,15-di(methyl thiophene-2-carboxylate)10,20-diphenyl porphyrin (27a)
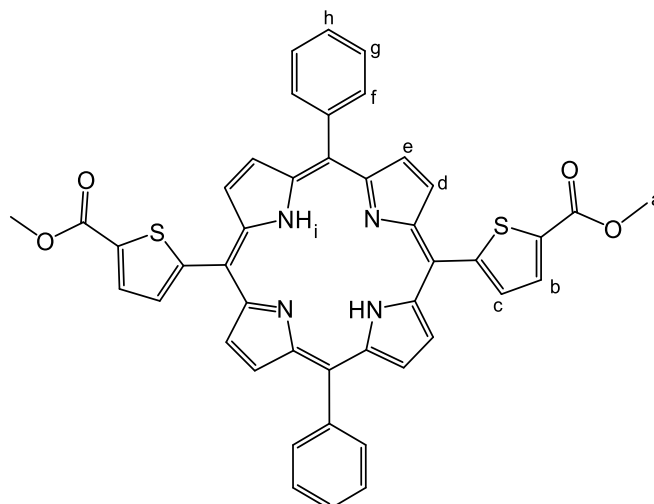
Compound (27a) was synthesised according to general procedure B, using 0.042 g of compound (36) (0.068 mmol), 0.086 g methyl 5-(4,4,5,5-tetramethyl-1,3,2-dioxaborolan-2-yl)thiophene-2-carboxylate (0.32 mmol), 0.248 g K_2PO_4 (1.22 mmol) and 0.012 g of [Pd(PPh$_3$)$_4$] (0.010 mmol) and 50 mL of THF, with a reaction time of 24 h. Column chromatography (silica gel: DCM) yielded a purple solid (0.022 g, 0.029 mmol, 43 % yield).

^{1}H NMR (400 MHz, CDCl$_3$) δ$_H$**: e** 9.03 (d, $^3J_{H-H}$ = 3.6, 4H, 4 x C*H*), **d** 8.86 (d, $^3J_{H-H}$ = 4.3, 4H, 4 x C*H*), **c/g** 8.18 (overlayed m, 6H, 6 x C*H*), **b** 7.92 (d, $^3J_{H-H}$ = 3.8, 2H, 2 x C*H*), **f/h** 7.78 (m, 6H, 6 x C*H*), **a** 4.01 (s, 6H, 2 x C*H$_3$*), **i** - 2.11 (s, 2H, 2 x N*H*).

^{13}C NMR (101 MHz, CDCl$_3$) δ$_C$: 163.1, 150.2, 141.7, 135.6, 134.6, 134.5, 132.5, 128.1, 126.9, 121.5, 110.5, 52.5.

APCI-MS: calc. for C$_{44}$H$_{31}$N$_4$O$_4$S$_2$ [M+H]$^+$ m/z 743.1781, found m/z 743.1806 [M+H]$^+$.

UV/Vis (CHCl$_3$): λ$_{max}$ (ε) = 421 (2.12 x x 10^8), 517 (8.75 x 10^6), 554 (4.98 x 10^6), 592 (2.84 x 10^6), 648 (2.29 x 10^6).

Fluorescence (CHCl$_3$): λ$_{em}$ at excitation 418 nm: 659 and 722 nm.

Quantum Yield (CHCl$_3$): Φ$_a$ = 0.016.

IR (FTIR): 2922, 1718, 1453, 1257, 1095, 997, 798, 748, 724.

5.3.8.4. Zinc (II) *trans*-di(methyl thiophene-2-carboxylate)10,20-diphenyl porphyrin (27b)
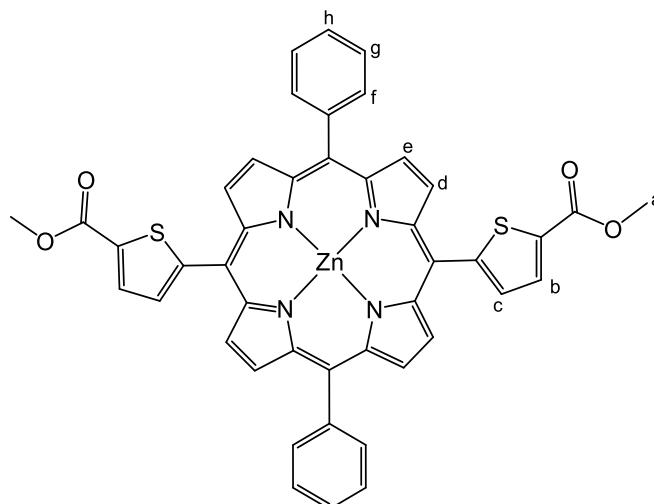
Compound (27b) was synthesised according to general procedure B, using 0.049 g of compound (36) (0.072 mmol), 0.073 g methyl 5-(4,4,5,5-tetramethyl-1,3,2-dioxaborolan-2-yl)thiophene-2-carboxylate (0.27 mmol), 0.260 g K_2PO_4 (1.23 mmol) and 0.010 g of [Pd(PPh$_3$)$_4$] (0.009 mmol) and 50 mL of THF, with a reaction time of 48 h. Column chromatography (silica gel: DCM) yielded a pink/pale purple solid (0.013 g, 0.016 mmol, 22 % yield).

^{1}H NMR (400 MHz, CDCl$_3$) δ_H**: e** 9.11 (d, $^3J_{H\text{-}H}$ = 4.1, 4H, 4 x C*H*), **d** 8.95 (d, $^3J_{H\text{-}H}$ = 4.1, 4H, 4 x C*H*), **c/g** 8.19 (overlayed m, 6H, 6 x C*H*), **b** 7.89 (d, $^3J_{H\text{-}H}$ = 4.2, 2H, C*H*), **f/h** 7.77 (m, 6H, 6 x C*H*), **a** 4.01 (s, 6H, 2 x C*H$_3$*).

^{13}C NMR (101 MHz, CDCl$_3$) δ_C: 161.8, 138.5, 136.5, 134.1, 131.6, 126.2, 117.4, 52.3.

APCI-MS: calc. for $C_{44}H_{29}N_4O_4S_2Zn$ [M+H]$^+$ m/z 805.0916, found m/z 805.0874 [M+H]$^+$.

UV/Vis (CHCl$_3$): λ_{max} (ε) = 423 (6.42 x 10^8), 551 (1.99 x 10^7), 592 (6.64 x 10^6).

Fluorescence (CHCl$_3$): λ_{em} at excitation 419 nm: 610 and 655 nm.

Quantum Yield (CHCl$_3$): Φ_a = 0.045.

IR (FTIR): 2931, 1692, 1455, 1257, 1097, 1002, 978, 794, 753, 696.

6. References

1. NASA Global Climate Change, https://climate.nasa.gov/faq/16/is-it-too-late-to-prevent-climate-change/, (accessed 16/11/2022).

2. United Nations Framework Convention on Climate Change, https://unfccc.int/process-and-meetings/the-paris-agreement/the-paris-agreement, (accessed 11/11/2022).

3. Department for Business, Energy & Industrial Strategy, 2021, Net Zero Strategy: Build Back Greener, Her Majesty's Stationery Office (HMSO), 1-368.

4. Our World in Data, https://ourworldindata.org/sources-global-energy, (accessed 16/11/2022).

5. D. Archer, *Global Warming: Understanding the Forecast.*, John Wiley & Sons, Danvers, 2011.

6. IEA, Solar PV, https://www.iea.org/reports/solar-pv, (accessed 16/11/2022).

7. K. Pawlus and T. Jarosz, *Appl. Sci.*, 2022, **12**, 3442.

8. G. Reginato, M. Calamante, L. Zani, A. Mordini and D. Franchi, *Pure Appl. Chem.*, 2018, **90**, 363-376.

9. C. Gautam, A. Singh, S. W. Gosavi, R. Chauhan, V. K. Sharma, A. Alarifi, M. Afzal, M. Muddassir and A. Kumar, *Appl. Organomet. Chem.*, 2022, **36**, e6608.

10. A. B. Muñoz-García, I. Benesperi, G. Boschloo, J. J. Concepcion, J. H. Delcamp, E. A. Gibson, G. J. Meyer, M. Pavone, H. Pettersson, A. Hagfeldt and M. Freitag, *Chem. Soc. Rev.*, 2021, **50**, 12450-12550.

11. H. Tian, J. Gardner, T. Edvinsson, P. B. Pati, J. Cong, B. Xu, M. Abrahamsson, U. B. Cappel and E. M. Barea, in *Solar Energy Capture Materials*, ed. E. A. Gibson, The Royal Society of Chemistry, London,1st edn, 2019, ch 3 , pp. 89-152.

12. N. Serpone, A. V. Emeline and S. Horikoshi, in *Photochemistry: Volume 37*, ed. A. Albini, The Royal Society of Chemistry, London, 1st edn, 2009, vol. 37, pp. 300-361.

13. C. E. Housecroft and E. C. Constable, *Chem. Sci.*, 2022, **13**, 1225-1262.

14. B. O'Regan and M. Grätzel, *Nature*, 1991, **353**, 737-740.

15. J-M. Ji, H. Zhou and H. K. Kim, *J. Mater. Chem. A*, 2018, **6**, 14518-14545.

16. N. Tomar, A. Agrawal, V. S. Dhaka and P. K. Surolia, *Solar Energy*, 2020, **207**, 59-76.

17.   H. Ozawa, T. Sugiura, T. Kuroda, K. Nozawa and H. Arakawa, *J. Mater. Chem. A*, 2016, **4**, 1762-1770.

18.   Y-J. Yuan, Z-T. Yu, D.-Q. Chen and Z-G. Zou, *Chem. Soc. Rev.*, 2017, **46**, 603-631.

19.   L-H. Yu, J-Y. Xi, K. C. Lo, L. J. Antrobus, D. L. Phillips and W. K. Chan, *J Inorg Organomet Polym Mater*, 2015, **25**, 169-175.

20.   E. Longhi and L. De Cola, in *Iridium(III) in Optoelectronic and Photonics Applications*, ed. E. Zysman-Colman, John Wiley & Sons Ltd, Chichester, 1st edn, 2017, ch 6, pp. 205-274.

21.   S. I. Bezzubov, I. S. Zharinova, A. A. Khusyainova, Y. M. Kiselev, I. V. Taydakov, E. A. Varaksina, M. T. Metlin, A. S. Tobohova, V. M. Korshunov, S. A. Kozyukhin and V. D. Dolzhenko, *Eur. J. Inorg. Chem.*, 2020, **2020**, 3277-3286.

22.   S. Zhang, J-C. Xia, Z-G. Wu, G-Z. Lu, Y. Zhao and Y-X. Zheng, *Eur. J. Inorg. Chem.*, 2016, **2016**, 2556-2561.

23.   H. Ozawa, Y. Yamamoto, H. Kawaguchi, R. Shimizu and H. Arakawa, *ACS Appl. Mater. Interfaces*, 2015, **7**, 3152-3161.

24.   H. Ozawa, K. Fukushima, A. Urayama and H. Arakawa, *Inorg. Chem.*, 2015, **54**, 8887-8889.

25.   A. Sinopoli, C. J. Wood, E. A. Gibson and P. I. P. Elliott, *Eur. J. Inorg. Chem.*, 2016, **2016**, 2887-2890.

26.   L. N. Ashbrook and C. M. Elliott, *J. Phys. Chem. A*, 2013, **117**, 3853-3864.

27.   Q. Zhang, S. Wei, S. Zhou, X. Wei, Z. Xu, Z. Wang, B. Wei and X. Lu, *ACS Appl. Electron. Mater.*, 2020, **2**, 2141-2150.

28.   O. S. Wenger, *Chem. Eur. J.*, 2019, **25**, 6043-6052.

29.   Y. Liu, T. Harlang, S. E. Canton, P. Chábera, K. Suárez-Alcántara, A. Fleckhaus, D. A. Vithanage, E. Göransson, A. Corani, R. Lomoth, V. Sundström and K. Wärnmark, *Chem. Commun.*, 2013, **49**, 6412-6414.

30.   L. Liu, T. Duchanois, T. Etienne, A. Monari, M. Beley, X. Assfeld, S. Haacke and P. C. Gros, *Phys. Chem. Chem. Phys.*, 2016, **18**, 12550-12556.

31.   J-M. Ji, H. Zhou, Y. K. Eom, C. H. Kim and H. K. Kim, *Adv. Energy Mater.*, 2020, **10**, 2000124.

32.	S. Ito, H. Miura, S. Uchida, M. Takata, K. Sumioka, P. Liska, P. Comte, P. Péchy and M. Grätzel, *Chem. Commun.*, 2008, **41**, 5194-5196.

33.	J. Yang, P. Ganesan, J. Teuscher, T. Moehl, Y. J. Kim, C. Yi, P. Comte, K. Pei, T. W. Holcombe, M. K. Nazeeruddin, J. Hua, S. M. Zakeeruddin, H. Tian and M. Grätzel, *J. Am. Chem. Soc.*, 2014, **136**, 5722-5730.

34.	Y. Oshida, in *Bioscience and Bioengineering of Titanium Materials*, ed. Y. Oshida, Elsevier, Oxford, 2nd edn, 2013, ch 4, pp. 87-115.

35.	P. Wang, S. Guo, H. J. Wang, K. K. Chen, N. Zhang, Z. M. Zhang and T. B. Lu, *Nat. Commun.*, 2019, **10**.

36.	W. R. McNamara, Z. Han, P. J. Alperin, W. W. Brennessel, P. L. Holland and R. Eisenberg, *J. Am. Chem. Soc.*, 2011, **133**, 15368-15371.

37.	M. A. Bryden and E. Zysman-Colman, *Chem. Soc. Rev.*, 2021, **50**, 7587-7680.

38.	C. D. Windle, M. W. George, R. N. Perutz, P. A. Summers, X. Z. Sun and A. C. Whitwood, *Chem. Sci.*, 2015, **6**, 6847-6864.

39.	H-J. Son, S. Jin, S. Patwardhan, S. J. Wezenberg, N. C. Jeong, M. So, C. E. Wilmer, A. A. Sarjeant, G. C. Schatz, R. Q. Snurr, O. K. Farha, G. P. Wiederrecht and J. T. Hupp, *J. Am. Chem. Soc.*, 2013, **135**, 862-869.

40.	X. Liu, J. Zhou, M. Meng, G. Y. Zhu, Y. Tan, X. Chen, J. Wei, D.-B. Kuang, Y. Y. Wu, S. Su, T. Cheng, Y. Zhou and C. Y. Liu, *Appl. Catal. B*, 2021, **286**, 119836.

41.	K. Maeda, *Adv. Mater.*, 2019, **31**, 1808205.

42.	E. Nikoloudakis, I. López-Duarte, G. Charalambidis, K. Ladomenou, M. Ince and A. G. Coutsolelos, *Chem. Soc. Rev.*, 2022, **51**, 6965-7045.

43.	R. Kuriki and K. Maeda, *Phys. Chem. Chem. Phys.*, 2017, **19**, 4938-4950.

44.	J. Hawecker, J.-M. Lehn and R. Ziessel, *J. Chem. Soc., Chem. Commun.*, 1985, **2**, 56-58.

45.	Y. Arikawa, I. Tabata, Y. Miura, H. Tajiri, Y. Seto, S. Horiuchi, E. Sakuda and K. Umakoshi, *Chem. Eur. J.*, 2020, **26**, 5603-5606.

46.	S. Das, R. R. Rodrigues, R. W. Lamb, F. Qu, E. Reinheimer, C. M. Boudreaux, C. E. Webster, J. H. Delcamp and E. T. Papish, *Inorg. Chem.*, 2019, **58**, 8012-8020.

47.	D. R. Whang, K. Sakai and S. Y. Park, *Angew. Chem. Int. Ed.*, 2013, **52**, 11612-11615.

48.	J. Zhao, K. Xu, W. Yang, Z. Wang and F. Zhong, *Chem. Soc. Rev.*, 2015, **44**, 8904-8939.

49.	M. Tahoun, C. T. Gee, V. E. McCoy, P. M. Sander and C. E. Müller, *RSC Adv.*, 2021, **11**, 7552-7563.

50.	H. Shinokubo and A. Osuka, *Chem. Commun.*, 2009, DOI: 10.1039/B817941G, 1011-1021.

51.	M. O. Senge, *Chem. Commun.*, 2011, **47**, 1943-1960.

52.	B. Vaz, R. Alvarez, M. Nieto, A. I. Paniello and A. R. de Lera, *Tetrahedron Lett.*, 2001, **42**, 7409-7412.

53.	W. Zheng, N. Shan, L. Yu and X. Wang, *Dyes Pigm.*, 2008, **77**, 153-157.

54.	M. A. Bakar, N. N. Sergeeva, T. Juillard and M. O. Senge, *Organometallics*, 2011, **30**, 3225-3228.

55.	S. G. Dimagno, V. S. Y. Lin and M. J. Therien, *J. Org. Chem.*, 1993, **58**, 5983-5993.

56.	A. Nakano, H. Shimidzu and A. Osuka, *Tetrahedron Lett.*, 1998, **39**, 9489-9492.

57.	A. N. Kiselev, S. A. Syrbu, N. S. Lebedeva and Y. A. Gubarev, *Inorganics*, 2022, **10**, 63.

58.	E. Leary, B. Limburg, A. Alanazy, S. Sangtarash, I. Grace, K. Swada, L. J. Esdaile, M. Noori, M. T. González, G. Rubio-Bollinger, H. Sadeghi, A. Hodgson, N. Agraït, S. J. Higgins, C. J. Lambert, H. L. Anderson and R. J. Nichols, *J. Am. Chem. Soc.*, 2018, **140**, 12877-12883.

59.	M. O. Senge, N. N. Sergeeva and K. J. Hale, *Chem. Soc. Rev.*, 2021, **50**, 4730-4789.

60.	P. Chen, O. S. Finikova, Z. Ou, S. A. Vinogradov and K. M. Kadish, *Inorg. Chem.*, 2012, **51**, 6200-6210.

61.	J. Rochford, S. Botchway, J. J. McGarvey, A. D. Rooney and M. T. Pryce, *J. Phys. Chem. A*, 2008, **112**, 11611-11618.

62.	R. Bonnett, A. Harriman and A. N. Kozyrev, *J. Chem. Soc., Faraday Trans.*, 1992, **88**, 763-769.

63.	G. T. Rohde, J. R. Sabin, C. D. Barrett and V. N. Nemykin, *New J. Chem.*, 2011, **35**, 1440.

64.	M. Uttamlal and A. Sheila Holmes-Smith, *Chem. Phys. Lett.*, 2008, **454**, 223-228.

65. A. Shinohara, G. Shao, T. Nakanishi and H. Shinmori, *Front. Chem.*, 2021, **9**.

66. X. Cui, C. Zhang, K. Xu and J. Zhao, *J. Mater. Chem. C*, 2015, **3**, 8735-8759.

67. B. Minaev, *Spectrochim Acta A Mol Biomol Spectrosc*, 2004, **60**, 3213-3224.

68. A. Wiehe, C. Ryppa and M. O. Senge, *Org. Lett.*, 2002, **4**, 3807-3809.

69. A. D. Adler, F. R. Longo, J. D. Finarelli, J. Goldmacher, J. Assour and L. Korsakoff, *J. Org. Chem.*, 1967, **32**, 476-476.

70. S. Eu, S. Hayashi, T. Umeyama, A. Oguro, M. Kawasaki, N. Kadota, Y. Matano and H. Imahori, *J. Phys. Chem. A*, 2007, **111**, 3528-3537.

71. M. Cariello, S. M. Abdalhadi, P. Yadav, J.-D. Decoppet, S. M. Zakeeruddin, M. Grätzel, A. Hagfeldt and G. Cooke, *Dalton Trans.*, 2018, **47**, 6549-6556.

72. J. S. Lindsey, in *Metalloporphyrins Catalyzed Oxidations*, ed. F. Montanari and L. Casella, Springer Netherlands, Dordrecht, 1st edn, 1994, ch 2, pp. 49-86.

73. J. S. Lindsey, *Acc. Chem. Res.*, 2010, **43**, 300-311.

74. A. Nowak-Król, R. Plamont, G. Canard, J. A. Edzang, D. T. Gryko and T. S. Balaban, *Chem. Eur. J.*, 2015, **21**, 1488-1498.

75. S. Shanmugathasan, C. Edwards and R. W. Boyle, *Tetrahedron*, 2000, **56**, 1025-1046.

76. B. Godlewski, D. Baran, M. De Robichon, A. Ferry, S. Ostrowski and M. Malinowski, *Org. Chem. Front.*, 2022, **9**, 2396-2404.

77. K. Sonogashira, Y. Tohda and N. Hagihara, *Tetrahedron Lett.*, 1975, **16**, 4467-4470.

78. R. Chinchilla and C. Nájera, *Chem. Rev.*, 2007, **107**, 874-922.

79. M. Schilz and H. Plenio, *J. Org. Chem.*, 2012, **77**, 2798-2807.

80. A. Yella, C.-L. Mai, S. M. Zakeeruddin, S.-N. Chang, C.-H. Hsieh, C.-Y. Yeh and M. Grätzel, *Angew. Chem. Int. Ed.*, 2014, **53**, 2973-2977.

81. F. Gou, X. Jiang, R. Fang, H. Jing and Z. Zhu, *ACS Appl. Mater. Interfaces*, 2014, **6**, 6697-6703.

82. C-Y. Lin, C-F. Lo, L. Luo, H-P. Lu, C.-S. Hung and E. W-G. Diau, *J. Phys. Chem. A*, 2009, **113**, 755-764.

83. T. J. Whittemore, H. J. Sayre, C. Xue, T. A. White, J. C. Gallucci and C. Turro, *J. Am. Chem. Soc.*, 2017, **139**, 14724-14732.

84.   X.-y. Yu, H. Su, X. Zheng, W.-b. Liu, Y. He, N.-n. Fei, R. Qiao, Y.-l. Ren and C.-y. Niu, *J. Mol. Struct.*, 2021, **1237**, 130358.

85.   T. E. O. Screen, I. M. Blake, L. H. Rees, W. Clegg, S. J. Borwick and H. L. Anderson, *J. Chem. Soc., Perkin Trans. 1*, 2002, **3**, 320-329.

86.   P. B. Dzhevakov, M. A. Topchiy, D. A. Zharkova, O. S. Morozov, A. F. Asachenko and M. S. Nechaev, *Adv. Synth. Catal.*, 2016, **358**, 977-983.

87.   S. M. Marschner, R. Haldar, O. Fuhr, C. Wöll and S. Bräse, *Chem. Eur. J.*, 2021, **27**, 1390-1401.

88.   B. J. Littler, M. A. Miller, C.-H. Hung, R. W. Wagner, D. F. O'Shea, P. D. Boyle and J. S. Lindsey, *J. Org. Chem.*, 1999, **64**, 1391-1396.

89.   S. Shanmugathasan, C. K. Johnson, C. Edwards, E. K. Matthews, D. Dolphin and R. W. Boyle, *J. Porphyr Phthalocyanines*, 2000, **4**, 228-232.

90.   R. W. Boyle, C. K. Johnson and D. Dolphin, *J. Chem. Soc., Chem. Commun.*, 1995, **5**, 527-528.

91.   S. M. Marschner, R. Haldar, O. Fuhr, C. Wöll and S. Bräse, *Chem. Eur. J.*, 2021, **27**, 1390-1401.

92.   M. L. Dean, J. R. Schmink, N. E. Leadbeater and C. Brückner, *Dalton Trans.*, 2008, **10**, 1341-1345.

93.   A. Manda, M. B. Maradolla, C. Garimella and G. Lingamallu, *J Chem Res*, 2007, **2007**, 390-391.

94.   G. R. Seely and M. Calvin, *J. Chem. Phys.*, 1955, **23**, 1068-1078.

95.   A. Orbelli Biroli, F. Tessore, M. Pizzotti, C. Biaggi, R. Ugo, S. Caramori, A. Aliprandi, C. A. Bignozzi, F. De Angelis, G. Giorgi, E. Licandro and E. Longhi, *J. Phys. Chem. A*, 2011, **115**, 23170-23182.

96.   T-G. Zhang, Y. Zhao, I. Asselberghs, A. Persoons, K. Clays and M. J. Therien, *J. Am. Chem. Soc.*, 2005, **127**, 9710-9720.

97.   M. Balaz, H. A. Collins, E. Dahlstedt and H. L. Anderson, *Org. Biomol. Chem.*, 2009, **7**, 874-888.

98.   L. Zhang, L. Favereau, Y. Farre, A. Maufroy, Y. Pellegrin, E. Blart, M. Hissler, D. Jacquemin, F. Odobel and L. Hammarström, *RSC Adv.*, 2016, **6**, 77184-77194.

99. M. Zawadzka, J. Wang, W. J. Blau and M. O. Senge, *Photochem. Photobiol. Sci.*, 2013, **12**, 996-1007.

100. J. Lu, B. Zhang, S. Liu, H. Li, H. Yuan, Y. Shen, J. Xu, Y. Cheng and M. Wang, *Phys. Chem. Chem. Phys.*, 2014, **16**, 24755-24762.

101. Y-C. Chang, C-L. Wang, T-Y. Pan, S-H. Hong, C.-M. Lan, H-H. Kuo, C-F. Lo, H-Y. Hsu, C-Y. Lin and E. W-G. Diau, *Chem. Commun.*, 2011, **47**, 8910-8912.

102. J. Hatano, N. Obata, S. Yamaguchi, T. Yasuda and Y. Matsuo, *J. Mater. Chem.*, 2012, **22**, 19258-19263.

103. A. G. Hyslop, M. A. Kellett, P. M. Iovine and M. J. Therien, *J. Am. Chem. Soc.*, 1998, **120**, 12676-12677.

104. D. Blakemore, in *Synthetic Methods in Drug Discovery: Volume 1*, ed. D. C. Blakemore, P. M. Doyle, Y. M. Fobian, The Royal Society of Chemistry, Cambridge, 2016, vol. 1, ch 1, pp. 1-69.

105. N. Oka, T. Yamada, H. Sajiki, S. Akai and T. Ikawa, *Org. Lett.*, 2022, **24**, 3510-3514.

106. T. Ishiyama, J. Takagi, Y. Yonekawa, J. F. Hartwig and N. Miyaura, *Adv. Synth. Catal.*, 2003, **345**, 1103-1106.

107. K. D. Mulholland, S. Yoon, C. C. Rennie, E. K. Sitch, A. I. McKay, K. Edkins and R. M. Edkins, *Chem. Commun.*, 2020, **56**, 8452-8455.

108. A. J. J. Lennox and G. C. Lloyd-Jones, *Chem. Soc. Rev.*, 2014, **43**, 412-443.

109. M. O. Senge, M. Fazekas, M. Pintea, M. Zawadzka and W. J. Blau, *Eur. J. Org. Chem.*, 2011, **2011**, 5797-5816.

110. J. Pijeat, Y. J. Dappe, P. Thuéry and S. Campidelli, *Org. Biomol. Chem.*, 2018, **16**, 8106-8114.

111. Z. Ahmadi and J. S. McIndoe, *Chem. Commun.*, 2013, **49**, 11488-11490.

112. X. Sun, J. Zhang and B. He, *J. Photochem. Photobiol. A*, 2005, **172**, 283-288.

113. C. Brückner, P. C. D. Foss, J. O. Sullivan, R. Pelto, M. Zeller, R. R. Birge and G. Crundwell, *Phys. Chem. Chem. Phys.*, 2006, **8**, 2402-2412.

114. I. Gupta and M. Ravikanth, *J. Photochem. Photobiol. A*, 2006, **177**, 156-163.

115. H-Z. Yu, J. S. Baskin and A. H. Zewail, *J. Phys. Chem. A*, 2002, **106**, 9845-9854.

116.   K. Suzuki, A. Kobayashi, S. Kaneko, K. Takehira, T. Yoshihara, H. Ishida, Y. Shiina, S. Oishi and S. Tobita, *Phys. Chem. Chem. Phys.*, 2009, **11**, 9850-9860.